CARDIFF UNIVERSITY
SCHOOL OF ENGINEERING

Fuel Flexibility with Low Emissions for Gas Turbine Engines

By

Hayder Jabbar Kurji

Supervisors:
Prof Philip J Bowen
Dr Agustin Valera-Medina

A Thesis submitted to Cardiff University
For the Degree of Doctor of Philosophy
In Mechanical Engineering, 2017

DECLARATION

This work has not been submitted in substance for any other degree or award at this or any other university or place of learning, nor is being submitted concurrently in candidature for any degree or another award.

Signed ……. (Candidate) Date ….....

STATEMENT 1

This thesis is being submitted in partial fulfilment of the requirements for the degree of PhD

Signed ……. (Candidate) Date ….....

STATEMENT 2

This thesis is the result of my independent work/investigation, except where otherwise stated, and the thesis has not been edited by a third party beyond what is permitted by Cardiff University's Policy on the Use of Third Party Editors by Research Degree Students. Other sources are acknowledged by explicit references. The views expressed are my own.

Signed ……. (Candidate) Date ….....

STATEMENT 3

I hereby give consent for my thesis, if accepted, to be available online in the University's Open Access repository and for inter-library loan, and for the title and summary to be made available to outside organisations.

Signed ……. (Candidate) Date ….....

ACKNOWLEDGMENTS

*First and foremost, I would like to praise and thank **GOD** for helping me to complete This thesis.*

*I wish to express my gratefulness to my supervisors, **Prof. Philip Bowen and Doctor Agustin Valera-Medina** for their continuous supervision, real discussions and valuable ideas through this research work.*

*I would like to thank **Dr Richard March** for his support during this research.*

*My great thanks also extended to all technicians of the laboratory and their help in offering me the facilities to complete my experiments. Special recognition to **Mr Malcolm Seaborne** and **Mr Paul Malpas,** whose technical knowledge contributed to the successful completion of this work.*

*I would like to thank the staff of School of Engineering, the staff of the Gas Turbine Research Centre (GTRC), the staff of the Mechanical Engineering. And special thanks for whom I will never forget to go to the following: **Dr Andrew Crayford, Dr Tony Giles, Dr Daniel Pugh, Gina Goddard, Chris Lee, Jeanette Whyte, Aderyn Ried.***

*I would like to extend my thanks to the **Iraqi Government** for sponsoring my PhD study, and many thanks to the staff of the **Iraqi cultural attaché in London** for their help during my stay in the UK.*

*My deepest thanks, love and gratitude for all of my family, **parents, brothers, sisters** and extraordinary thanks for my **wife** and my lovely daughter, **Fatimah***

ABSTRACT

This work examined the performance of swirl burners using different injection strategies for various substitute fuels. The research procedure involved various stages; firstly, an assessment study between two liquid fuels, a pure biodiesel and saturated biodiesel, compared to kerosene. Atomization forms were obtained, and a combustion test campaign was initiated using a generic swirl burner. Emissions and power outputs were measured at gas turbine relevant equivalence ratios. Excess oxygen and atomization trends in the biodiesel seem to be playing a significant role in the creation of emissions and flame stability when compared to kerosene.

Secondly, an experimental study on the combustion of methane-carbon dioxide mixtures was achieved. Gas mixtures were examined by using different injection strategies with and without swirl and with and without central injection. A smaller 20-kW swirl burner was used to analyse stability and emissions performance by using these blends and to study the impact of CO_2 addition. The burner configuration comprised a centre body with an annular, premixed gas/air jet introduced through five, 60° swirl vanes. CO_2 dilution reduced flame stability and operability range. The introduction of CO_2 decreases temperatures in the combustion zone thus producing a lessening in emissions of nitrous oxides across all equivalence ratios. Regarding injection regimes, the external purely premixed injection system has lower NO_x and CO. Addition of CO_2 increases the lean blowout limit of all blends.

In the last section, a new burner was finally employed to carry out trials using multi-phase injection, where, experimental work investigated the performance of a swirl burner using various mixtures of CO_2/CH_4 blends with either diesel or biodiesel derived from cooking oil. The swirl burner was employed to analyse gas turbine combustion features under atmospheric conditions to quantify flame stability and emissions by using these fuels.

The results revealed that the use of biodiesel and CO_2/CH_4 blends mixtures led to lower CO production. Results showed that a notable reduction of ~50% in NOx was obtained at all conditions for the biodiesel blends.

Publications

[1] H. Kurji, Agustin Valera-Medina, Jon Runyon, Anthony Giles, Daniel Pugh, Richard Marsh, N. Cerone, F. Zimbardi, and V. Valerio., "Combustion characteristics of biodiesel saturated with pyrolysis oil for power generation in gas turbines," *Renew. Energy*, vol. 99, pp. 443–451, 2016.

[2] H. Kurji, Aniekan Okon, Agustin Valera-Medina, and C. Cheng-Tung. "Reduction of emissions by using various syngases with different injection strategies under premixed combustion mode." In *Students on Applied Engineering (ISCAE), International Conference for*, pp. 407-412. IEEE, 2016.

[3] H. Kurji, A. Valera-Medina, Aniekan Okon, C. Cheng-Tung, " Combustion and emission performance of CO2/CH4/biodiesel and CO2/CH4/diesel blends in a Swirl Burner Generator." In the 9th International Conference on Applied Energy, ICAE2017, 2017.

[4] H. Kurji, A. Valera-Medina, Aniekan Okon, C. Cheng-Tung, " Carbon dioxide blends to reduce emissions under premixed combustion mode." In 13th International Conference on Energy for a Clean Environment July 2-6, São Miguel, Azores, Portugal,2017.

[5] Aniekan Okon, H. Kurji, A. Valera-Medina, and Yiqin Xue, " Acoustic dynamics of a swirl premixed combuster with different operating conditions." in the 9th International Conference on Applied Energy, ICAE2017, 2017.

[6] Aniekan Okon, H. Kurji, A. Valera-Medina, and Yiqin Xue. "Heat release rate and pressure fluctuation of lean premixed flame at different forcing levels." In *Students on Applied Engineering (ISCAE), International Conference for*, pp. 232-236. IEEE, 2016.

[7] Aniekan Okon, A. Valera-Medina, H. Kurji, and Yiqin Xue. " Effects of Flame Temperature on Combustion Instabilities of a Premixed Burner." In 8th European Combustion Meeting (ECM 2017), Dubrovnik, Croatia, 2017.

Table of Contents

List of Figures

List of tables

Nomenclature

Alphabetic symbols

AFR	Air-fuel ratio	-
(CH)'/(CH)	Gain (Heat release fluctuations)	-
d	Burner inner central diameter	[m]
D	Droplet diameter	[m]
Dh	Swirler hub diameter	[m]
Ds	Swirler diameter	[m]
FAR_{act}	Actual Fuel Air Ratio	-
FAR_{stoich}	Stoichiometry Fuel Air Ratio	-
K	the molar fraction ratios of additional gas in methane	-
$\dot{m}air$	Air mass flow rate	[kg/s]
$\dot{m}fuel$	Fuel mass flow rate	[kg/s]
MFRs	mass flow rates	[kg/s
P	The pressure	[bar]
Re	Reynolds number	-
S	Swirl number	-
t	Blade thickness	[m]
T	temperature	[K]
u	Swirl axial velocity	[m/s]
We	Weber number	-
Z	Ohnesorge number	-

Greek symbols

θ	Swirl angle	deg
ρ	density	[kg/m^3]
σ	Surface tension	[N/m]
μ	Viscosity	[Pa.s]
υ	Kinematic viscosity	[m^2/s]
Φ	Equivalence ratio	-

List of abbreviations

$C_2H_4O_2$	Methyl-formate
C_3H_6	Cyclopropane
C_5H_{10}	Cyclopentane
CCS	Carbon Capture and Storage
CFD	Computational fluid dynamics
CH_4	Methane
CO	Carbon monoxide
CO_2	Carbon dioxide
CP	specific heat
CRZ	Central Recirculation Zone
EIPPCB	European Parliament by the Pollution Prevention and Control Bureau
EPA	Environmental Protection Agency
FAME	Fatty Acid Methyl Ester
FID	Flame Ionisation Detector
GC	Gas Chromatography
GTRC	Gas Turbine Research Centre
H_2	Hydrogen
H_2O	water vapour
HHV	Higher Heating Value
HMFR	High Momentum Flow Region
HPOC	high-pressure optical chamber
HSP	High-Speed Photography
ICAO	International Civil Aviation Organisation
IEA	The International Energy Agency
IGCC	Integrated Gasification Combined Cycle
LHV	Lower Heating Value
N_2	Nitrogen
NG	natural gas
NO	Nitric Oxide
NO_2	Nitrogen Dioxide
NOx	Nitrogen oxides
O_2	Oxygen
OH-PLIF	Hydroxyl Planar Laser-Induced Fluorescence
PAH	Polycyclic Aromatic Hydrocarbons
PLL	Phase-Locked Loop
PM	particulate matter
ppm	parts per million
SMD	Sauter mean diameter
SO_2	Sulphur Dioxide
SO_x	Sulphur Oxides
UHC	unburned hydrocarbons

Chapter1
Introduction

The true sign of intelligence is not knowledge but imagination
Albert Einstein

1.1 Energy supply

The International Energy Agency (IEA) has expected that worldwide energy request will increase about 1.6% per year between the years 2006 – 2030 [1] with increasing contribution required from both gas powered and renewable energy sources to achieve demand, figure 1.1. Although renewable energy technologies are already meeting demand, the current limited output of these technologies means that power generation of optimised fossil fuelled systems will be vital for the future, most of which is produced by gas turbines. While the power output and efficiency of modern gas turbine units have both increased, to reduce emissions, new fuel blends are in the process of being put into use. As a consequence, the operational flexibility of these systems is one of the leading issues for the industry [1].

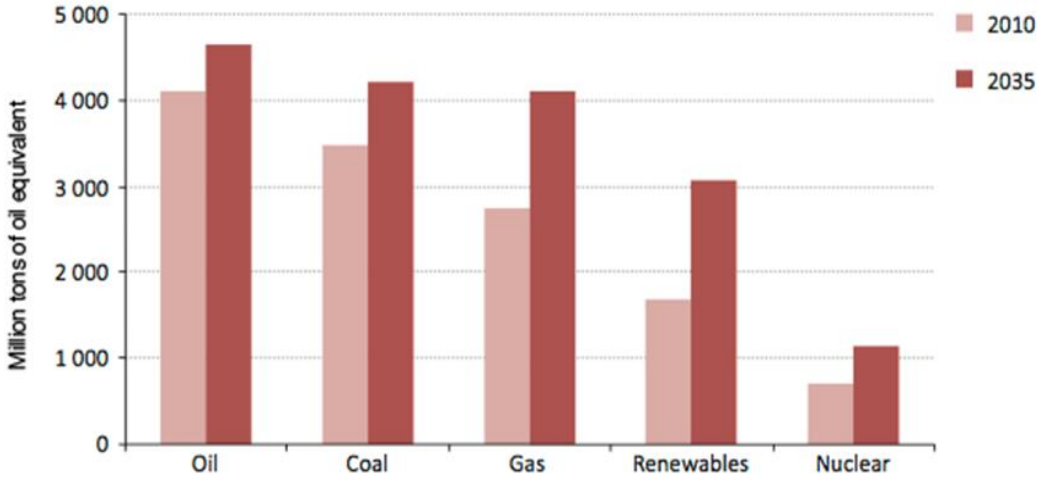

Figure 1-1 World primary energy demand by fuel [2]

First gas turbine began to generate electricity successfully in 1939. It produced energy on a commercial scale at the local power station in Neuchâtel, Switzerland. Designed and built by A. B. Brown Boveri, the turbine had a thermal efficiency of 17% and a power output of 4MW [3]. Nowadays, commercial gas turbines are far more powerful and efficient. For instance, as part of a combined cycle, the Siemens' H-class SGT5-8000H has a net thermal efficiency of 60.75% and has an output of 578MW [4].

From the early stages of the 21st century, gas-fired turbines have been giving more than 33% of the UK's power. During 2011 this quantity was about 40% [5].

1.2 Gas turbine combustion

Stationary gas turbine engines are used to produce shaft power. The shaft power can then be converted to electrical energy with a generator, or it can be used to turn mechanical devices such as pumps and gas compressors for pipelines. Figure 1.2 shows a conventional gas turbine engine [6].

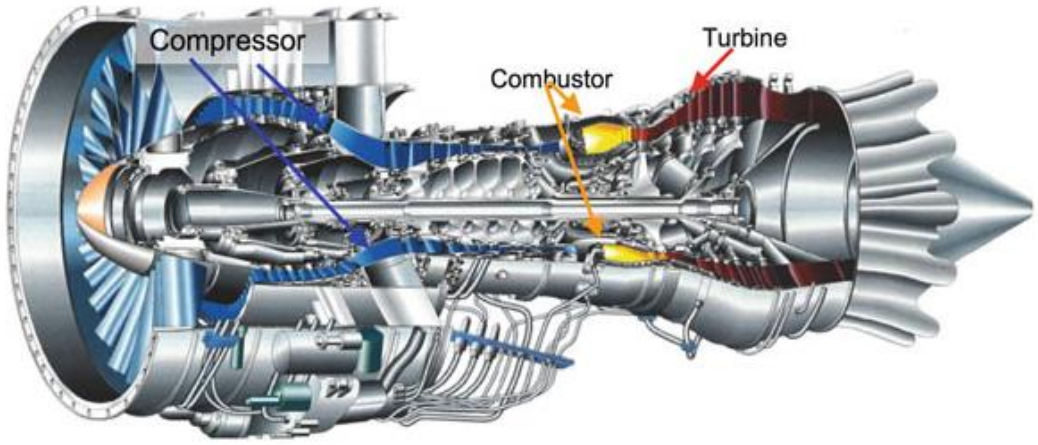

Figure 1-2 Basic components of a turbine engine [6]**.**

The engine works by pulling ambient air into and through the compressor, where the pressure and temperature rise because of the compression. Then the air is then mixed with fuel and reacts inside a combustion chamber or combustor for short. The heat liberated from combustion increases the temperature of the new product gas to relatively high temperatures.

This gas then passes through a turbine where the thermal energy is transformed into shaft power. The product gas is exhausted out of the turbine and back into the atmosphere. Part of the shaft power produced by the turbine is used to spin the compressor, while the remaining power is available for turning an electrical generator or other devices. The primary difference between the stationary gas turbine and the propulsion gas turbine engine is that the stationary gas turbine does not use the thrust of the exhaust gas to push an aircraft. Rather, it extracts as much energy out of the exhaust gas by having additional turbine stages to produce maximum shaft power.

Also, stationary gas turbines do not have severe size and weight limits and are designed to work with a wider range of fuels. They often use both axial and radial turbines and compressors and finally have strict pollutant emission regulations.

The basic thermodynamic process of a gas turbine can be represented by a Brayton cycle. Figure 1.3 shows pressure-volume and temperature-entropy diagrams for this cycle. The numbers at each state point correspond to the numbers in figure 1.3. The inlet to the combustor is stated point 2, and the combustor exit/turbine inlet is stated point 3. The ratio of the pressure at the combustor inlet to ambient conditions is known as the compressor pressure ratio.

The primary aim of any gas turbine design is to maximise the power output and efficiency. Figure 1.3 shows how the two change with variations in the pressure ratio and combustor exit/turbine inlet temperature for the simple-cycle engine. The turbine inlet temperature, T3, is limited in any design by the material and cooling process used on the turbine blades and rotor. For higher turbine inlet temperatures, the maximum efficiencies occur at higher pressures. Similarly, the optimal pressure ratio for specific output increases with higher turbine inlet temperatures.

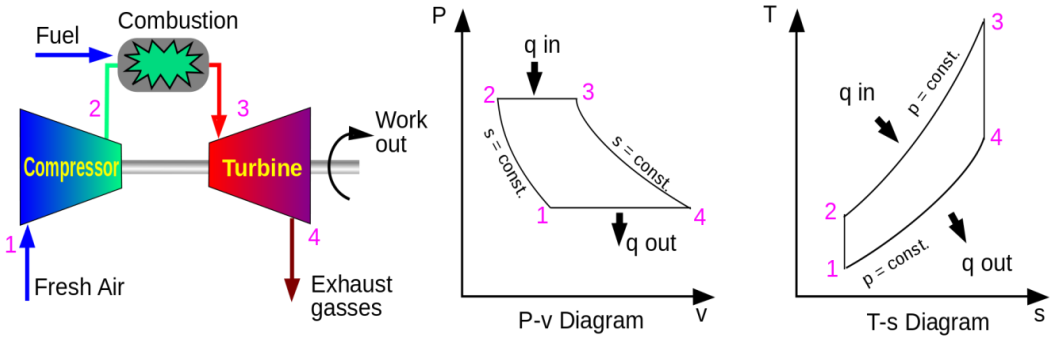

Figure 1-3 Gas turbine components, PV and TS diagrams of a Brayton cycle [7]

Some designs incorporate a heat exchanger between the compressor and combustor to preheat the air from the hot exhaust products. Higher heat exchanger effectiveness leads to lower optimal pressure ratios and higher efficiencies.

Although this trend is preferred over the simple, the simple cycle is still often used in practice. That is because the increased efficiency in the recuperated cycle comes at the

extra cost and complexity of adding the heat-exchanger to the system. Smaller gas turbines with low turbine inlet temperatures and fewer compressor stages utilise heat exchangers while larger gas turbines continue to favour from the simple cycle design.

Modern gas turbines are often part of combined cycle power plant. A combined cycle gas turbine plant turns a generator much like a basic cycle plant; however, it uses exhaust gases to heat water to form steam.

As fuel expenses are a huge factor in power production, the efficiency of the turbine and the total system must be considered, while always attempting to lower emissions. A further challenge for the units is to increase operational flexibility [5]. As renewable energy production increases, it is likely that gas turbine systems will be used to provide backup power generation.

Backup systems will need to react fast enough to ensure demand can be met if needed. Also, it is special if the units can work on together liquid and gaseous fuels. If fuel costs vary or if the supply of a particular fuel type is limited, being capable of work on many fuels would be valuable. The last considerations relate to dependability and stability. As the units will be quick to react when required, it is essential that they are reliable and stable at all operation stages [5].

1.3 Gas turbine alternative fuels

Fossil fuels rule in aerospace transportation, industrial energy, production, agricultural energy and electrical power generation [8]. Right now 25% of fossil fuels are consumed by the transportation sector, and the aviation section consumes about 13% of the transportation fuel, being the second greatest sector after road transportation. About 15,750 aircraft work using fuel derived from fossil fuels, thus contributing to 2-3% of worldwide carbon emissions [9]. Therefore the aeronautic sector could benefit from alternative fuels.

Alternative fuels are playing a more and more important role in the power supply. These fuels can be taken out, for example, from the gasification of biomass or coal. They are categorised by a high concentration of H_2 and CO and have different combustion features in comparison to natural gas [9].

Hydrocarbon fuels are organic compounds consisting wholly of carbon and hydrogen. Dependent on the number of carbon atoms and their molecular structure, they can be classified as either gaseous, liquid or solid in standard conditions. Gaseous fuels have up to four carbon atoms while fuels with twenty or more are solid, and those in between are liquid [10].

There are three reasons for using renewable fuels: fuel security, carbon reduction and NOx and soot reduction. There has been extensive research on feedstocks and process transformation of the biomass feedstock into aviation fuels. Aviation biofuels are harder to get approval than road transport biofuels as they need tighter fuel requirement, flight-testing, and life cycle impact assessment of these fuels. They must also meet all the operational specification of current kerosene jet fuels [11].

Both synthetic and renewable jet fuels are the most common alternative fuels in aviation [12] and not the oxygenated methyl ester biofuels used in diesel. These Jet fuels such as Fisher-Tropsch fuels are aromatic and sulphur free which has the benefit of reducing particulate emissions [13]. However, oxygenated diesel biofuels have the additional benefit of soot reductions through the incorporation of oxygenated components in the fuel which are known from diesel engine work to reduce soot emissions.

Regarding power generation, there are many types of fuels used in industrial gas turbine combustors. These include natural gas, liquid distillate, diesel fuel, residual fuel oil, etc. The effect of pollutant emissions from combustion processes of these fuels on the health and environment have become a primary concern for the public and have led to wide research and development in combustion technologies, fuels, and other sectors to meet more and more stringent air quality and emissions regulations. New alternative fuels have a significant advantage dealing with these issues, therefore the importance of conducting active research on many of them.

For instance, biofuels include biogas, bioethanol, and biodiesel that has become more attractive recently as they are carbon neutral as plants absorb CO_2 emissions while they grow up [14] releasing it when the biodiesel is burned. In other words, the CO_2 released by burning a gallon of biodiesel today is absorbed from the atmosphere by soybean plants tomorrow. Nonetheless, this process is not carbon neutral if carbon

emissions are generated in the developing, harvesting and biomass to biofuel manufacturing process [14].

1.4 Dual injection nozzles

There are varied types of spray nozzles, each developed for a particular use and a special sort of flows, and to produce the desired droplet size and velocity scattering. Spray nozzles can be classified based on mass flow rate, liquid mass distribution, spray pattern, spray angle, spray effect, and droplet size [15].

The flow rate is reliant on the nozzle area, nozzle geometry, quality of the fluid and the supply pressure. In twin-fluid nozzles, there are two mass flows, one for the liquid and one, commonly, for the gas. For the same nozzle, a higher liquid flow rate tends to lead to greater droplet sizes, while a higher gas flow rate leads to smaller droplets[16].

Twin-fluid atomising nozzles can produce fine droplets at low liquid flow rates. In these nozzles, a high-velocity gas stream is brought in interaction with a liquid stream. Applications for this kind of nozzles contain humidification, dust control, gas cooling, accuracy coating and spray drying[17].

Twin-fluid atomising nozzles are available in different designs. Some employ the pressure principle, where the liquid is delivered from a pressurised source. Others use the gravity principle, wherever the liquid supply is placed above the nozzle, invoking gravity for the liquid flow.

The syphon principle is used too in some twin-fluid atomising nozzles where the liquid source is self-aspirating. The spray influence, flow rate and droplet size distribution differ for each nozzle. However, many twin-fluid nozzles can produce very fine droplets. Gas and liquid can be brought in contact either in the nozzle (internal mix) or outside of the nozzle (external mix)[16]. Furthermore, nozzles can be classified based on the flow rate of the atomising gas and the method the gas is brought into contact with the liquid. These differences are air blasting (figure 1.4), air-assisting, and effervescent nozzles. The main variation between each of the three is the velocity and quantity of air used in the atomising process. The additional difference relates to when the air is mixed with the liquid stream[18].

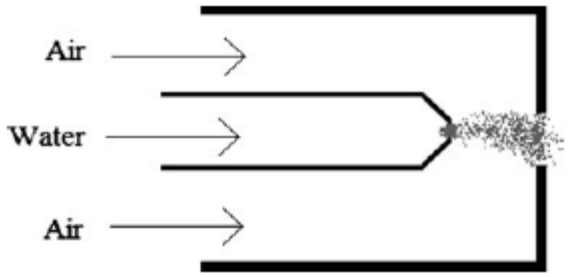

Figure 1-4 A schematic for a simple air blast nozzle design [6]

1.5 Gas turbine emissions and health impact

Industrial gas turbine emissions are very low for CO and UHC but significant in NOx emissions at high powers. Industrial gas turbines do not operate at idle, but for aero gas turbines, CO and UHC emissions are high at idle conditions and hence are important for air quality at airports [19]. The composition of gas turbine exhaust gases and their environmental impacts and sources are summarised in table 1.1. There are two particular classes of gas turbine emissions.

The main exhaust gases are carbon dioxide (CO_2), water vapour (H_2O), Nitrogen (N_2) and Oxygen (O_2), and their concentration is presented at percentage levels. Of these gases, only CO_2 is a greenhouse gas pollutant [13].

The composition of these major species can be computed if the fuel composition and working conditions are known, as these are complete combustion products. The second category is minor species that are environmentally harmful and dangerous to human health: carbon monoxide (CO), particulate matter (PM), unburned hydrocarbons (UHC), smoke (carbon), oxides of sulphur (SO_X) and oxides of nitrogen (NO_X).

These cannot be calculated and require careful measurement. The power generation sector contributes with the largest share of CO_2 emissions at 40% [20]. Thus, in gas turbines, the regular greenhouse gas is CO_2, which is a natural product of combustion and can only be reduced by using less fuel (less usage or better thermal efficiency) or alternative renewable fuels [20]. Aviation emissions are a relatively small compared to power generation sources and depend on fuel type, aircraft and engine type, engine load and flying altitude [21].

The need to locate an alternative cost-effective environmentally friendly fuel becomes essential when global warming and airport air quality issues are to be decreased [22]. Moreover, there is growing political and public pressure directing air transportation to reduce greenhouse gas emissions, which are changing rapidly because of the quick development of the aviation area.

Table 1. 1. Gas turbine exhaust emissions burning conventional fuels [23]**.**

Major Species	**Typical Concentration (% Volume)**	**Source**
Nitrogen (N_2)	**66 - 72**	**Inlet Air**
Oxygen (O_2)	**12 - 18**	**Inlet Air**
Carbon Dioxide (CO_2)	**1 - 5**	**Oxidation of Fuel Carbon**
Water Vapor (H_2O)	**1 - 5**	**Oxidation of Fuel Hydrogen**
Minor Species Pollutants	**Typical Concentration (PPMV)**	**Source**
Nitric Oxide (NO)	**20 - 220**	**Oxidation of Atmosphere Nitrogen**
Nitrogen Dioxide (NO_2)	**2 - 20**	**Oxidation of Fuel-Bound Organic Nitrogen**
Carbon Monoxide (CO)	**5 - 330**	**Incomplete Oxidation of Fuel Carbon**
Sulphur Dioxide (SO_2)	**Trace - 100**	**Oxidation of Fuel-Bound Organic Sulphur**
Sulphur Trioxide (SO_3)	**Trace - 4**	**Oxidation of Fuel-Bound Organic Sulphur**
Unburned Hydrocarbons (UHC)	**5 - 300**	**Incomplete Oxidation of Fuel or Intermediates**
Particulate Matter Smoke	**Trace - 25**	**Incomplete Oxidation of Fuel or Intermediates, Fuel Ash, Inlet Ingestion**

Carbon Monoxide reduces the oxygen-carrying of the blood through the formation of carboxyhemoglobin, and this increases the heart's pumping rate to increase the supply of oxygen, which prompts heart-related medical problems. CO additionally participates in atmospheric reactions with sunlight and NOx to form ozone [24].

Some hydrocarbons are cancer-causing (benzene, toluene, aldehydes, polycyclic aromatic hydrocarbons [PAH]). Nonetheless, the primary concern for UHCs is the production of ozone when they react with NOx in the existence of sunlight [20].

Ozone reduces lung function and decreases the oxygen-carrying capacity of the blood and subsequently impacts the heart by influencing the flow of oxygen into the blood.

NOx is one of the essential pollutants of concern from the gas turbine and is the most critical at high power conditions [20]. In industrial gas turbines, the formation of NOx is influenced by the primary zone flame temperature [25] such as the compressor exit temperature which is controlled by the engine pressure ratio.

Also, NOx interacts with moisture and ammonia in the air to form small particles of nitric acid which cause certain respiratory disease, for example, emphysema and bronchitis and can trigger heart disease.

The formation of nitric acid likewise prompts acid rain which harms plant growth in sensitive soils, such as in Scandinavian forests [24].NOx additionally interacts with common organic compounds including ozone to form toxic chemicals such as nitroarenes, nitrosamines and nitric radicals which can cause biological mutations. Numerous studies have shown that NOx can deplete the stratospheric ozone layer and increase the penetration of solar ultraviolet radiation which expands the risk of skin cancer [20, 23].

1.6 Aim and Objectives

The main target of the thesis to control the emission and reducing their environmental impact.

To meet this aim, several specific objectives needed to be met:

1. Experimental study of different liquid fuels will determine.The comparison study will be between kerosene and biodiesel, the last as pure fuel and as a saturated mixture with pyrolytic oil will be performed to understand the conclusion of using liquids fuels in a gas turbine and check if saturated biodiesel of fuel is appropriate to operate in a gas turbine. Providing evidence

of the potential to use this biodiesel as substitutes or backup of conventional gas turbines, as these kinds of alternative fuels can reduce harmful emissions.

2. Investigate the effect of CO_2 addition to methane by measuring the flame stability, emission performance and CH* production. Using methane-carbon dioxide mixtures at atmospheric conditions, to examine the effect of CO_2 addition alongside different levels of premixing with various injection strategies with and without swirl and with and without central injection, where CO_2 helps to reduce emissions.
3. Investigate the effect of using different mixtures of CO_2/CH_4 blends with either diesel or biodiesel derived from cooking oil under atmospheric conditions, then flame stability and emissions will be determined by using these fuels. Comparison between the blends will be carried out at different equivalence ratios. CH* chemiluminescence diagnostics will also use and linked with the levels of emissions created through the trials. Where biodiesel and CO_2 help to reduce emissions.

1.7 Thesis organisation

This thesis consists of seven chapters.

Chapter 1. The introduction illustrates the basic principles of gas turbines including the problems of emissions, alternative fuels and health impacts from emissions.

Chapter 2. This chapter comprehensively reviews previous work in the area and discusses atomization, combustion technologies, pollutant formation, fuel blends, gas turbine emissions regulations and liquid and gases multiphase studies.

Chapter 3. A review of the measuring techniques used in this work.

Chapter 4. Comparison study from experimental results through analysis of atomization and combustion of kerosene, pure biodiesel and saturated biodiesel.

Chapter 5. Study of methane and methane-carbon dioxide with a swirl burner. Flame stability characterisation, temperature profile, CH* production and emissions studies using different flow rates.

Chapter 6. Multi-phase studies were performed using a swirl burner. Flame stability, temperature profile, CH* production and emissions measurements at various flow rates were conducted.

Chapter 7. Conclusions and further work, providing a summary of the main findings obtained with this project, suggesting several research programmes that can be carried out for future experiments.

The thesis concludes with an alphabetical list of references to the works of the literature, cited in the text. Some of the work described in this thesis has been published or is in the process of publication, and has been presented at three conferences. For easy reference, the publications are at the beginning of this thesis.

Chapter 2

Literature review

Science walks forward on two feet, namely theory and experiment.
But continuous progress is only made by the use of both.

Robert A. Millikan

2.1 Gas turbine power

One area demanding significant research within the industry is the development of fuel flexible and dual fuel capable gas turbines. As the price of conventional fuels carries on to change, it is vital that modern gas turbine units can expand to a full difference of fuels depending on available and economically viable supply.

That could provide new blends of fuels, which often have lower qualities. While fuel flexibility is beneficial, control and reduction of emissions is necessary and must be taken into consideration as well.

Gas turbines have historically been able to run on many sorts of fuels, for example during improvement of turbine units in the 1920s; the fuels used were blasted furnace gas, pulverised coal and oil [3]. Current gas turbine units use a range of fuels dependent on their application:

- Aerospace engines mostly use kerosene due to its high calorific content which lessens the amount needed and therefore weight [3].

- Marine turbines consume diesel as it is cheap, weight being of less concern and it has a lower risk of explosion – significant in military applications.

- Finally, the majority of industrial power generation turbines use natural gas as fuel because of its cost and minimal corrosive element content. Assuming suitable engineering modifications have been made, these turbines can also employ compatible liquid fuels as a backup in case of gas shortage [26].

As a result of a stable supply of comparatively cheap, low sulphur natural gas during the 1990s, an increased deregulation of the power generation industry and need to decrease CO_2 emissions, high-efficiency combined cycle natural gas powered turbines became the preferred method of power generation [28].

2.2 Combustion fundamentals

Combustion in Gas Turbines is divided into three types: diffusive (non-premixed) flames; premixed flames and partially premixed flames. In diffusive combustion, the fuel is injected into the combustion chamber in a different position to the air, where it burns upon mixing with the air. Most aero-engine combustors are of this type.

In premixed systems, before entering the combustion zone fuel and air are mixed [20], [27]. The latter type of combustion is partially premixed flame fronts this kind occurs in the transition of non-premixed and premixed combustion.

Figure 2.1 shows a conventional gas turbine. This one mostly utilised non-premixed or partially premixed combustion due to these wide flame stability and simplicity of ignition. Non –premixed flames have a wider range of Air-fuel ratio (AFR) over which stable combustion can occur. However, NOx emissions have a trend to be higher as a consequence of the diffusion combustion with local stoichiometric reaction zones.

A traditional diffusion flame combustor design as utilised in aero-engines contains a primary zone, a secondary zone, and a dilution zone. A constant airflow velocity is kept up, and the fuel flow is then increased or decreased to control the overall air-fuel ratio (AFR) inside the primary zone. The (AFR) is set to achieve the preferred combustor exit temperature or turbine inlet temperature.

Engine power is changed by decreasing this temperature from that of maximum power. The maximum power turbine entry temperature has increased since the gas turbine was developed as turbine blade cooling systems and materials have been developed [28].

H class industrial gas turbines have the maximum turbine entry temperature around 1750K. The F class has about 1600K being presently the most common power generation gas turbine [103, 104]. Older E class systems have turbine entry temperature of 1450K covering most current power generation gas turbines.

There is a precise AFR value in which complete combustion occurs for any specified fuel and air mixture. This value is called the Stoichiometric air-fuel ratio (AFR st). Mixtures with higher AFR than AFR st are called lean as they have excess air, while mixtures with lower AFR values are termed rich as they have extra fuel.

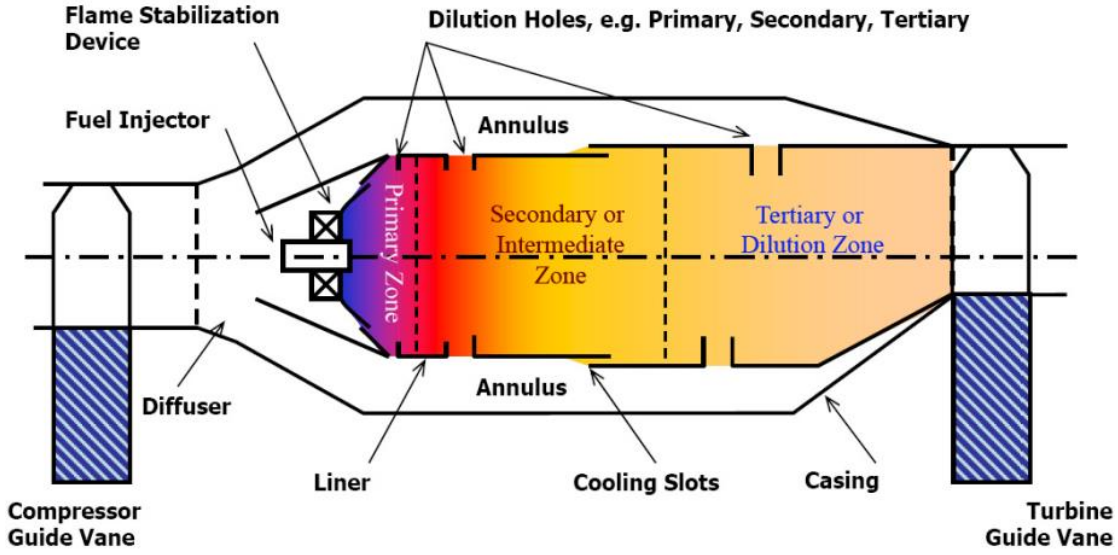

Figure 2-1 The components of a conventional combustor in gas turbine[28]

The AFR is usually given on a mass basis [27]. In diffusion burning systems there is a wide variation of local A/F around the mean A/F. The primary zone is usually designed to be close to stoichiometric values at maximum power. Inside this local zone will be rich and lean zone.

The rich zone will give difficulties with CO and soot emissions; the stoichiometric interface region will be where most NO_X formation occurs. The aim for well-mixed or quickly mixed combustion is to mix the fuel and air before the primary combustion occurs [82, 105], thus increasing combustion efficiency.

Actually, in practice, lean combustion, and hence low NOx is limited by the highest AFR (leanest) value at which stable combustion can happen. This value is known as the weak extinction value.

Various authors [82, 105, 106] have reviewed published data on weak extinction for well mixed and premixed low NOx gas turbine flame of stabiliser designs. They demonstrated

that all the best weak extinctions are similar to the lean flammability limit for laminar flames.

2.3 Gas turbine fuels

Renewable fuels are in demand to reduce carbon effects from fossil fuels. Industry and research groups are considering many alternative fuels. The most viable options are synthetic kerosene, Fatty Acid Methyl Ester (FAME), hydrogenated vegetable oils, liquid hydrogen, methane, and ethanol/methanol.

For the short term, synthetic liquid fuels of primary interest will be mostly derived from biomass, coal, heavy oil, and oil shale/tar sands. For the longer term, liquefied gaseous fuels (methane and hydrogen) are among the candidate fuels now being considered. All these fuels must be compatible with the engine and fuel system requirements.

Hydrocarbon fuels are organic compounds consisting entirely of carbon and hydrogen. The combination of these fuels supports flexibility for energy independence in various countries across the world. Hydrocarbons in petroleum fuel are usually classified into three main groups: paraffinic, naphthenic and aromatic.

1) Paraffinic oils are straight series with a general formula (CnH2n + 2) they can be found mostly in the United States, North Africa and Nigeria. The simplest hydrocarbons are methane and propane. They have a higher hydrogen/carbon ratio, high gravimetric calorific value, lower density and freeze point compared to other heavier of hydrocarbon fuels.

2) Naphthenes are saturated hydrocarbons with general formula $(CH_2)n$; the carbon atoms are linked to form rings instead of chains as in the case of paraffin. Their contributions to Jet fuel are about 25-35%, and they have the high gravimetric heat of combustion and low soot formation. Cyclopropane, (C_3H_6) and Cyclopentane (C_5H_{10}) are members of Naphthenes.

3) Aromatic hydrocarbons are unsaturated molecules, ring compounds containing one or more six-member rings with the equivalent of three double bonds. They contain less hydrogen and lower specific energy and have a similar structure to naphthenes.

The general formula of aromatics is (CnH_2n-6) and benzene, toluene and naphthalene are examples. The main advantage of aromatic compounds in the fuel is that they help to seal the high-pressure fuel system. However, aromatic compounds have a higher tendency to form soot and a substantial solvent action on rubber, which damages fuel systems. The chemical analysis determines the three primary sorts concentration of compounds.

Another alternative option is biofuels; they reduce CO_2 emissions for both industrial and aero gas turbines. Industry applications are more applied compared to aero derivatives because of low-temperature waxing problems at high altitude. Using of biofuels in industrial gas turbines must also attain low NO_x.

Table 2-1 Classification variety of gas turbine fuels [33].

Industry branch	Origin process	Fuel name	State (L/G)	Characteristics range	Ashless (AL), ash forming (AFo)
Oil	Oil extraction	Crude oil	L	Light to heavy	AFo
	Oil distillation	LPG: propane, butane	L/G	Variable C_3/C_4	AL
		Naphtha, kerosene, diesel fuels	L		AL
			L	Light to heavy	AL
		Heavy oils	L	Atm. and vac. resids	AFo
	Catalytic cracking	Light cycle oil	L	Highly aromatic	AL
Natural gas (NG)	NG extraction	Natural gas	G	Rich to weak	AL
				Soft to sour	AL
	NG extraction/ treatment	Gas condensates	L	Light to heavy	AL to AFo
	NG reforming	NGL			AL
Coal and lignite	Coal extraction	Coalbed gas	G	Low-BTU gas	AL
	Coal liquefaction	Synfuels	L	Highly aromatic	AL
		Methanol	L	Medium BTU liquid	AL
	Coal gasification	Syngas (CO/H_2)	G		AL (purified)
		SNG	G	Medium to low BTU	AL
Steel	Coal pyrolysis	Coke oven gas	G	Medium BTU	AFo
	Iron production	Blast furnace gas (BFG)	G	Low BTU	AFo
Petrochemical industry	Naphtha cracking	Olefins	G	Variable olefin %	AL
	Aromatics synthesis	H_2-rich gas	G	Variable H_2 %	AL
	Butadiene unit, etc.	Propane/butane-rich gas	G	Variable C_3/C_4 ratio	AL
Residuals	Fermentation	Biogas: CH_4–N_2–CO_2 syngas	G	Medium to low BTU	AL (purified)
	Gasification		G	Medium to low BTU	AL (purified)
Renewables	Vegetable processing	Biofuels from farming	L	DF number 2 substitute	AL

On the other hand, as table 2.1 highlights, there are many other alternative fuels appropriate for gas turbine use. Before alternative fuels are considered, it must be noted that the properties of the fuels have a significant influence on their suitability.

For alternative fuels to act as a suitable replacement, the following criteria must be met [34].

1. Needed resistance to spontaneous auto-ignition within the premixer.
2. The appropriate level of resistance to a flashback where this is one of common combustion instabilities.

3. Comply with emissions production (CO_2, UHC, NO_x).
4. Combustion dynamics are acceptable.
5. Appropriate lean blow-off limits where blow-off occurs when the heat required by the combustible stream exceeds the one received from the recirculation zone.

2.3.1 Gaseous fuels

By far the most common gaseous fuel for industrial gas turbines is natural gas. However, the diminishing supply of natural gas has led to increased interest in other gaseous fuels, including by-products from industrial processes, low-energy gas from coke or oil, and coke-oven gas. All gaseous fuels are advantageous regarding high thermal stability and clean (soot- and ash-free) combustion. Table 2.2 lists the typical properties of common gaseous fuels [35].

One alternative gaseous fuel is syngas, short for synthetic gas. It is produced by gasifying coal, or other carbon-based sources, and providing carbon capture technologies are applied it can represent a real possibility source of a low carbon fuel. Jones et al. [35] stated that the fuel could be directly cleaned of carbon and the outcome is a hydrogen-rich fuel that can be used in a gas turbine systems.

Table 2-2 Properties of common gaseous fuels [10]

Property	Natural Gas	Coal Gas (Low Btu)	Coal Gas (High Btu)	Coke-Oven Gas	Blast-Furnace Gas	Producer Gas
Energy density (Btu/ft³)	950–1150	110–165	500–700	525–650	90–100	120–140
Energy density (MJ/m³)	35–43	4.1–6.1	19–26	20–24	3.4–3.7	4.5–5.2
Relative density (air = 1.0)	0.58–0.72	0.80–0.92	0.41–0.48	0.40–0.45	0.95–1.05	0.86
Composition (vol%)						
Methane	75–97	0.5–4.5	20–35	28–32		1.2
CH–other hydrocarbons	2–20		2–4	2–4		
Hydrogen		12–16	40–55	50–55	1–4	16.5
Carbon monoxide		2–32	5–15	5–7	25–30	24
Nitrogen	1–16	30–55	4–11	1–6	55–60	50.8
Carbon dioxide	0.1	0.5–10	2–4	2–3	8–16	7.5

On the other hand, syngas is not identical to natural gas. The flame speed of hydrogen, and therefore hydrogen-rich syngas, is higher, and it has a lower (per mole) calorific value. From an oxygen gasifier, this value is typically one-third of natural gas [36]. As a result, the air/fuel ratio, AFR, will need to increase to accommodate the lower calorific value and the speed at which the fuel is supplied may need to be raised to avoid flashback.

Furthermore, Wright and Gibbons [36] explained that mass flow rates, MFRs, would have to change throughout sections of the turbine when compared to one that is designed to run on natural gas.

The compressor, for example, would produce a lower output whereas the MFR within the combustor and turbine would both need to increase.

The higher fuel volumes could require an increase in piping and valve sizes which can result in higher cost [37]. One last concern when using syngas is the existence of impurities in the fuel and the possible adverse effects on the materials used within the turbine [26]. Despite the technological challenges, some turbines use syngas today.

Carbon Dioxide /Methane blends have also been attempted [32, 33]. The major aim of introducing CO_2 into the gas turbine combustor is to decrease the emissions of NO_x while increasing CO_2 concentration for carbon capture and storage. CO_2 cools the flame. Thus the Zeldovich mechanism of NO_x production can be reduced [40]. The thermal mechanism (Zeldovich), where the contaminant is formed under high-temperature conditions by reaction between nitrogen and oxygen, especially at temperatures greater than 1600^{o}C. The appearance of hot spots in the combustion chamber contributes to the formation of these contaminants, and engineers aim to minimise their formation.

Previous experimental and numerical studies researched the influence of diluting syngas fuels with various additives, including carbon dioxide, nitrogen, and steam [35, 36]. The studies concentrate on essential characteristics of the combustion process. The work by Lee et al. [41] essentially examined the influence of diluting the premix fuel had on the emission of NO_x and CO from a model gas turbine. Lee et al. [41] showed that lessening in ppm NO_x per unit power is logarithmically correlated to the heat capacity of the total additional diluent.

H. Kurji et al. carried out an experimental study on the combustion of methane-carbon dioxide mixtures at atmospheric conditions by using different levels of premixing with various injection strategies. Results were shown that the introduction of limited amounts of CO_2 (15%) had controlled reaction rates and temperatures in the combustion zone, thus producing a reduction in emissions with a decrease in flame stability at low equivalence ratios [43].

Furthermore, using of CO_2 from carbon capture and storage facilities could reduce also costs capture equipment further downstream the combustion zone [41]. Through, the CO_2 injected the premixed blend will reduce the reaction rate, thus reducing the temperature.

Since carbon dioxide has a bigger heat capacity than nitrogen or steam, a smaller mass flow rate is required for a comparable reduction in NO_x. Furthermore, the use of CO_2 from carbon hold and storage facilities could decrease costs as well as catch equipment further downstream the combustion zone.The high temperature of the CO_2 in the CRZ will guarantee a quick chemical reaction of the diluted reactants, thus giving low NO_x and CO. As well as synthesis gas, known as syngas, produced from gasification processes, is considered as one of the hopeful substitutional energies due to its clean fuel characteristics. Synthesis can be produced via gasification of several feedstocks, including coal, biomass and solid waste.

Swirl flows are related to the high momentum flow region (HMFR). The central recirculation zone (CRZ) is moved from the central axis and generates the high momentum flow region placed on the shear layer. The high momentum flow region that accompanies swirling flows has attracted the attention of several groups interested in blowoff and stretching phenomena [44]. The swirl will join into high momentum flow region (HMFR), which is highly correlated with the CRZ. That will increase the strength of the CRZ but reduce its dimensions. The addition of CO2 affects the velocity of the flow, the mixing and the combustion characteristics, thus generating slower profiles than with pure methane. At the same time, it seems that the dimensions of the CRZ with CO2 are increased [44].

Using syngas as a fuel source can reduce CO_2, NO_x and other pollutants [42]. One model of using syngas is in Integrated Gasification Combined Cycle (IGCC) power plants wherever syngas fuel is combusted in gas turbines to generate power and electricity [38, 39]. Regardless of the confirmed feasibility of syngas, the difficulty that syngases confront is the variation in their composition due to various feedstock and production procedures. Moreover, the shortage of understanding of the combustion characteristics of syngases poses difficulty in the design of syngas-specific systems and combustors [47], thus making flexible plans a challenge that requires further research.

Regarding hydrogen, the higher combustibility of this gas has received bigger attention as an additive to fuels for extending the lean combustion limits of gaseous fuels as it resulted in favourable flame temperatures and decreased NO_x emissions.

Mixtures with the higher air-fuel ratio (AFR) than stoichiometric air-fuel ratios (AFRst) are termed lean as they have excess air, whereas mixtures with lower AFR values are termed rich as they have excess fuel. Lean premixed combustion has become the most promising technology for emission reduction in gas turbine combustion systems [48]. Increase lean premixed combustion limit is possible by mixing hydrogen with gaseous hydrocarbon fuels for combustion in traditional gas turbines and can produce power with low emissions of nitrogen oxides (NOx) [48].

2.3.2 Liquid fuels

While natural gas is now the fuel of traditional use for land-based gas turbines, liquid fuels are used in areas where natural gas has a restricted supply or is not available as can be seen in figure 2.2 [37]. They can be utilised as a backup fuel driven by a global effort to reduce emissions and our dependency on fossil fuels. One of the replacements that are probable to increase in popularity is biodiesel.

The fuel can be created from the following branches: coco, palm, rape-seed, sunflower, peanut, soya, cotton, sugar cane, jatropha, algae or animal fat by-products [33]. Moliere [33] states that the fuel has a 10% lower heating value than that of diesel oil.

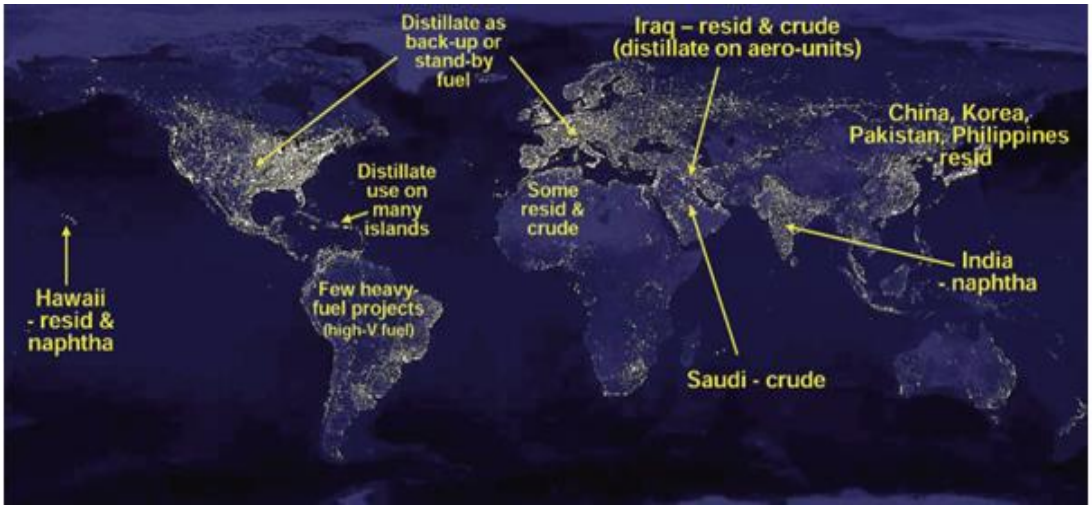

Figure 2-2 Examples of liquid fuel usage with gas turbines on a global scale [37]**.**

Therefore, biodiesel, like syngas, would require a higher volumetric flow rate to accomplish the same power output. The benefits of using biodiesel over diesel include better lubricity [49], and carbon dioxide net emissions are reduced by ~60%, inclusive of the crop growing and related absorption. The flash point of biodiesel is also higher (>100°C), this is especially beneficial to increase the flash point of conventional diesel. For example, in India, the average diesel flash point is 44°C, 11°C lower than the world average [49]. That increases the safety of the system as there is a reduced risk of accidental ignition. Despite the positives, there are some disadvantages in using the fuel. The fuel can harmfully affect the elastomers found in gaskets and seals within the gas turbine, so selecting compatible components is a must [50].

Table 2-3 The kinematic viscosity at various temperatures for diesel, pure biodiesel (BD100) and vegetable oils. [51]

Temp. (°C)	Kinematic viscosity ($mm^2 s^{-1}$)							
	Diesel	BD100	Rapeseed	Sunflower	Soybean	Palm	Corn	Grapeseed
10	5.39	9.00	119.48	118.72	107.62	–	113.39	100.63
20	4.15	6.78	74.19	73.45	67.12	–	70.29	64.32
30	3.30	5.30	48.88	48.46	44.69	–	46.54	42.94
40	2.70	4.26	34.06	33.78	31.42	45.34	32.53	30.19
50	2.26	3.51	24.68	24.48	23.00	28.19	23.74	22.29
60	1.92	2.94	18.62	18.52	17.47	20.84	17.96	17.04
70	1.64	2.51	14.48	14.44	13.67	15.60	14.01	13.34
80	1.43	2.16	11.58	11.53	11.17	12.35	11.39	10.88
90	1.27	1.90	9.45	9.44	9.13	9.94	9.34	8.96
100	1.14	1.69	7.89	7.78	7.71	8.21	7.83	7.53
110	1.03	1.51	6.70	6.50	6.58	6.88	6.65	6.42
120	0.93	1.36	5.86	5.62	5.68	5.85	5.70	5.49
130	0.85	1.23	5.09	4.91	4.99	5.02	4.93	4.77
140	0.78	1.13	4.47	4.37	4.45	4.38	4.34	4.21

Gupta et al.[50] explained that alternative fuels (jatropha-based) have a higher viscosity in vegetable oil form and a lower calorific value. The higher viscosity then increases the trouble of atomization, clogs fuel nozzles and affects combustion. The variation of kinematic viscosity for diesel, biodiesel and various vegetable oils can be seen in table 2.3. It is clear that viscosity can be reduced by heating the fuel. Transesterification is another procedure that can be used to achieve the same result [52].

Biodiesel is considered a more environmentally benign fuel that can be used in gas turbines without significant modification and has advantages over diesel regarding sulphur content flash point, aromatic carbon content and biodegradability [53]. In gas turbines, biodiesel has demonstrated a reduction of un-burnt hydrocarbons (UHC), carbon monoxide (CO) and particulate matter (PM) without reducing the power output significantly [54]. Experiments have shown a reduction of 12% in both CO and PM emissions and 20% of UHC emissions by co-firing 20% biodiesel in diesel fuel blends.

Emissions reduction was about 48% for CO and PM and 68% for UHC when using 100% biodiesel. However, there was a minor increase in NOx (1–6%) [50]. The presence of extra (fuel-bound) oxygen produced overall leaner combustion, which has the benefit of increasing the thermal efficiency [55]. Uncontrolled emissions such as Polycyclic Aromatic Hydrocarbons (PAH) were also found to be less prevalent during biodiesel combustion.

CO_2 emissions aside, biodiesel can be considered a cleaner fuel than fossil-derived diesel because it has almost no sulphur content (typically less than 15 ppm), no aromatics and contains about 10% oxygen, which can improve the overall combustion process. Biodiesel also has a comparatively high lubricity and can hence be used as a lubricating agent for traditional diesel blends [56].

Panchasara et al. studied the combustion performance of biodiesel and diesel – vegetable oil blends in a simulated gas turbine combustor [57]. These experiments were performed at atmospheric pressure with air-assisted injector/atomisers and swirling flows. The results showed that fuel chemistry effects were minimal since combustion emissions for a given fuel were largely dependent on the atomization process.

Campbell et al. studied alternative fuels available for gas turbines and, amongst others, focused on vegetable oils [58]. They highlighted several features of vegetable oils that would require special consideration such as transportation, storage, delivery and injection into industrial gas turbines.

Hashimoto et al. [8] compared the emissions of palm-derived biodiesel with those of fossil-derived diesel in a gas turbine burner. The result indicated that NO_X emissions for palm biodiesel were consistently lower compared to those of diesel when plotted as a function of excess air ratio, average droplet diameter, atomising air pressure and viscosity. These results indicate that biodiesel has the potential to produce lower NO_X emissions than diesel under gas turbine conditions, opposing to the higher NOx emissions measured in reciprocating compression-ignition engine experiments [59].

Biodiesel and diesel have differences in physical properties, and it is, therefore, necessary to study the spray characteristics of biodiesel about its application in internal combustion engines and gas turbines.

Senatore et al. [60] analysed results of an experimental study fuelling a common-rail diesel engine with 100% rapeseed biofuel, comparing his findings with a blend of rapeseed and Used Fried Oil (UFO), showing good correlation between fuels. Zhao et al. [61] observed that the spray penetration and spray cone angle of biodiesel were larger than those of diesel.

Likewise, Lee et al. [62] studied the atomization characteristics of biodiesel-blended fuels using a spray visualisation system and phase Doppler particle analyser. They deduced that the blended biodiesel fuels had comparable spray tip penetrations to traditional diesel, but higher Sauter Mean Diameter (SMD) because the viscosity and surface tension of the biodiesel was upper than the regular diesel fuel. Being a crucial topic for the improvement in burnout and a key factor in emissions, advanced laser-based spray quantification techniques have been used and developed to understand atomization patterns for diesel and biodiesel [57, 58].

The biodiesel was used in chapter four is a by-product of a biomass gasification process; specifically a liquid condensate from the product gas cleaning process. That a crucial stage in the thermal conversion of biomass, particularly when the main product gas components CO and H_2, are used for Fischere-Tropsch synthesis, or as high purity fuel [65]. Biodiesel is widely used for scrubbing the raw syngas as it effectively removes the condensable (heavier) hydrocarbons produced from biomass pyrolysis. Experimental investigations have been carried out on similar post-scrubbing liquids where combustion of blends of pyrolytic oil, biodiesel or ethanol in engines and boilers [60, 61] have proved the suitability of the approach. That has included large-scale applications and highlighted a need to standardise the trade of this product [68].

Cappelletti et al. redesigned a micro gas turbine to permit stable combustion of pyrolysis oil showing that the combustion is only stable in the combustor's secondary zone [69]. H. Kurji et al. investigated a comparison among three fuels, kerosene and a biofuel in unsaturated and saturated form, were tested to compare the relative performance of the saturated biodiesel for gas turbine applications.

It was observed that use of the saturated blend would result in higher NOx concentrations in the exhaust with less oxygen and CO emissions. It has been shown that the ideal operability region for the saturated biodiesel is at very lean conditions [70].

Hashimoto et al. [71] investigated the potential of jatropha biodiesel using a swirl liquid flame gas turbine burner. It was reported that larger jatropha biodiesel droplet was generated compared to baseline diesel fuel. Emission wise, jatropha spray flame produces higher CO at a low flame temperature (<1300^{o}C) due to low fuel evaporative, but similar NOx emission level as diesel was detected.

The radiation intensity and soot emission were reported to be lower with the increase in a blend ratio of jatropha pure oil/jatropha biodiesel with diesel. In a separate test conducted by the same group [8], the spray combustion characteristics of palm biodiesel were compared against baseline diesel fuel.

Apart from the reported lower NOx emission, the tendency to form soot and the luminous flame was found to be lower for palm biodiesel. Chong and Hochgreb [72] compared the spray combustion properties of palm biodiesel with baseline fuels of Jet-A1 and diesel using a model gas turbine burner. The result shows that NOx emission was reduced in the case of palm biodiesel, while CO emission was not affected. The burner flow field has been extensively characterised under reacting and non-reacting conditions [73].

Sequera et al. [74] utilised an airblast-injector type axial swirl combustor to compare the emissions of soy methyl ester, soy methyl ester and bio-oil pyrolysed from hardwood against diesel fuel. The result shows lower emissions of NOx and CO for biodiesel-blended fuels under constant mass flow rate test condition. Bolszo and McDonell [75] reported higher NOx emission when using soy-based biodiesel in a 30 kW MGT (Capstone C30) test conducted under non-reacting and reacting conditions.

Under cold spray condition, soy-based biodiesel was observed to generate larger droplet size compared to diesel. That subsequently led to higher NOx emission for biodiesel under reacting condition due to longer evaporation time scale [76]. It was further demonstrated that increasing atomization air-to-liquid mass ratio resulted in improved spray atomization quality for biodiesel, which is effective in lowering post-combustion NOx emission [75].

Biodiesel for a gas turbine to improve the fuel flexibility was studied to meet emissions goal and reducing operating cost. The characteristics of spray combustion of rapeseed biodiesel/methyl esters (RME) and 50% RME/diesel blend were examined and compared

with conventional diesel fuel, using a model swirl flame burner [77]. The reacting droplet distribution within the flame was determined using phase Doppler particle anemometry. Blend 50% RME with diesel outcomes a significant reduction in soot radiation. RME emits 22% on average lower NOx emissions compared to diesel under lean burning conditions.

2.4 Multiphase combustion

Studying multiphase combustion is vital because at this time a very high percentage (80%) of energy is produced by combustion of liquids such as gasoline, solids such as coal, and gases such as natural gas.

For instance, during the first decades of the twenty-first century, more than 50% of the electricity in the United States was made by coal-fired furnaces [78]. This tendency is expected to continue for several decades. Therefore, energy generation will remain heavily dependent on combustion technology.

Most practical devices include turbulent combustion, which needs an understanding of both turbulence and combustion, in addition to their influences on each other. Industrial furnaces, liquid rocket engines, diesel engines and devices using solid propellants contain multiphase and turbulent combustion.

Single-phase turbulent reacting flows are complex enough for modelling and numerical solutions, some of these flows are still unsolved problems of our time. The difficulty of the problem rises even further with the existence of multiple phases.

On the other hand, to decrease pollutants means reducing maximum flame temperature and lessen the size of fuel-rich zones where the concentration of fuel rich and high-temperature gradients can arise. To complete these aims an in-depth knowledge of multiphase flow processes, spray dynamics, and the interface between the liquid and gas phase is essential. Therefore, various modelling approaches have been developed that include attention of many multiphase gas-liquid flows and spray phenomena, for example, primary and secondary atomization, droplet propagation and evaporation, droplet collisions, etc. Reviews by [73, 74]. The resultant multi-phase flows are very complex processes, including turbulence, mass and heat transfer, droplet dynamics and phase changes that are strongly connected.

Thus, a full understanding of spray behaviour is very challenging yet critical regarding the upgrading of the efficiency of modern combustion devices to meet future restrictions on pollutant emissions.

There is an ever-increasing need to understand multiphase combustion because of their extensive application in energy, transportation, environment, propulsion, industrial safety, and nanotechnology. More engineers and researchers with skills in these areas are required to solve many multifaceted problems. Multiphase reacting flows have been main research issues for many decades, and studies in these regions are expected to continue at even greater speed.

Theoretical methods have accomplished some degree of success. However, in the past 20 years, improvements in computational ability have enabled major progress to be made toward comprehensive theoretical modelling and numerical simulation.

Experimental diagnostics, especially nonintrusive laser-based measurement techniques, have been developed and used to get accurate data, which have been used for model validation.

One of the challenging subjects is to deal with combustion in two-phase flows. Such as gas turbines, for instance, the fuel is introduced in a liquid form. The liquid fuel is atomised, and the scattering phase interacts with the air flow which is usually swirled to obtain compact flames.

This two-phase turbulent reactive flow is characterised near the flame region by a polydispersity evaporating spray interacting with an unsteady flow and a flame. Therefore, one simply infers the key role of evaporating sprays and spray interactions with vortices in the understanding of the dynamics of combustion systems.

Burners were fed by liquid fuels are also inclined to instabilities which often feature large synchronised coherent flow structures carrying the scatter fuel phase periodically to the flame [75, 76].

The modelling of two-phase combustion should take into account complex physical phenomena like the evaporation of sprays, droplet interactions, and the spray interaction with the flow and flame.

Here again, measurements come as a key input in the understanding of fundamental physical mechanisms, and as a benchmark for links with simulations in well-controlled patterns.

Lemaire et al.[82] examined the interaction of a vortex with flat diffusion flame in a two-phase flow imaging the flame front with Laser Induced Fluorescence (LIF) on CH radicals. In the experimental field, attempts have been made in the last decades to reach quick and dependable measurements on the vapour and liquid phases of droplets simultaneously in sprays. Many laser-based techniques have been developed for the discrete characterisation of either vapour phase or the liquid phase of evaporating droplets.

Different modelling method currently exists for multiphase flows such as Eulerian-Lagrangian, Eulerian Multiphase, Volume of Fluid (VOF), etc. The most commonly used are the Eulerian-Lagrangian method, also known as the Discrete Droplet Model (DDM). This method is particularly appropriate for modelling dilute sprays but has some disadvantages in the near-nozzle area on the lack of the physics in a dense spray, where particle contact is strongly affected by the collision [83].

Several researchers have used the Lagrangian-Eulerian approach, and various improvements to the basic scheme have been suggested [77, 78]. This method has been controlled in guessing the behaviour of spray.

Although many researchers and engineers have used the Lagrangian-Eulerian formulation as a numerical simulation tool for an estimate of characteristics of complex multiphase flows to guide their engineering devices design, the concept and application have severe limits.

The near-nozzle region, this formulation is very sensitive to the grid resolution [85] and is restricted to the adequate representation of dense spray. Oppositely, the main benefit of the Lagrangian-Eulerian formulation is finding a detailed physical explanation of single parcels of the dispersed phase in the gaseous flow field.

Harlow [86] developed a numerical technique for the multiphase flow dynamics in which several areas interface and interact with each other.

An efficient use of liquid fuel and produced pollutant emissions depend on the fuel-air mixture process, which is strongly affected by the spray dynamics.

One of the main issues this doctoral thesis has been focused on that multi-phase studies were performed using a swirl burner. Flame stability, temperature profile, CH* production and emissions measurements were conducted.

However, the complexity of multiphase combustion still requires rest researchers on atomization and combustion fundamentals, some the aims of this study.

2.5 Atomisation

The atomization procedure within modern gas turbines is imperative as the resulting smaller droplets of fuel let it burn easier and more reliably within the combustor. As the droplets are formed, the surface area to volume ratio of the fuel is expanded.

A perfect atomiser would supply consistent spray quality (SMD for example) during the operating range of the gas turbine. However, the variable amounts of fuel required at different power outputs and the variable pressure at which it is supplied mean this is not frequently completed [10]. The atomization process can, for the most part, be divided into fragments; primary and secondary atomization [10].

Essential atomisation considers the initial stage where the liquid first leaves the exit orifice and breaks into ligaments and shreds. Secondary atomization is the procedure of these ligaments and shreds disintegrating further into spherical droplets. The atomization process is "a disruption of the consolidating impact of surface tension by the activity of internal and external forces'' [10].

As these forces go over the uniting force of the surface tension and initially break up the fuel, the surface tension then pulls the liquid back into a form of minimum surface energy into the shape of a sphere. As expressed by [10], there are also many variables which affect the atomization quality including the atomiser's dimensions, the properties of the fuel used and the gas into which the fuel is released.

2.5.1 Breakup of liquid droplets in air

Liquid breakup in the air is the simplest manner of atomization, the theory of which has been widely examined and assessed. Aerodynamic forces (induced by increased liquid droplet velocity or atmospheric air velocity), surface tension and the inertia of the liquid all add to the breakup procedure, and four primary systems of a breakup have been acknowledged [87]. These are shown in figure 2.3.

- The first is the Rayleigh drop breakup. For this situation, droplet diameters are greater than the jet diameter with breakup occurring downstream of the nozzle.
- The second is the first wind-induced regime. Droplets in this regime are a similar size to that of the jet diameter. Finally, the breakup happens downstream of the nozzle.
- The third is the second-wind induced regime. The average droplet diameters are smaller than that of the jet diameter, and the breakup launches to occur closer to the nozzle orifice.
- The last regime is known as atomization. The drop sizes are considerably smaller than that of the jet diameter, and breakup launches as the liquid exits the orifice of the nozzle –this is the regime that is required for modern combustion systems.

As Lin and Reitz [81] state, for both the Rayleigh and the first wind-induced regime, "the growth of long-wavelength, small-amplitude disturbances" is thought to initiate the breakup of the liquid. These disturbances are the outcome of the interaction between the flow itself and the ambient gas in which the flow is present.

Higher speed liquid jets, as seen in figure 2.3 (C) and (D), are believed to result from waves with shorter wavelengths. As the relative velocity of the liquid grows about the ambient air, the surface tension faces the formation of unstable waves and so the liquid breaks into droplets [27]. For gas turbine combustion systems, the atomization regime is required because this is where the smallest droplets are made and later the largest surface area to volume ratio can be accomplished.

Figure 2.4 details the same four regimes of flow. These restrictions were the result of jet breakup length experimentation by Ohnesorge [88]. Baumgarten [88] also states that

Ohnesorge showed that the breakup process could be defined by the Weber number (equation 2.1) of the liquid and the Reynolds number (equation 2.2).

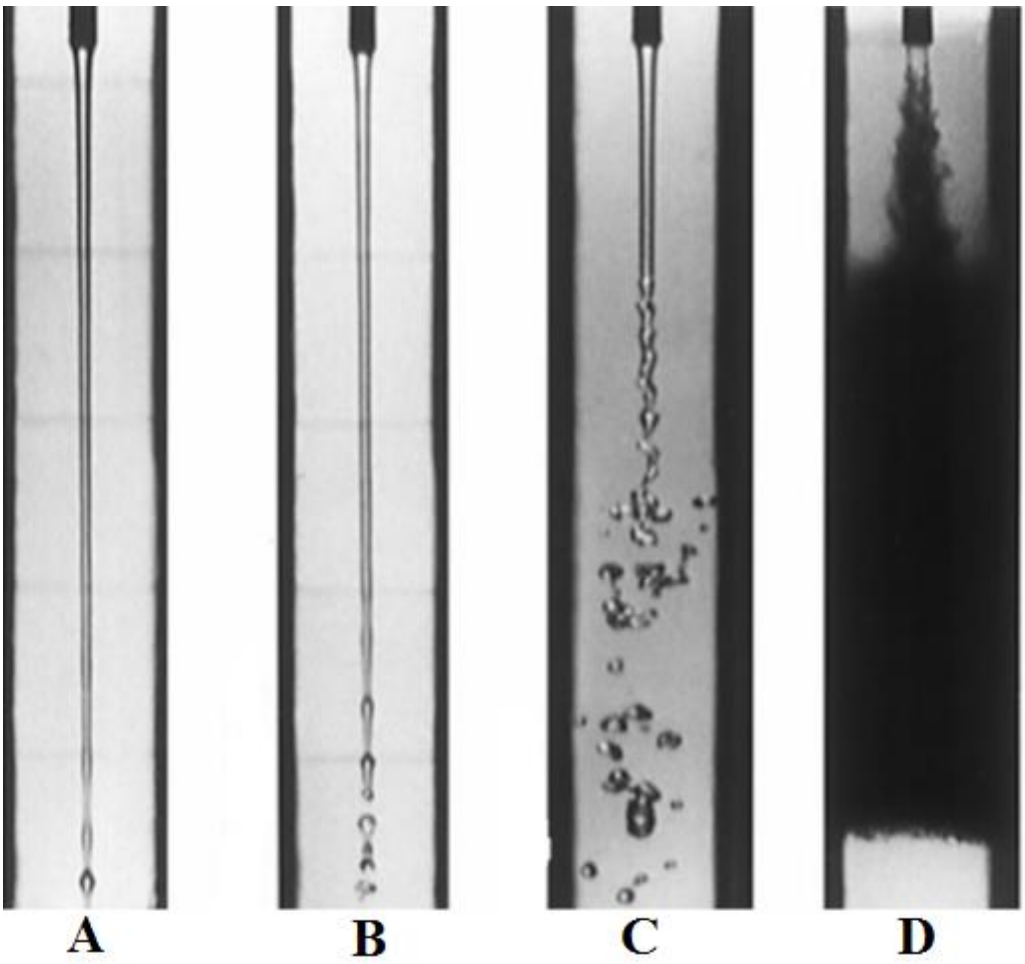

Figure 2-3 The four regimes of a breakup [89]

$$We = \frac{u^2 D \rho}{\sigma} \qquad (2.1)$$

$$Re = \frac{u D \rho}{\mu} \qquad (2.2)$$

Where

u : Relative velocity [m/s]

D : Droplet diameter [m]

ρ : Density of liquid [Kg/m^3]

σ : Surface tension [N/m]

μ : Viscosity [Pa.s]

By then eliminating the velocity of the jet u, Ohnesorge derived the Ohnesorge number, Z, equation 2.3. The number is dimensionless and as Baumgarten [88]

states, contains all the connected properties of the fluid as well as the orifice diameter from which the liquid exits.

$$Z=\frac{\sqrt{We}}{Re}=\frac{\mu}{\sqrt{\sigma\rho D}} \qquad (2.3)$$

Figure 2.4 shows the fact that atomization needs a high Reynolds number and that a large Ohnesorge number is also desirable. Equation 2.3, the Ohnesorge number, dictates that low surface tensions, liquid densities and orifice diameters are all beneficial factors while trying to achieve atomization [88].

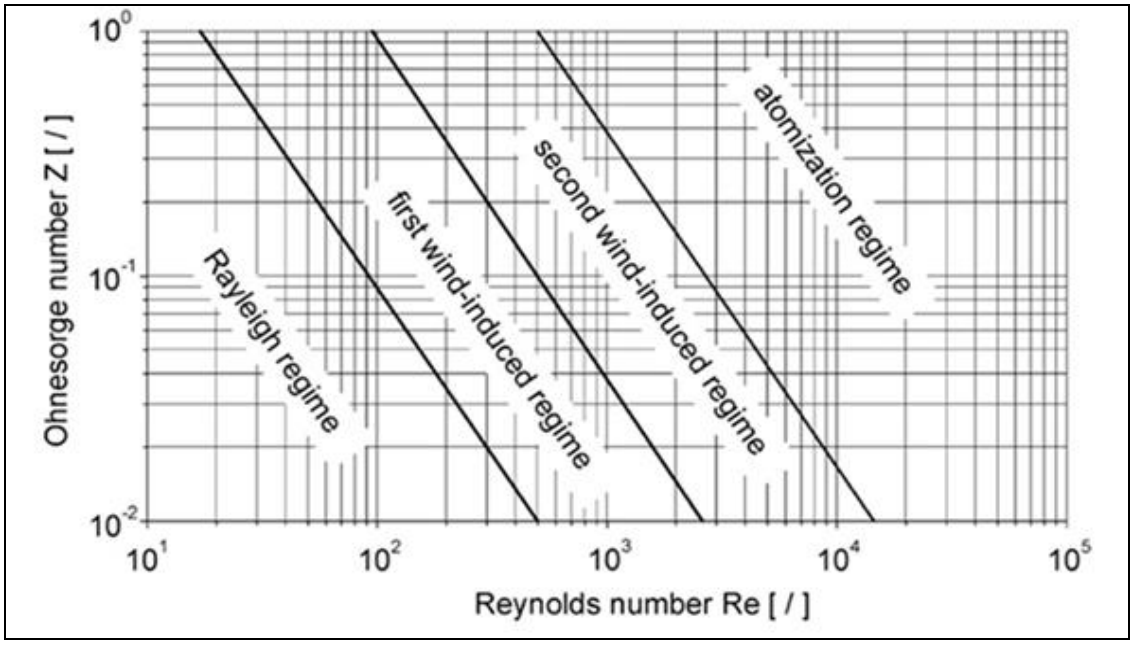

Figure 2-4 Modes of disintegration [88]

2.5.2 Classification of atomisers

The atomiser is an instrument that is used for liquid atomization. Varied sorts of shapes of atomisers are used in practice, and their design can be divided into three main sets listed below. None of them is perfect, and each atomiser has its advantages and disadvantages above others.

A. Pressure atomizers

Pressure atomisers are established on the conversion of pressure into kinetic energy to accomplish a high relative velocity between fuel and surrounding air. These sorts of atomisers are the most widely used. Their main advantages are simple construction and no requirement for additional energy or medium [90].

B. Twin-fluid atomizers

General twin fluid atomisers use the kinetic energy of pressurised air or stream to fragment liquid into drops. Two different groups are recognised air-assisted and airblast atomisers. Typical advantages of these types are good atomization with low liquid pressure and the capacity to atomise more viscous liquids [18].

C. Other atomizers

In the industry, a lot of other atomisers may be an encounter like effervescent, rotary, electrostatic, acoustics, ultrasonic, etc. [91].

2.5.3 Traditional atomization issues

There are numerous applications for which improvements in atomization, or atomiser operational parameters, would be helpful. Several areas, confront the issue, of atomising.

High viscosity liquids, including paint applications [92], pharmaceutical granulation, coating, spray drying [93], waste incineration [94], as well as combustion of biofuels[95], low-grade fuel oils [96], used oil [97], and coal slurries [98].

Many of these liquids have solid particles suspended within them, either by design or as contaminants, which present the challenges of clogging and nozzle corrosion [98]. To achieve proper atomization, many nozzles incorporate a small exit orifice diameter, which decreases the liquid jet diameter.

However, increasing the liquid velocity may increase shear between the jet and ambient air. While the exit diameter is reduced, clogging becomes more prevalent [98].

Moreover, reducing the exit diameter results in an increased liquid velocity then promoting erosion, particularly when solid particles are in the liquid. These problems lead to increased repairs costs or change rates for the atomisers [98].

Perhaps the greatest stringent factor for enhancing atomization processes originates from increasingly strong regulations on pollutant emissions from combustion. The formation of emissions is submissive to a massive grade on droplet size [99], air-fuel mixing [100]

and fuel distribution [101]. The power, wear, carbon deposits and efficiency of an engine are influenced by these reasons also.

Despite most combustion processes helping from smaller drop sizes, there are applications which care with the range of droplet sizes for instance paint spraying [92] and crop spraying [102].

For the spray applications, droplets below a particular size do not reach their intended surface and are lost to the environment with potentially harmful influences, whereas if black liquor droplets are too small, they are transferred away by flue gases into boiler tubes where their sedimentation can cause clogging difficulties.

2.5.4 Effervescent atomisation

The twin-fluid atomisers defined above, in which air is used either to increase atomization or as the main driving force for atomization, commonly has one vital feature. In the beginning, the bulk liquid is atomised and transformed into a jet or sheet before being exposed to high-velocity air.

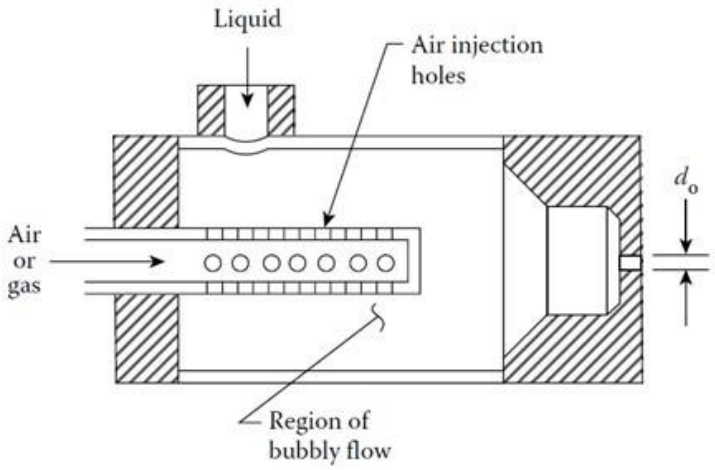

Figure 2-5 Plain-orifice effervescent atomiser

An alternative method is to introduce the air directly into the bulk liquid at some point upstream of the nozzle discharge orifice. This air is injected at low velocity and shapes bubbles that produce a two-phase effervescent flow at the discharge orifice. When the air bubbles appear from the nozzle, they expand so quickly that the surrounding liquid is shattered into droplets [18].

Most of the research achieved on effervescent atomization [18, 98] has used atomisers of the plain-orifice type shown in figure 2.5. A disadvantage to this simple concept is that the spray cone angle is quite small, naturally around 20° [104].

Most gas turbine combustors need injectors that distribute the fuel in the form of a conical spray of approximately 90° involved angles. Whitlow et al. [105] have studied some different types of effervescent atomisers designed to produce wide-angle sprays.

The single design was the same as the atomiser shown in figure 2.5., except that the single-hole orifice was changed with four equally spaced holes drilled at an angle of 40° from the axis of the mixing tube.

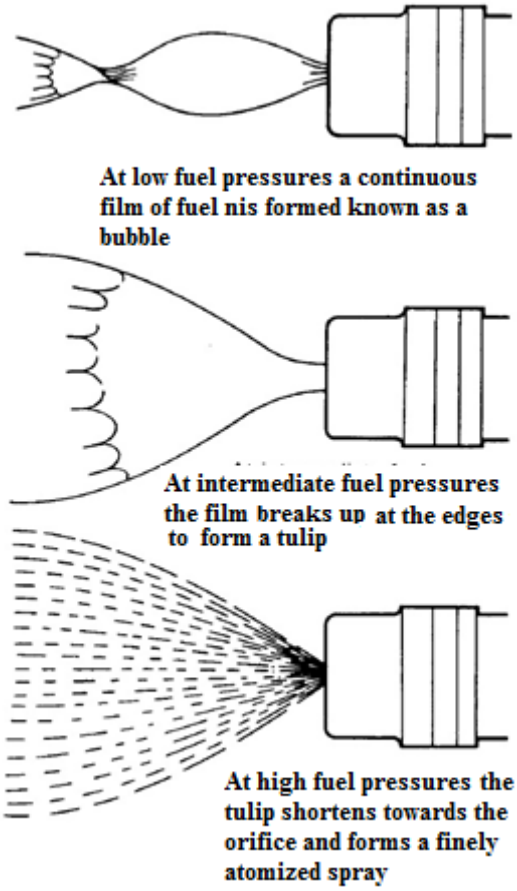

Figure 2-6 Stages of fuel atomization with varying pressures in a traditional pressure atomiser [26]**.**

The essential quantity with effervescent atomization of atomising gas is far less than that of traditional air assisted atomisers, and so the likelihood of using fuel gases instead of air is possible. The technique produces a two-phase flow within the atomiser. As the two-phase flow leaves the exit orifice, if the primary pressure drop exists, the threads and

ligaments of the liquid are shattered into droplets as the gas phase of the flow expands downstream [101] as can be seen in figure 2.6.

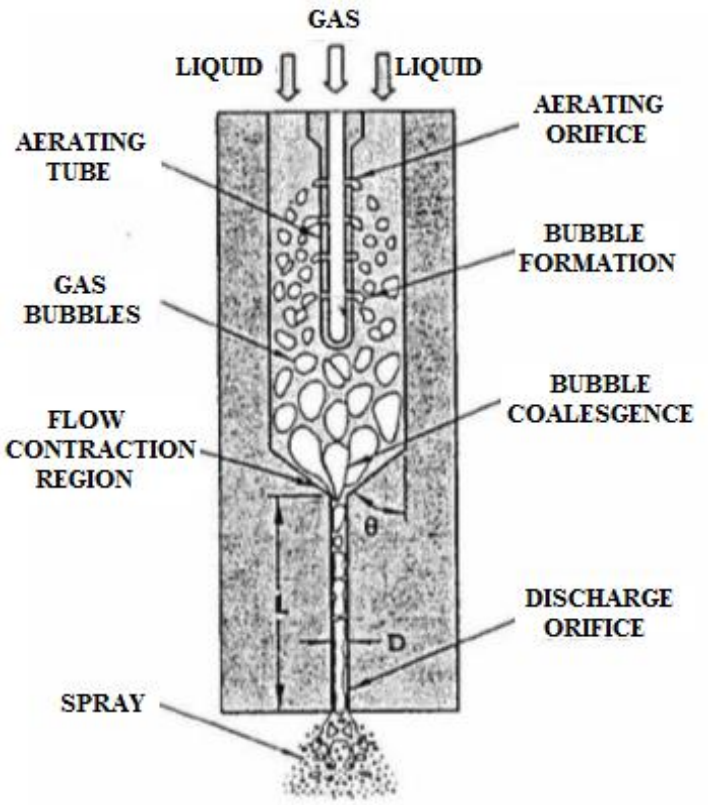

Figure 2-7 Operation of an effervescent atomiser [106]**.**

The injector employs inside-out gas injection for the gas insertion as shown in figure 2.7. Primarily, effervescent injectors could be defined into two configurations based on the gas injection method: inside-out and outside-in configurations.

Inside-out is superior when using low liquid flow rates, while outside-in is better with high liquid flow rates [103].

2.6 Pollutant formation

2.6.1 Oxides of nitrogen (NOx)

The term NOx is expressing the formation of NO and NO_2. Nitric oxide (NO) formed in the combustion process, with factors appropriate to NOx formation being those of high temperature, long residence time and high pressure.

On the other hand, NO_2 shaped by oxidation of NO by HO_2 in the reaction zone under very lean conditions at low temperature where a high amount of excess air also exists.

The degree of oxidation is too slow to provide major transformation in short residence times, and the concentrations of nitrogen dioxide are commonly less than that of NO. Four different mechanisms can form nitric oxides: thermal, nitrous oxide, prompt, and fuel nitrogen [82, 107].

2.6.2 Carbon monoxide (CO)

This kind of pollution is a hazardous gas that forms carboxyhemoglobin with blood, which lessens the oxygen-carrying capacity of the blood and puts an extra effort on the heart. Death happens after 30 minutes for concentrations over 3000ppm of Carbon monoxide. Otherwise, in low levels, it still acts in the oxygen-carrying capacity of the blood.

On the other hand, CO is a reactive gas, which takes part in ozone construction chemistry in the atmosphere. Carbon monoxide emissions emit from traditional gas turbines are usually under 10 ppm at maximum power, but often increase at low loads or parts loads [10]. CO is formed through different ways [10].

Carbon monoxide equilibrium is very high for rich mixtures and low for lean blends and can be calculated at the equilibrium adiabatic flame temperature.

2.6.3 Unburned hydrocarbon (UHC)

Incomplete combustion of hydrocarbons fuels leads to generate unburned hydrocarbons. That can be due to insufficient residence time [31], the addition of quench air too soon and poor fuel and air mixing.

Poor fuel atomization for liquid fuels can give the extra source of UHC [82, 107]. UHC has unreleased chemical energy, and that provides increased to the combustion efficiency. Escott et al. [108] showed that for a 330 mm long combustor the critical temperature (1700K) for UHC increases because of insufficient residence time, beyond this temperature UHC emissions were very low at ~1ppm.

2.6.4 Particulate matter

Particulate matter (PM) is characterised by diesel emissions regulation as any material collected on a specified filter paper when dilution cools the exhaust to between 42 and 52 ^{0}C [105, 109]. Particles contain a volatile portion produce from unburned liquid fuel and lube oil, and from carbon emissions.

There are methods for estimating particle mass (first order approximation methods)[105, 109] that approximate the volatile fraction from the total hydrocarbons, the sulphate fraction from fuel sulphur and the carbon fraction of the smoke number (filter reflectance or blackness) [105, 109].

Various sources produce particulates, including industrial processes, power generation, and transportation activities. These emissions from combustion sources burning fossil fuels have raised certain interest in recent years from environmental regulatory agencies because of health effects [110].

2.7 Swirler aerodynamics

2.7.1 Characteristics of swirl flow

To improve the mixing pattern and control the flame to attain a minimum level of NOx emissions and a high intensity of combustion, swirling flows are used for stabilisation as shown in figure 2.8 [20, 111, 112]. The swirling flow has a rotational velocity around a central axis in addition to an axial flow.

It produces a toroidal reversal flow which entrains and recirculates a portion of the hot combustion products to mix by entering the air and fuel to stabilise the flame [20, 111, 112]. This sort of recirculation zone (figure 2.8) delivers better mixing and active shear regions, high turbulence and rapid mixing rates [20]. The flow recirculation is generated by the low static pressure in the central core downstream of the swirl, which becomes low enough for the formation of a reverse flow as the swirl number reaches a critical value [20]. Swirling flows represent one of the main advantages of swirling devices, with of centrifugal forces which incline to accelerate the mixing of two flows having different densities [20, 111, 112].

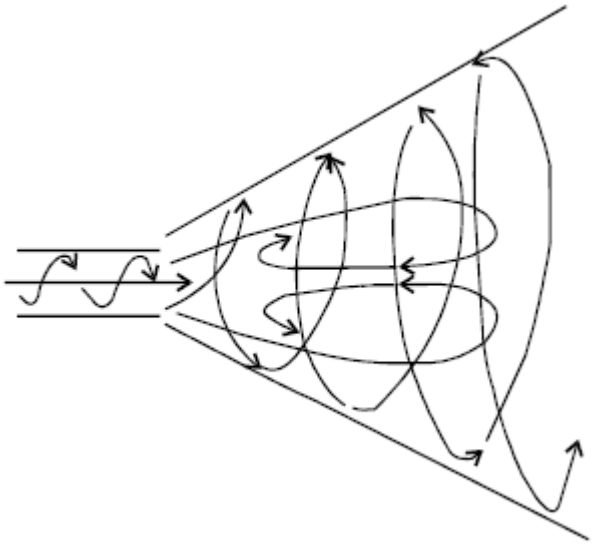

Figure 2-8 Swirl flow with internal zone recirculation [10]

Regarding adding carbon dioxide to methane blends in swirl burner, where the high temperature of the CO2 in the CRZ will guarantee a quick chemical reaction of the diluted reactants. Thus giving low NOx and CO, as well as synthesis gas, known as syngas, produced from gasification processes, is considered as one of the hopeful substitutional energies due to its clean fuel characteristics. Synthesis can be produced via gasification of several feedstocks, including coal, biomass and solid waste.

Swirl flows are associated with the high momentum flow region (HMFR), the central recirculation zone (CRZ) is displaced from the central axis and generates the high momentum flow region (HMFR) placed on the shear layer [44].

2.7.2 Swirler type and configuration

Several low NOx gas turbines use swirling flows in the primary zone [19, 20]. However, the flow in this section has high shear stresses and strong turbulence intensity due to vortex breakdown, providing better mixing compared to bluff bodies [19, 20].

Figure 2.9 shows axial and radial swirl; these swirls are used in both tubular and annular combustors depending on the use. The air is directed through angled routes, which causes the air to rotate about the combustor centre line. The swirling flow then increases, with a recirculation zone being formed.

The size of the recirculation zone is increased as the vane angle, and swirl number is raised [20]. The air enters the combustor straight from the compressor outlet in the axial direction than in the axial configuration, while in radial configuration the air passes across the combustor walls before making a 180° turn to enter the combustor.

Axial swirls continuously have a large diameter compared to radial swirl for the same flow capacity and pressure loss. The higher swirl airflow required for lean low NOx combustion needs larger flow capacity swirls, which need a larger axial swirl diameter. On the other hand, radial swirls do not require a larger diameter, and the flow can be increased by increasing the vane depth [31].

A radial swirl produces a stronger central recirculation zone and delivers a widely dispersed, flat swirling mechanism attached to the swirl face, with more chance of fuel impingement on the wall compared to axial swirl [19].

Multiple swirlers can be arranged into either a counter-rotating or a co-rotating direction. The effects of both configurations on the flow field have been investigated [19]. The main differences between co-rotating and counter-rotating are the distribution of turbulent kinetic energy and shear stress near the exit [19].

The performances of counter-rotating and co-rotating swirls have been examined and found that the organisation of counter-rotating is more appropriate than its co-rotating counterpart [113].

Counter-rotating swirls are more necessary because of the strong shear layer and high intensity for these type. Which increase the level of mixing in the downstream section of the fuel injector. On the other hand, low NOx emission levels were found with the co-swirl formation compared to counter-swirling for both gaseous and liquid fuels [19].

Andrews et al. [114] found that a counter-rotating radial swirl with vane channel injection has low NOx emissions compared to co-rotating which has better flame stability. The same researchers reported that using a splitter plate between the two swirls formed a separation of the upstream airflow, which enhanced the flame stability with a central pilot injector [99, 100]. A 40mm splitter plate between the two 76mm outlet radial swirls was used in this work to improve the flame stability and to increase the mixing.

Swirling flow intensity is indicated by the swirl number (S), which is defined as ''the ratio of the axial flux of angular momentum to the axial flux of axial momentum'' [19, 20, 112]. The swirl number has a great impact on the shape and size of the recirculation zone. Numerous examinations on the influence of swirl number showed that the size of the central recirculation zone increased as the grade of swirl increased [20].

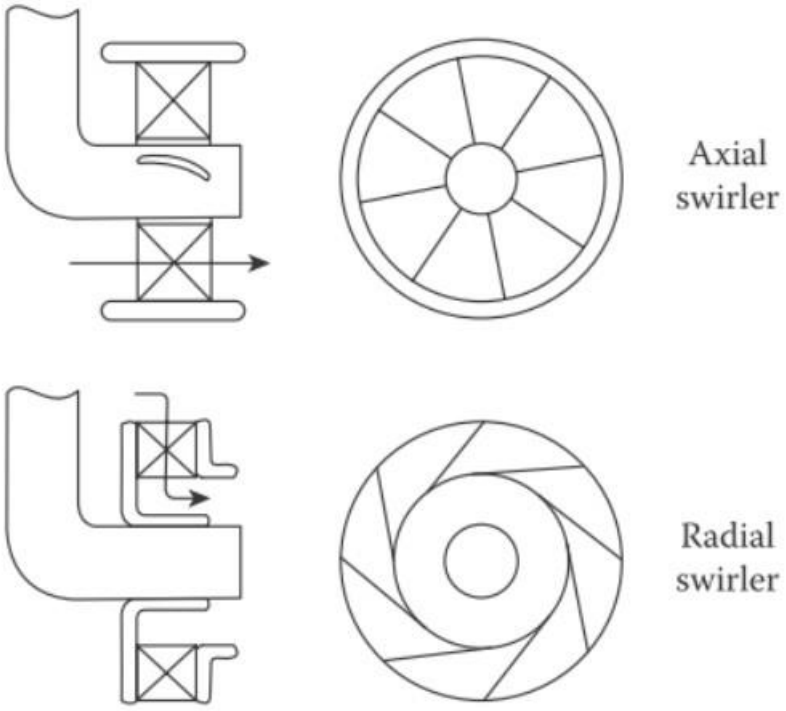

Figure 2-9 Axial and radial swirl [10]**.**

2.8 Combustion instabilities

Usually, premixed combustion systems incline instabilities. Barrere and Williams [115] listed three different types;

1. System instabilities – Instabilities that happen because of interfaces between procedures occurring within the combustion chamber and other components of the system.
2. Combustion chamber instabilities – These types are confined to the combustor.
   2.1. Acoustic Instabilities – The influence of acoustic waves propagating throughout the combustion chamber.

2.2. Shock instabilities – These due to detonation waves or steep-fronted shock waves.

2.3. Fluid-dynamic instabilities – Correlated to special sorts of flow patterns within the combustion chamber.

3. Intrinsic instabilities – Take place because of the reactants themselves irrespective of the system.

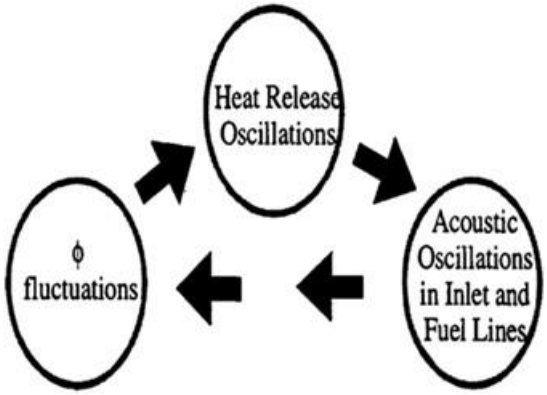

Figure 2-10 Feedback loop is potentially explaining combustion instabilities [116]**.**

The primary mechanisms of combustion instability are that of heat release dynamics and acoustic oscillations. Since these processes happen within a closed system, given the correct conditions, these mechanisms can interact with each other as demonstrated in figure 2.10 [19].

If the pressure fluctuations are small-amplitude (less than 5% of the mean chamber pressure), the combustion is considered stable. However, a combustion process with large-amplitude periodic pressure oscillations can be described as unstable [19]. Mongia et al. [117] showed that low-frequency instabilities are those that have a frequency less than 30Hz and are observed under lean running conditions near blowout.

Between 100-1000Hz, frequencies are described as transitional and are usually associated with equivalence ratio and acoustic fluctuations. Often arise in flame temperature results in higher amplitudes for intermediate frequencies. Interactions between acoustic oscillations and flame growth are stated as the reason for high-frequency instabilities, those over 1000Hz.

Stable and an unstable flame are shown in figure 2.11. Where the steady flame is blue in colour, conical in shape and the corner recirculation zone can be seen to be free of

chemical reactions. The unstable flame is red and seems far less organised. Sun et al. [118] suggested a method of assessing flame stability regarding its colour, geometry, and luminance in fossil-fuel-fired furnaces, and proved the method by applying it to a heavy-oil-fired combustion trial device.

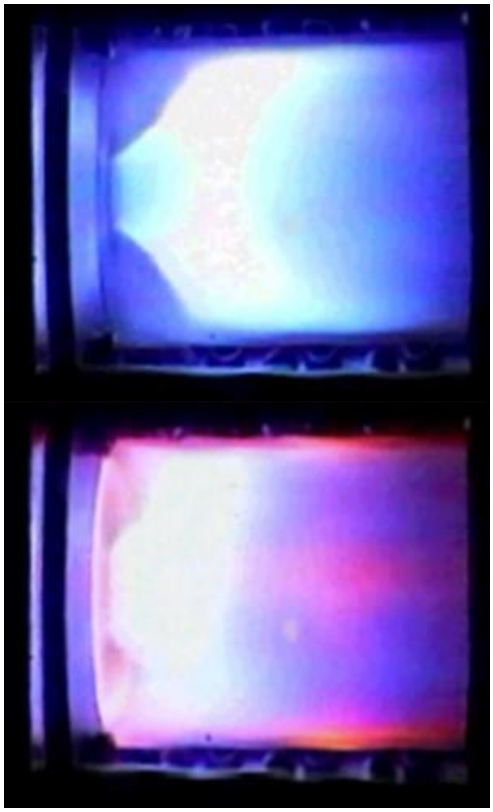

Figure 2-11 Comparison between a stable and unstable flame, top, and bottom respectively [19].

2.9 Gas turbine emission regulations

Emissions legislation to stationary gas turbines varies from country and region depending on the different governments and the existing level of pollution in the region. This legislation usually for full power conditions is expressed as part per million (ppm) on a dry gas basis and corrected to 15 % oxygen.

For example, in the USA, Environmental Protection Agency (EPA) manage the emissions, and 75 ppm of NOx emissions were the previous limits for natural gas. Nowadays, NOx limits are under 25 ppm (governed by the federal government) and less than 10 ppm in California [7, 18]. However, in Europe, the European Parliament by the Pollution Prevention and Control Bureau (EIPPCB) control emissions legislation, where NOx limits being less than 25 ppm for NG and less than 45 ppm for liquid fuels.

Stationary gas turbines working at full power the normal CO limit is from 10 to 40 ppm at 15 % Oxygen [7, 18]. On the other hand, aircraft engines the exhaust gas emissions must submit with applicable regulations represented by the International Civil Aviation Organisation (ICAO). Limits for emission are further complex because of the variation of power setting through a standard flight (much higher emissions during take-off than when idle) [7, 18].

2.10 Chemiluminescence spectroscopy

Chemiluminescence, as the name proposes, is the light that is created due to chemical reactions. It is the spontaneous electromagnetic radiation that is created when chemically produced motivated states return to a lower energy state [107]. Chemiluminescence forms a part of the wider field of emission spectroscopy. Especially, it deals with emissions from the excited molecules OH*, CO_2* and CH*[120].

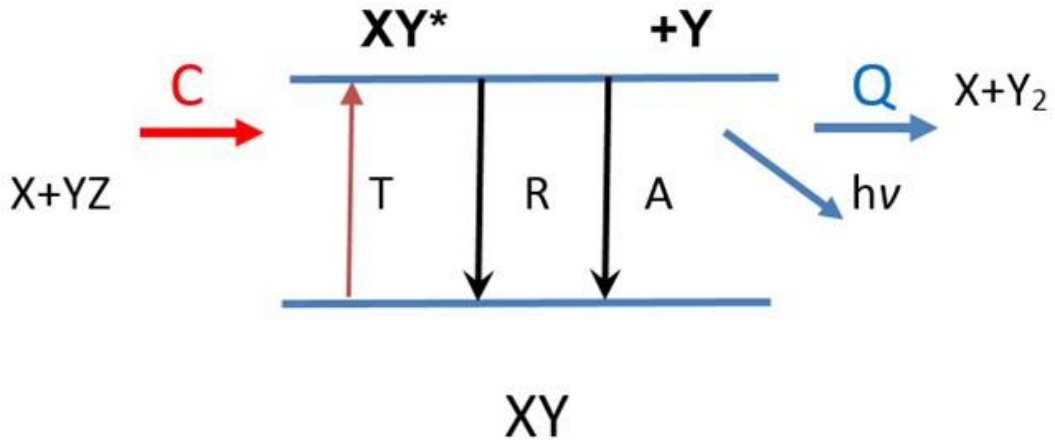

Figure 2-12 General stages involved in a chemiluminescence reaction mechanism.

The spectrum variation in electronic states of the molecules limits the location of the molecular band system overall. The place of the single band within the band system is determined by the variations in the vibrational energy states of the molecule [122, 124].

Furthermore, the fine line structure of the individual bands is determined by the changes in the rotational energy states in the molecule.

Because of the net photon emission, chemiluminescence from an excited molecule for example (OH*), can be determined by the following steps as shown in figure 2.12 [124, 125].

1) Excited state formation via chemical reactions (C),
2) Excited state formation via thermal excitation (T),
3) Quick collisional quenching reactions that eliminate the excited state, decreasing to the ground electronic configuration non-radiatively (R),
4) Reactive collision with a different molecule (Q).
5) Spontaneous radiative transitions to the ground state (A).

Radiant species usually formed through chemiluminescence in hydrocarbon flames contain OH*, C_2*, and CH* [124]. Table 2.4 gives their primary emission band locations and the reactions.

Some researchers have correlated these chemiluminescent features to significant flame factors, for example, the equivalence ratio [128, 130], heat release fluctuations and flame front motion [131, 135, 136] or flame temperature [132, 137]. The hydroxyl radical is given specific attention, because of its dominance as an emission feature, and for its critical role in reaction pathways in the total combustion process[132, 137].

Figure 2.13 shows the fluctuations in emission intensity (in arbitrary units) for the reactive radiating species found in a methane-air flame, between equivalence ratios of 0.8 and 1.5.

Table 2-4 Dominant combustion intermediates, connected formation reactions, and band head locations.

Species	Main Formation Reaction in Hydrocarbon Flame [126, 127]	Main Band Locations(nm) [131]
OH*	$CH+O_2=CO+OH^*$	283,306-315
CH*	$C_2+OH=CO+CH^*$ $C_2H+O=CO+CH^*$	390,431
C_2^*	$CH_2+C=H_2+C_2^*$ $CH+C=H+C_2^*$	469-473,510-516
CO_2^*	$CO+O+M=CO_2^*+M$	300-500

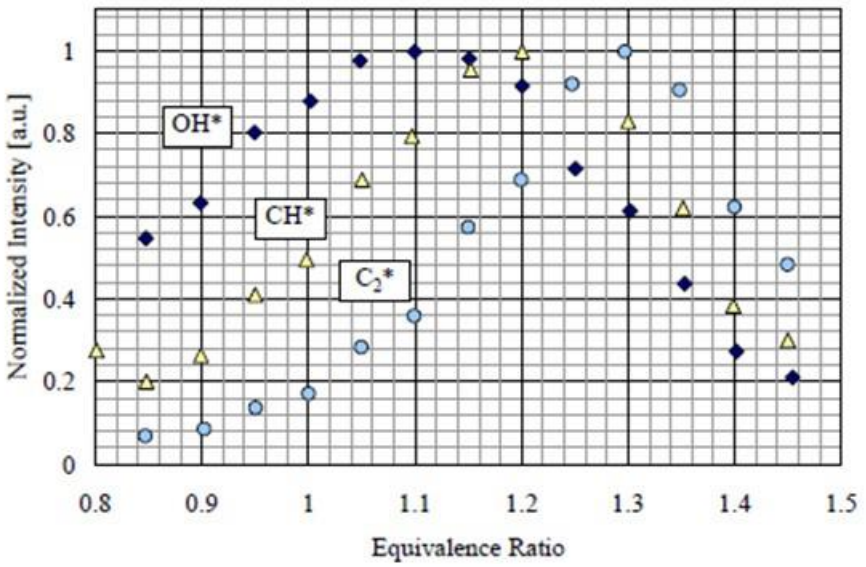

Figure 2-13 Published results are showing normalised chemiluminescent emissions for OH*, CH*, and C_2*, for a laminar premixed methane-air flame [132]**.**

The intensity of each chemiluminescent signal rises with the equivalence ratio and peaks for OH*, CH*, and C_2* take place at different equivalence ratios. Further work has shown that stronger signals are expected at lower pressures and greater flow rates [133].

A study by Higgins et al. [133] separated these properties for a premixed methane-air flame. The authors were capable of collapsing the OH* signal from all experiments onto a single line, reliant on equivalence ratio, the mass flow rate, and pressure [133]:

The CH*/OH* ratio has been defined as the greatest sensitive to variations in equivalence ratio, so this ratio has formed the basis for many suggestions including its use as an equivalence ratio monitor [132, 139].

2.11 Summary

A literature review of some subjects related to alternative fuels, multiphase flow, swirl combustor characteristics and associated combustion instabilities such as blowoff, has accomplished in this chapter. It can be concluded that,

- The need to find an alternative environmentally friendly fuel becomes vital when global warming and airport air quality problems are to be decreased. Additionally, there is increasing political and public pressure directing air transportation to

reduce greenhouse gas emissions, which are changing quickly because of the quick development of the aviation area.

- Combustion equipment has been developed to get together minimum pollutant level requests, however, keeping high operation efficiency of gas turbines. Premixed combustion using alternative fuels has verified as the best hopeful technology in this context.

- Swirl is important and can influence the formation of critical combustion processes such as inner recirculation zone. The equivalence ratio and velocity at which fuel is supplied can also have effects on the system. If the flame becomes unstable, combustion instabilities can happen. These are undesired phenomena, and hardware damage can result.

- Multiphase flow has widely existed in many industrial applications and academic studies, and mostly the gas-liquid two-phase flow can be considered as one of the greatest extensively applied flow conditions. Examples of both alternative liquid and gaseous-fuelled systems exist.

Varying fuel properties mean that suitable changes need to be made so the fuel can be used in their pure form, however providing sensible blend ratios are used, some units can run on alternative fuels without modification, it is clear that a two-phase system is a hopeful method for the use of alternative fuels.

However, it has been noted that there are several design limits of importance that need to be considered during the design procedure. It is vital to obey to these restricts the reduction of the mean droplet diameter as the proposed atomiser needs to provide a fine spray appropriate for combustion.

Chapter 3

Experimental setup

The science of today is the technology of tomorrow.

Edward Teller (American Physicist)

3.1 Introduction

Different techniques and various gas analysers were used to measure different rigs configurations to determine the combustion emission regimes while using different fuel blends, atomization, and temperatures. Calorific values, density, and surface tension were also measured, and proximate analyses were performed to act as a comparison between the fuels. Finally, High-speed imaging has used to detail the atomization parameters, namely, spray angle.

Chemiluminescence spectroscopy was also used to show OH*, CH* reactive combustion species to provide basic measures of flame structure and heat release.

Atomization characterisation was achieved in a spray chamber located at Cardiff University. High-speed imaging was used to specify the atomization parameters, namely, spray angle. The atomiser nozzle was placed in the top of the experimental test rig to atomise the fuel at operating pressures from 8 to 26 bar (abs).

Experiments were achieved at the Gas Turbine Research Centre (GTRC). The rig able to deliver 5 kg/s of air at 900K and 16 bars (abs), the HPOC rig was fitted with a generic pre-mixed swirl burner in this work as shown in figure 3.2. The generic swirl burner included a central lance that was used for liquid injection and the main body that receives both the premixed (gaseous) fuel and oxidiser.

In chapter five an axial swirling flame burner was utilised to establish continuous swirling flames. The swirler is positioned concentrically into with the inner tube of the burner. Two methods of injection were used, one through the centre via a central injector, and one through the outer, primary premixed zone. Gases and air for central

and outer parts were premixed together in separate tubes to certify sufficient mixing before inflowing the burner.

In chapter six for the last burner, the liquid flows were supplied independently to the atomiser through the centre via a central injector. The air-gas mixture passes through swirl-generating vanes which create swirling effects on the combination before exiting the injector through the discharge orifice. A Delavan 0.4 x 60 A, nozzle atomiser was used as the fuel injector to atomise liquid fuel before mixing with swirling premixed.

3.2 High-speed photography

The technology of High-Speed Photography (HSP) has been developed in the last decades [130]. The guideline situated in the context of pixels of a Charge-couple device (CCD) camera, which is an analogue shift register that permits analogue signals to be transported through continuous stages controlled by a clock signal, digitalising them in the camera [125].

These can be used as a type of memory or for postponing sampling signals. These are put in arrays as photoelectric light sensors.

Digitalization frequently happens at 8 bits, which is associated with the number of colours (or grey levels) noticeable by the device [135]. CCD cameras started in 1980 permitting higher resolution. The addition of image intensifiers allowed to capture thousands of frames per second [120]. Modern cameras can work at more than 250000 frames/s resulting in a massive stream of data.

A Photron Fastcam APX-RS high-speed camera operating at 1000 frames/s was used in work with Generic swirl burner to capture various phenomena, i.e. atomization and combustion processes with a 105 mm, 1:2.8 Nikon lens.

The camera was also used with a 20 kW burner to capture chemiluminescence results of CH* radicals; It was used with a Hamamatsu Intensifier attached with a UV lens and a 420±10nm, 85 transmissivities optical filter. Repetition rates were established at 60 Hz to provide an overview of CH fluctuations for each case. The resultant images were analysed using a Photron FASTCAM PFV software and MATLAB program.

3.3 Chemiluminescence and emission spectroscopy

3.3.1 Chemiluminescence for high-pressure optical chamber

OH* chemiluminescence measurements were taken using high-pressure optical chamber (HPOC) burner as shown in figures 3.1 and 3.2. A Dantec Dynamics Hi Sense Mk II CCD camera with a 1.3-megapixel resolution was joined to a Hamamatsu C9546-03L image intensifier; image intensifier units involve of a compact head, it integrates an image intensifier with a high-speed entrance operation circuit and a remote controller.

High sensitivity, high-speed shutter camera can be configured by simply connecting an image intensifier head to the front of a CCD camera. A speciality 78 mm focal length lens (f/2.8) able to capture light in the UV wavelength range was installed on the image intensifier alongside with a narrow bandpass filter centred at 307 nm (FWHM =10 nm).

The perfect filter must minimise the influence of the blackbody radiation and be broad enough to capture the OH* radiation with minimal effect of the narrow absorption feature [136]. In this work to settle the flame chemiluminescence, a concentrated high-speed camera equipped with an interference filter. This camera watches the flame via the side window. Due to the large quantity of collected data, it is not usually applied, but used only for studies of details of particular interest.

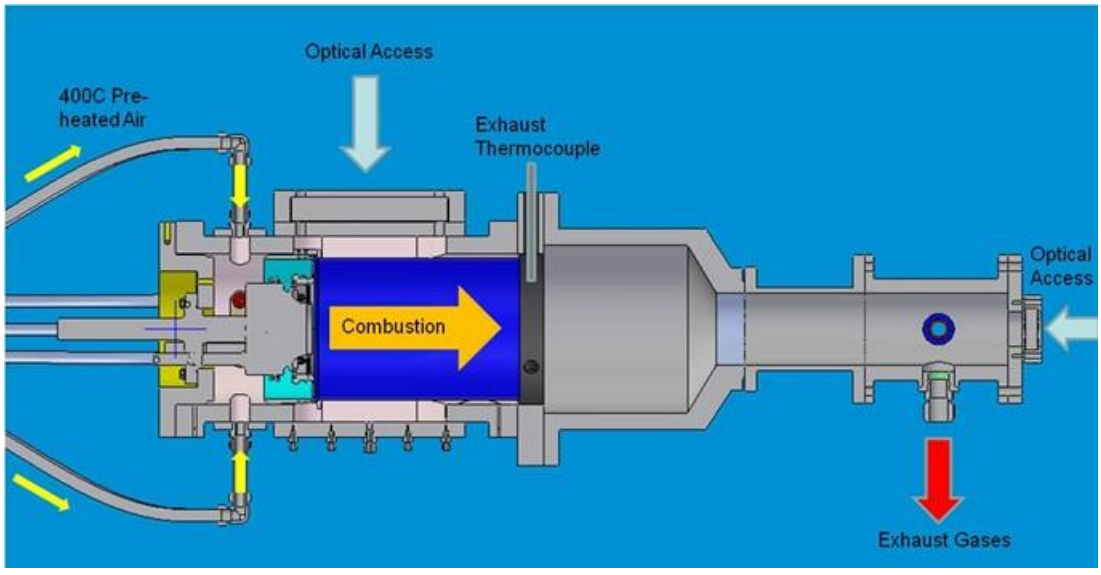

Figure 3-1 Schematics of the HPOC.

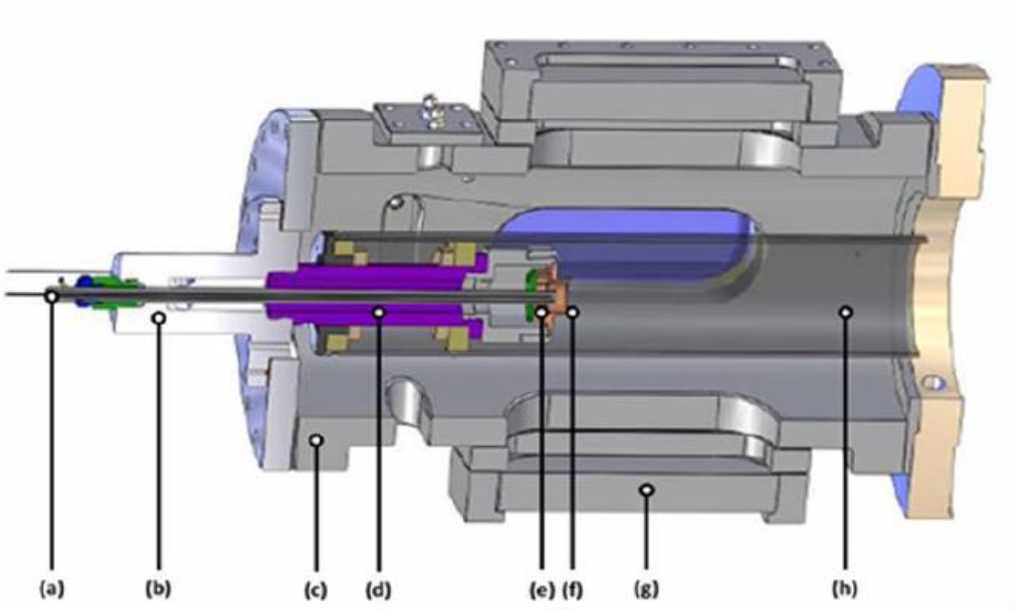

Figure 3-2 Sectioned detail view of the HPOC showing (a) instrumentation and pilot. (b) inlet plenum.(c) HPOC outer casing. (d) premixing chamber.(e) radial-tangential swirler insert.(f) exit nozzle.(g) Quartz window for OH* visualisation and (h) quartz confinement. Flow goes from left to right.

Two hundred images were taken at 10 Hz for each test condition using Dantec's Dynamic Studio software, though the image intensifier gain was carefully chosen via remote control. All images were taken over the top window of the HPOC at a 90° angle to the direction of flow as presented in figure 3.1.

Abel inversion of the resulting time-averaged images was used to deliver better recognition of the OH* distribution through the flame [24, 25]. Abel inversion was achieved on the temporal average of 200 images taken at 10 Hz (20 seconds of runtime) and then used the resulting image intensity values in the normalisation process.

3.3.2 Chemiluminescence for 20 kW burner

CH Chemiluminescence fluctuation was performed using A Photron Fastcam APX-RS high-speed camera, a Hamamatsu Intensifier coupled with a UV lens and a 420±10nm, 85 transmissivities optical filter. Repetition rates were fixed at 60 Hz to supply an outline of CH fluctuations for each case. The resultant images were analysed using a Photron FASTCAM PFV ver 2.4.1.1 software and MATLAB R2015a.

3.3.3 Emissions of high-pressure optical chamber (HPOC)

Two pieces of equipment were used to characterise combustion emissions; the first is an integrated system developed by signal instruments comprising several analysers: A Flame Ionisation Detector (FID) is employed within a Signal 3000HM to detect total Hydrocarbons (THCs), calibrated with propane in the range 0-890 ppmV.

A heated vacuum chemiluminescence analyser (Signal 4000VM) is simultaneously employed to quantify NOx concentrations, calibrated to 37.1 ppmV NO and 1.9 ppmV NO_2.

The system also contains a multi-gas analyser (Signal MGA), containing an infrared cell for measurement of CO (calibrated for 0-900 ppm) and CO_2 (0-9%), in addition to a paramagnetic O_2 sensor (up to 22.5%).

The second system is a standalone Rosemount NGA 2000 multi-gas analyser and provides secondary readings of CO, CO_2 and O_2 all calibrated to the same concentrations previously stated.

3.3.4 Emissions of 20 kW burner

To investigate the content of exhaust gases with 20 kW burner, a Testo 350 XL combustion analyser was used. The Testo exhaust gas analyser is a portable unit designed for taking measurements in furnaces and combustors, and as such may not be entirely suitable for analysing the broad range and quickly changing emissions of the combustion engine.

The Testo 350 XL gas analyser, its control unit and sampling probe is pictured in figure 3.3. Measurements of post-combustion emissions were performed using a TESTO 350-XL gas analyser, at about 500 mm downstream of the outlet of the burner. The sampling probe was positioned 10 mm inside the exit to the plenum. The measured emissions include NOx, CO, O_2 and CO_2, with the measurement range of 0-1000 ppm, 0-10,000 ppm, 0-25% and 0-99.9% respectively. The emissions readings from the gas analyser are reported in wet basis with the uncertainty of ± 5% ppm for NO, ± 5% ppm for CO, ± 0.8% for O_2 and ± 0.3% for CO_2 [138].

Figure 3-3 Testo 350 XL unit and probe [137]

A sampling of the post-combustion gases was performed in the steady state, for 1 minute until the reading became stabilised. The model TESTO 350-XL is a self-contained emission analyser system capable of measuring different types of emissions in combustion emission sources; figure 3.4 shows a schematic of the model 350 as tested [138].

The model 350 XL uses electrochemical sensors and can be calibrated, exchanged, and upgraded in the field without hand tools [138]. Electrochemical sensors are measured flue gas residents (O_2, CO, NO, NO_2, SO_2, H_2S) through the principle of ion-selective potentiometry.

This equipment enables the sensor to be pre-calibrated at Testo and connected in the field as a simple plug-in device, no essential to have calibration gases on site[139].

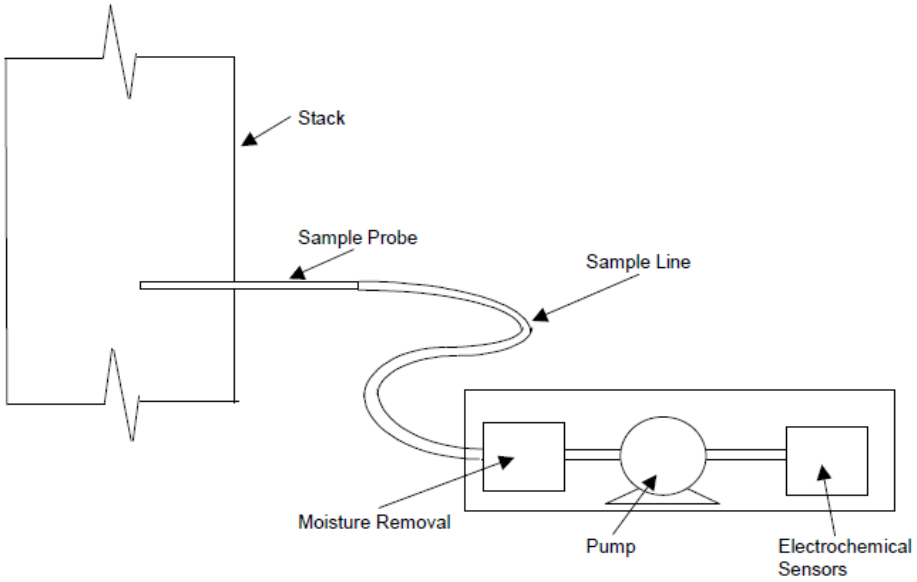

Figure 3-4 TESTO 350-XL sampling schematic[138]

3.4 Temperature measurements

An SL7000 series data logger was used to obtain temperature measurements with the 20 KW burner. The wire diameter was 1.5 mm, so it was small enough to not cause any significant interference to the flame structure while maintaining structural rigidity of the thermocouple. Gas temperature in the flame was measured using an isolated tip K-type thermocouple. The signals were recorded onto a PC using a data acquisition board.

The SL7000 series data loggers are joined to the computer via a USB cable. Data are downloaded to a PC using the Temp IT software via its USB interface. The SL7000 is a logger of data which has a very flexible combination of inputs from a temperature input linked with an internal temperature and RH in addition to an optional external temperature and RH sensor.

An onboard LCD, the display shows selected channel information and integral LED displays to provide quick scanning. The thermocouples had positioned on the burner wall as illustrated in figure 3.5.

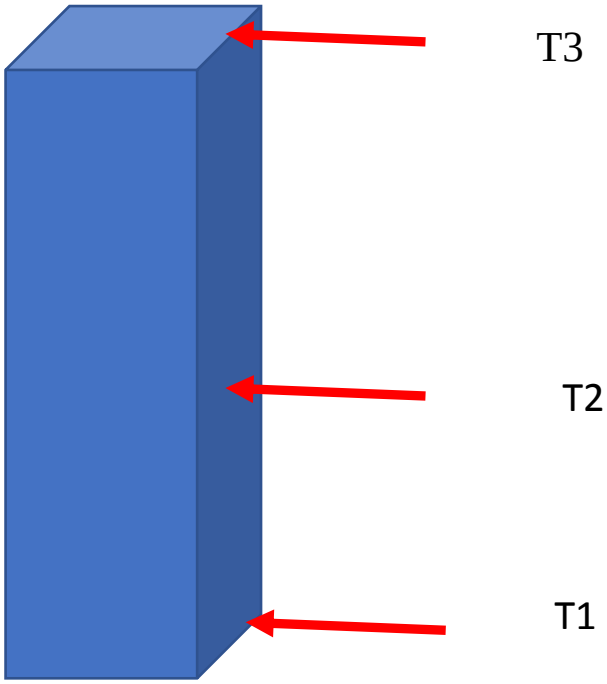

Figure 3-5 Thermocouples position in 20 KW burner, T1 at the burner, T2 at 10 cm from the burner and T3 at the exit

3.5 Gaseq

Gaseq is a chemical equilibrium program for Windows [140]. It can be used to compute a different parameter for equilibrium processes. It uses chemical thermodynamics to calculate final product species for equilibrium reactions, i.e. viscosity, temperature and density, etc. The initial reactant temperature, mole fractions, pressure and other different properties can be stated.

Gaseq has been used in this work with a variety of fuels to calculate different parameters of the mixtures used for a range of equivalence ratios. This program has some features like [140]: -

- **Excel interface**

This advantage helps of the increasing capabilities of the program to plot a graph of the results of auto-incremented calculations. An X-Y plot is created with the X being the first property stated (generally the incremented one), and the others are seeming as several Ys.

Two Y scales are used: mole fractions on a log scale are plotted and the other properties, e.g. temperature, on a linear scale. It is very hard to deliver a graphing

facility which meets all requirements, and it is unavoidable that it will usually be necessary to edit of the graph within Excel to improve its appearance and effectiveness.

- **New species**

It can be used any species in a thermodynamic calculation of the elemental composition, the enthalpy and entropy at 298K and the specific heat (CP) at different temperatures are known.

- **Reactants with different temperatures**

With gasseq each reactant species can have a changed temperature.

- **Specify the number of moles of product**

This feature is to handle "super-equilibrium" concentration of radicals which happen just after the reaction zone in low and moderate pressure flames. Where the reactions interchange radical species (H, OH, O, etc.) are fast and equilibrated, but the recombination reactions which eliminate radicals are slow.

- **Using mass units**

Concentrations of species entered and displayed in mass units.

3.6 Summary

The measurement instrumentation has been mentioned can be considered as vital regarding characterisation and verification of different combustion problems and in particular, for the understanding of flame alternative fuels properties and emission measurement.

Chemiluminescence diagnostics has the ability for investigating to the levels of emissions produced during all the trials.

Chapter 4

Combustion and atomisation characteristics of a saturated biodiesel in gas turbines

The gift of mental power comes from God, and if we concentrate our minds on that truth, we become in turn with this great power.
Nikola Tesla

4.1 Introduction

Biodiesel products are considered highly oxygenated fuels and have been used as substitute sources of fuel for diesel engines to improve combustion performance. Biodiesel can be regarded as a more environmentally friendly fuel if it is compared to fossil-based fuels. Thus, this fuel could be used in gas turbines without significant adjustments [56].

Biodiesel has proved a reduction of un-burnt hydrocarbons (UHC), carbon monoxide (CO) and particulate matter (PM) without decreasing the power output in a meaningful way [54]. Testing of biodiesel has often shown promising results where emissions are comparable to control studies using fossil-based diesel [141].

There are remarkable differences in physical properties of biodiesel and diesel; therefore, there is a need to examine the spray characteristics of biodiesel about its application in internal combustion engines and gas turbines, more so given that atomization behaviour has an important consequence on emissions.

The biodiesel used in this chapter is a by-product from a biomass gasification processes, in particular, a liquid condensate from product gas cleaning processes. That is an essential stage in thermal conversion of biomass, particularly when the main product gas components, CO and H_2, are used for Fischer–Tropsch synthesis or as high purity fuel [65].

The purpose of this chapter is a comparison study between two liquid fuels, a pure biodiesel and the biodiesel as a saturated blend with a pyrolysis by-product; these two

fuels were compared to standard kerosene as a baseline. The study methodology includes two stages: first of all, atomization patterns and injection systems were achieved using a high-speed imaging method. Secondly, a combustion trial campaign was undertaken using a swirl burner to quantify the operational performance and exhaust gas composition of the fuels.

Emissions, flame stability tendencies and power outputs were measured at gas turbine related to equivalence ratios, indicating the potential to use these biodiesels as alternatives or backup of conventional gas turbines. Chemiluminescence was used to provide proof of localised OH* production and flame profiles. The primary results are that the saturated biodiesel showed increased production of CO_2 compared to the other fuels.

Heavy organics seem to be acting as catalytic substances for OH production close to the burner mouth. Regarding stability and combustion, it is suggested that the saturated blend would be an appropriate candidate for power generation.

This chapter has been published in the journal 'Renewable Energy' (see publication 1 in the list in Chapter 1).

4.2 Experimental Setup

4.2.1 Characterisation of saturated biodiesel

The surface tension and density were experimentally achieved at ENEA, Italy by using a temperature controlled LAUDA TVT 1 Drop Volume Tensiometer. Drop volume tensiometer method is highly accurate measurement, low sample volume requirements and modern electronics. It used to measure the surface, interfacial tension and density of liquids. The drop volume detaching from the needle is measured very accurately.

This measurement principle is an easy test with the highly stable Phase-Locked Loop (PLL) speed controller of the direct-current motor; droplets can be shaped with a lifespan from one second up to many hours without vibrations [142].

The viscosity was experimentally determined using a U–Tube Viscometer. A Parr 6100 calorimeter bomb and an IKA C4000 calorimeter using benzoic acid as reference determined the Higher Heating Value (HHV). The 6100 calorimeter is a compact

calorimeter that works at room temperature taking full benefit of modern microprocessor abilities. The advantages of this system include less water, less energy, and less hardware although still giving good accuracy [143].

On another hand, IKA C4000 calorimeter used compact semi-automated calorimeter to limit calorific values of liquid and solid samples. It is appropriate for educational purposes and commercial, industrial laboratories [144].

The final analysis was gained by using an elemental analyser, a Perkin Elmer CHN/O according to UNI EN 15104. This Analyser allows fast determination of the carbon, hydrogen, nitrogen, sulphur or oxygen content in organic and other sorts of materials. It has the ability of treatment a wide variety of sample types, including solids, liquids, volatile and viscous samples[121].

Ash was analysed to determine the elemental content according to the methods CEN 343 or CEN 345 by using an ICP-OES Agilent 720ES. This Optical Emission Spectrometer involves the use of compressed gases, high voltage radio frequency energy and dangerous materials including corrosive fluids and combustible liquids [145]. Oxygen was calculated by the difference of species. Gas Chromatography (GC) is a public type of chromatography used in analytical chemistry for separating and analysing mixtures that can be vaporised without decay.

Typical applications of GC contain testing the limpidness of a particular substance or separating the different components of a blend. In some conditions, GC helps in classifying a compound. GC can be used to prepare pure mixtures from a combination [124, 125].

This method was employ by using an Agilent HP 6890 GC. It is gas chromatograph that delivers greater performance for all applications. It uses of progressive electronic pneumatic control modules and high-performance temperature control [129].

The experimental campaign included three test fuels: unsaturated and saturated biodiesels, and kerosene. Fuels properties are given in table 4.1, with the GC analysis of the methyl esters in table 4.2. The unsaturated biodiesel is originated from cooking oil, providing a composition similar to that carried out in methyl-ester. The fraction of

biodiesel that is included in the saturated sample has almost the same elemental composition (C 76.28%, H 12.55%, O 11.04 %) as that of the unsaturated biodiesel. However, since the biodiesel has been used to clean up the gas stream from a gasification procedure, the saturated biodiesel represents less than half of the total mass of the final sample.

Table 4-1 Fuel properties obtained at ENEA

Property	Kerosene	Unsaturated Biodiesel	Saturated Biodiesel
Viscosity [m^2/s] 20°C	3×10^{-6}	7.40×10^{-6}	7.60×10^{-6}
Viscosity [m^2/s] 40°C	2.00×10^{-6}	4.49×10^{-6}	4.68×10^{-6}
Density [kg/m^3]	820	859	879
Surface Tension [mN/m]	28	29.1	32.1
HHV [MJ/kg]	46	38.9	29.4
Water content [wt%]	2.6	0.7	19.0
Methylesters [wt%]	---	95.0	44.2

Table 4-2 Analysis of methyl esters by GC, relative abundance as wt%, obtained at ENEA

Molecule	Unsaturated Biodiesel	Saturated Biodiesel
C14:0	1.07	0.92
C16:0	32.10	24.60
C16:1	0.00	0.00
C18:0	3.36	3.25
C18:1	47.50	47.60
C18:2	12.80	19.60
C18:3	3.07	3.90
TOT	100	100

Besides water, the remaining 36.8% is a complex mixture of organic molecules containing formic acid (molecular mass 46 g/mol) and aromatic compounds (molecular mass 200 g/mol). This scrubbing process has been carried out to increase the quality of gases in a biomass gasification system at ENEA, Italy [146].

4.2.2 Atomisation experiments

The fuel injector used for atomization was A Delavan 0.23mm-60°A WDB nozzle atomiser. Atomization characterisation was achieved in a spray chamber located at Cardiff University, figure 4.1. This rig works with independent control of the ambient (chamber air) pressure (up to 15 bars) and temperature (up to 150 °C), such that chamber air conditions can range from simulated intake stroke to late compression stroke injection for the characterisation of automotive applications. Constant control of the pressure was carried out error reading of the pressure gauges was a ±0.5 bar.

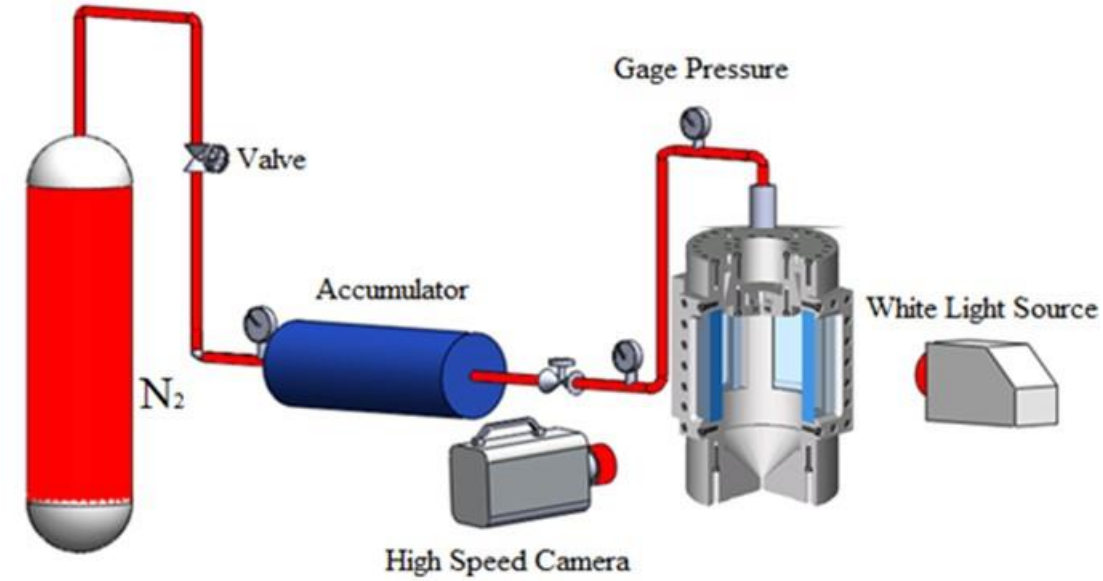

Figure 4-1 Spray rig and imaging setup diagram.

High-Speed Imaging was used to specify the atomization parameters, namely, spray angle. The spray angle was defined as the angle made by the cone of liquid leaving the nozzle orifice where two straight lines were surrounded by the maximum outer side of the spray [147]. A Photron Fastcam APX-RS high-speed camera working at 1000 frames/s was also used with a 105 mm, 1:2.8 Nikon lens.

A 50W straight projector bulb was used as a light source, accessing the chamber through one of its three quartz windows and located at a 90° angle to the high-speed camera. The atomiser nozzle was placed in the top of the experimental test rig to atomise the fuel at operating pressures from 8 to 26 bar (abs) as shown in figure 4.1. Using compressed nitrogen, passing into a liquid accumulator, collecting the bulk volume of the spray at the bottom of the rig. Photron FASTCAM PFV ver 2.4.1.1 software and MATLAB R2013a, used to analyse the resulting images.

4.2.3 Gas turbine burner experiments

Experiments were achieved at the Gas Turbine Research Centre (GTRC), which is a Cardiff University facility located at Port Talbot [148].

The rig used was the High-Pressure Optical Chamber (HPOC), able to deliver 5 kg/s of air at 900K and 16 bars (abs), thus allowing combustors to be studied at conditions applicable to gas turbine power generation.

Coriolis mass flow meters were used to accomplish accurate measurement of flowrates with an accuracy of ±0.5% RD plus ±0.1% FS. The HPOC rig was fitted with a generic pre-mixed swirl burner in this work as shown in figure 4.2.

The generic swirl burner included a central lance that was used for liquid injection and the main body that receives both the premixed (gaseous) fuel and oxidiser. The burner body contains a premixing chamber where most of the gas premixing occurs upstream of a swirl chamber. A quartz tube fitted with the system to simulate the proper expansion ratio from the burner into the engine's combustion chamber confines the burner; in this case, an expansion ratio of 4 was used.

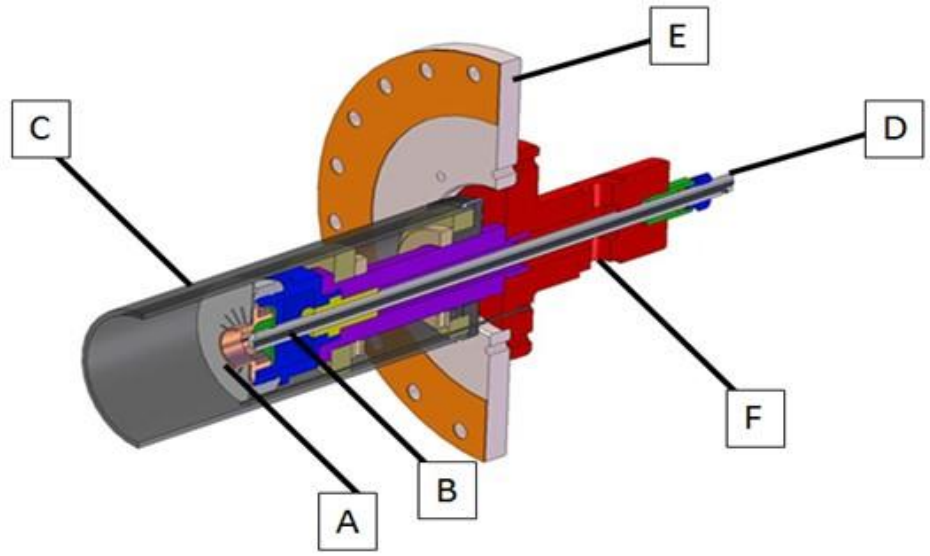

Figure 4-2 Generic swirl burner with lance attached. A - swirler head; B – liquid fuel lance with atomiser; C – quartz confinement tube; D – liquid fuel inlet; E – pressure casing wall; F – primary combustion air inlet.

At both atmospheric and pressurised conditions, combustion tests were performed. Pressures of up to 2.9 bar (abs) were examined for all fuels allowing for thermal power conditions ranging from 30 to 60kW. Images of the flame from radial and axial positions were captured by using high-definition (HD) video camera.

Flame shape, appearance and stability knowing how these parameters influence the combustion behaviour were documented; also, the exhaust gas composition of each fuel was examined.

OH* chemiluminescence measurements were taken using all fuels at several equivalence ratios. The Dantec Dynamics Hi Sense Mk II CCD camera with a 1.3-

megapixel resolution was combined to a Hamamatsu C9546-03L image intensifier. A speciality focal length lens, as described in chapter 3, was used. Image capturing methodology is explained in chapter 3.

An open-source MATLAB algorithm based on the Abel inversion method has been modified to provide a spatial representation of the OH* and CH* chemiluminescence measurements. This Abel inversion is based on a Fourier-series-like expansion which projects the radial pixel intensity distribution function onto a theoretical 2-D plane through cosine expansions.

The application of an Abel inversion assumes that the radial distribution being processed is symmetric about a central axis. Given the highly variable structure of the instantaneous turbulent swirl, flames investigated. Abel inversion was achieved on the temporal average of 200 images taken at 10 Hz (20 seconds of runtime) and then used the resulting image intensity values in the normalisation procedure.

Combustion equilibrium analyses were performed utilising GASEQ[140], under stoichiometric conditions to provide a better understanding of the development of some of the species that participate in the combustion process. The methyl formate reaction mechanism developed by Fisher et al.[149] has been used as a replacement for biodiesel.

Methyl-formate was selected as a surrogate molecule to achieve a reaction close to the one expected from biodiesel. Although methyl-formate mechanisms have presented changes to biodiesel [149], the results provide the basis for the discussion on exhaust gas composition.

4.3 Results and discussion

4.3.1 Spray characterisation

Table 4.1 shows characterisation studies; for the sprays, it is evident that the calorific value for the saturated biodiesel is lower than that of kerosene, and the unsaturated biodiesel, as expected although this was predictable.

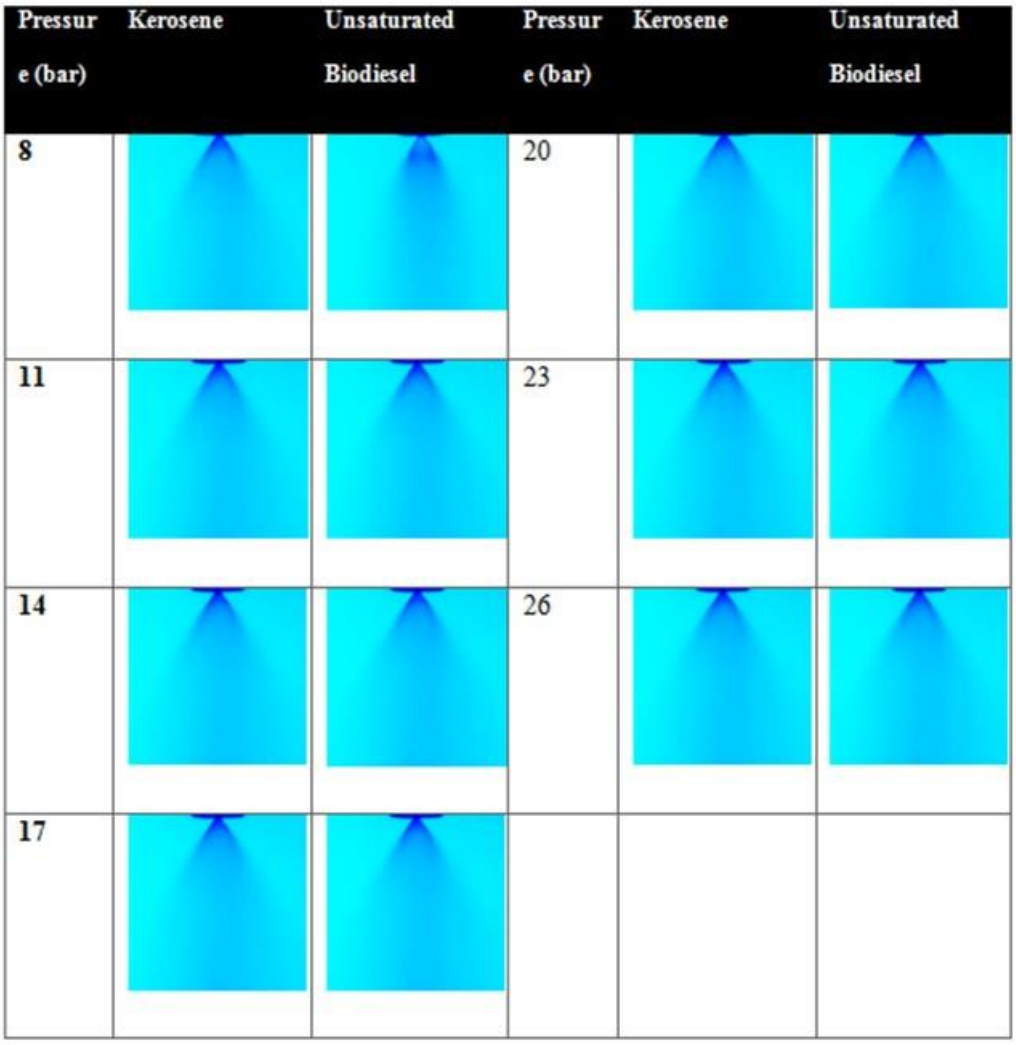

Figure 4-3 High-speed imaging at different pressures for fossil and biofuel blends. Average results out of 1000 images.

It is still a result which shows that the energy content of the saturated sample is high enough to be considered as an appropriate option for liquid fuel energy uses. This calorific value is dependent on the gasification process, scrubbing and aging, elements that need to be considered while using it as a support fuel [56].

Spray angle results showed that the unsaturated biodiesel has a narrower spray angle than kerosene as illustrated in figure 4.3. So biodiesel requires more pressure to accomplish an efficient droplet breakup previous to evaporation; this data is demonstrated clearly in figure 4.4 as a plot of spray angle vs. injection pressure for the three fuels is presented [53].

Similar results were achieved for the saturated biodiesel, figure 4.4, which showed a smaller spray angle linked to the existence of solid matter (from the particulate matter

contaminants present in the saturated fuel) and resultant larger viscosity. Narrower spray angles are a known issue for higher viscosity biofuels, which can result in combustion difficulties such as high smoke emission [18, 27].

Furthermore, the spray angle is known to be a function of the ratio between the ambient density and the sprayed fluid density, hence the results in figure 4.4 are logical given the properties discussed here. Proposed solutions to this problem include biofuel preheating to deliver lower viscosity and hence improve atomization, besides higher injection pressures to be used for scattering the saturated biodiesel.

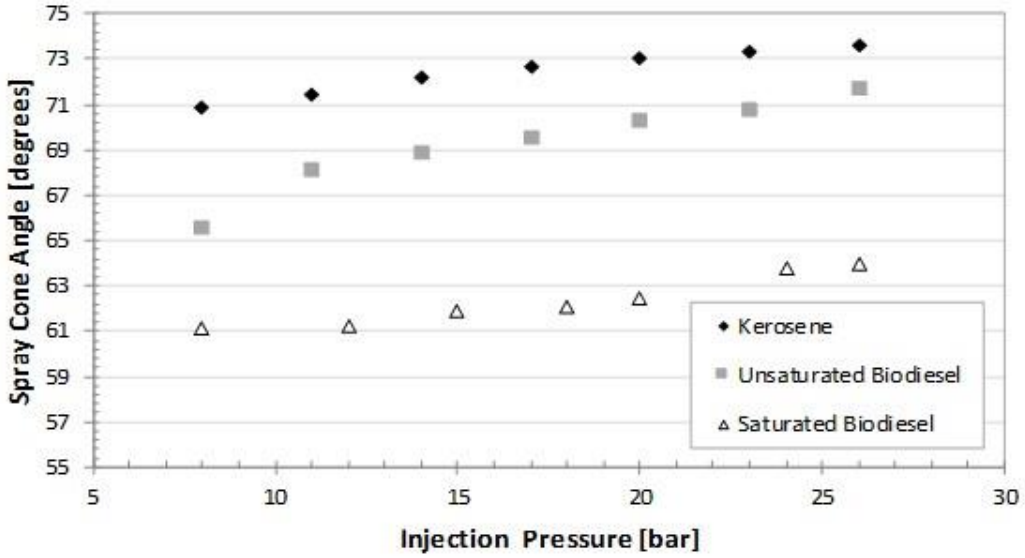

Figure 4-4 Effect of fuel injection pressure on spray angle

4.3.2 Combustion behaviour in the HPOC

4.3.2.1 Flame appearance

The flame was stable and sufficiently radiative for kerosene to show the production of soot that would be predictable with the lack of oxygen for complete burnout under rich conditions. Under comparable air to fuel ratios, the unsaturated biodiesel showed a lower amount of exhaust soot, perhaps because of the larger quantity of oxygen bound into the fuel.

Likewise, the saturated biodiesel burnt with a stable flame, but it was evident that the amount of soot coming from the saturated biodiesel was the highest of all the tested fuels, as shown in figure 4.5. The quartz confinement tube was stained with black soot residue after only a few seconds of operation under rich ($\phi \sim 1.2$) conditions due to soot formation. Also, there was undeniable proof that the atomization of the fuel was

partial, with the appearance of several glowing (probably fuel-rich) projections in the flame.

That was related to spray visualisation experiments, which showed that the saturated biodiesel formed into small droplets at a noticeably slower rate than the other fuels. Larger spray droplets need more time to evaporate, and hence thermal decomposition of the hydrocarbons will be obstructed, resulting in incomplete burn out, hence the observed soot.

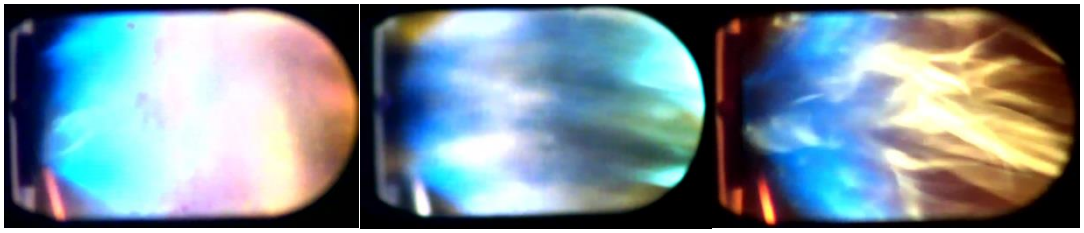

A. B. C.

Figure 4-5 Visible flame at equivalence ratios 0.6. A) Saturated biodiesel, high soot glowing. B) Unsaturated biodiesel and C) Kerosene.

It can be said that the saturated biodiesel blend under lean conditions (i.e. $\phi < 1$) worked positively regarding flame stability and burning processes compared to the other tested fuels.

Combustion instability refers to damaging oscillations driven by fluctuations in the combustion heat release rate. These undesirable oscillations can cause wear and damage to combustor components and, in some extreme cases, can cause breakage of components and resulting damage to downstream turbine components.

Gas analyses will show, if the flame can be stabilised at low equivalence ratios, the CO formation to be less with more CO2 produced, thus reflecting a higher combustion efficiency.

Completely unburned hydrocarbons will be lower, although NOx will increase because of the additional nitrogen and comparably higher temperatures generated during combustion. Nevertheless, if equivalence ratios of ~0.55 are accomplished, then measured outlet concentrations of NOx will be in the same magnitude order to those observed in kerosene flames.

4.3.3 Exhaust gas analysis magnitude

4.3.3.1 THC emissions

THC emissions as a function of equivalence ratio for the kerosene and tested biofuels under atmospheric conditions are shown in figure 4.6. A log scale has been used since the THC emission above stoichiometry was orders of magnitude higher than the values measured below. Apparently, it can be seen that the saturated biodiesel produced higher concentrations of unburnt hydrocarbon products, especially at higher equivalence ratios, which corresponds to the physical observations in the previous section. There was some proof to suggest that increasing the HPOC pressure had reduced net THC emissions, but more data would be necessary to confirm this.

Kerosene did not show significant concentrations of THC in the exhaust, demonstrating complete burnout of the fuel under the conditions studied. That correlates well with the spray results given that the kerosene spray was remarkably more atomised.

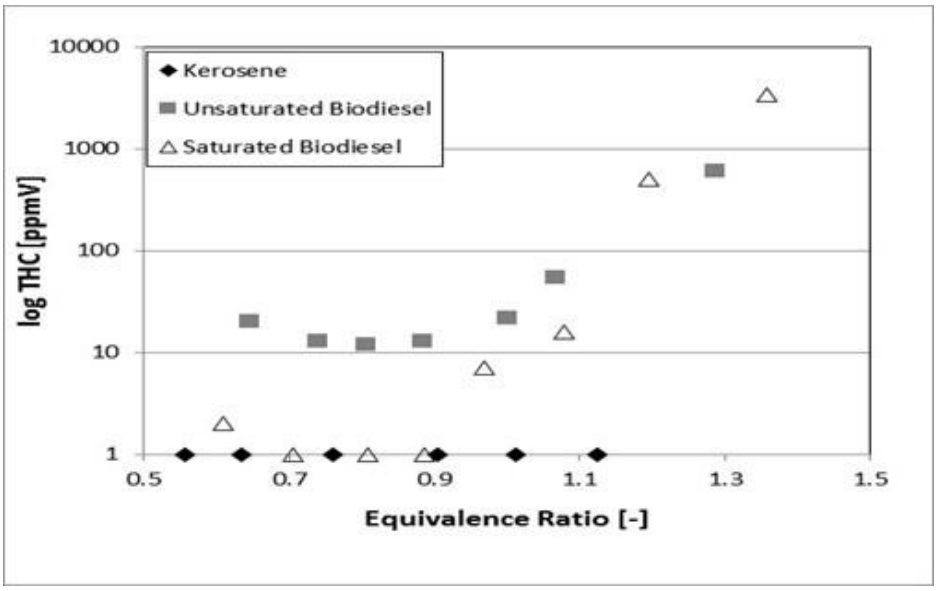

Figure 4-6 THC exhaust gas concentration (dry) as a function of equivalence ratio for kerosene and the two biofuels at atmospheric pressure.

4.3.3.2 O_2 emissions

O_2 concentration as a function of equivalence ratio under atmospheric conditions is presented in figure 4.7. This parameter is based on the measured fuel and air flow rates through the burner and the gas analysis. The measurement of oxygen and CO allowed for the identification of the near stoichiometry operating point. Among all fuels can

be seen different tendencies, with the unsaturated blend showing the maximum O_2 concentrations due to additional oxygen in the bio-blend.

However, the saturated biodiesel presented the lowest trend, which has been attributed to the existence of solid carbon-based particles present in the liquid fuel; therefore, more oxygen was necessary per unit mass of fuel burn because of a much greater average carbon composition.

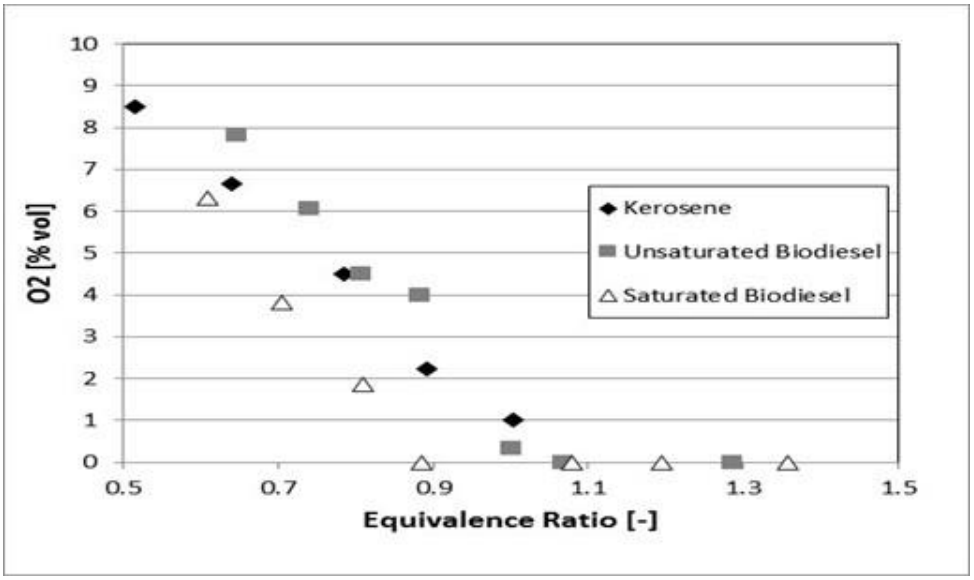

Figure 4-7 O_2 exhaust gas concentration (dry) as a function of equivalence ratio for kerosene and the two biofuels at atmospheric pressure.

4.3.3.3 CO_2 emissions

CO_2 emissions as a function of equivalence ratio for the kerosene and biofuels tested under atmospheric conditions are shown in figure 4.8. Compared to the kerosene, biofuels behaviour has a difference showed the peak CO_2 values at higher concentrations of the bio-blends.

Apparently, the biofuels made slightly more CO_2 than the kerosene under similar air flow rates, which is probably caused by the higher carbon to hydrogen ratio in the heavier fuels [50].

There is more CO_2 in the saturated fuel as expected because of the additional reactions of the solid particles; at higher pressures, this was also the case with this work [55]. These changes are relatively very small, therefore under these conditions, the results can be considered to be within the experimental uncertainty of the measurement.

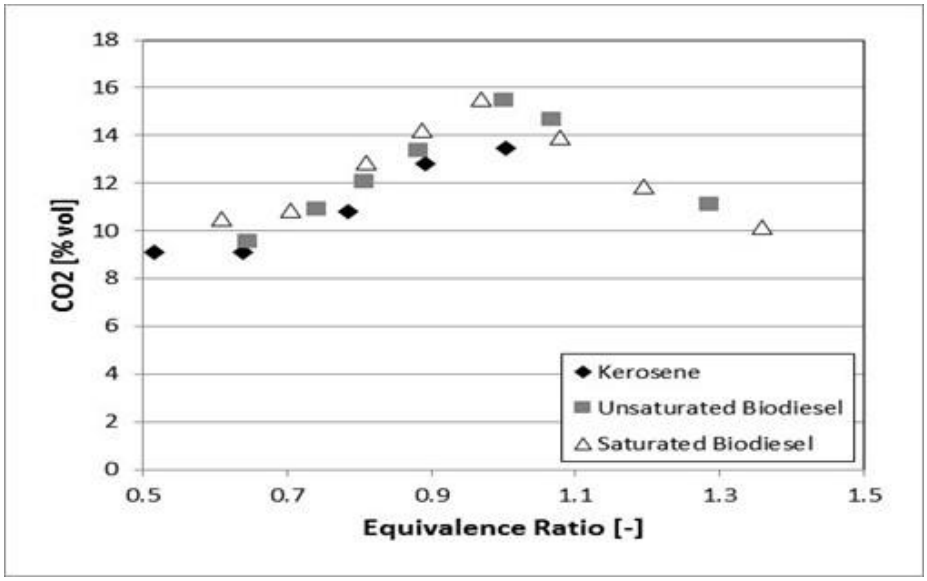

Figure 4-8 CO_2 exhaust gas concentration (dry) as a function of equivalence ratio for kerosene and the two biofuels at atmospheric pressure.

4.3.3.4 CO emissions

CO emissions as a function of equivalence ratio for the kerosene and tested biofuels under atmospheric conditions are shown in figure 4.9.

Incomplete combustion leads to CO emissions. At atmospheric and elevated pressure, results demonstrated that CO emissions are reduced with the biodiesel, probably as a consequence of the fuel-bound oxygen in the molecule which starts reacting further downstream than the oxygen contained in the airflow [50].

Relatively, the saturated biodiesel also showed lower CO concentrations, in some points even lesser than the unsaturated biodiesel [48, 49]. Although low emissions were predictable under lean equivalence ratios, there were three particular points, figure 4.9, which showed the highest production of the CO molecule while using kerosene and pure biodiesel.

Experimental trials showed highly changing patterns for these conditions indicating a lean blue flame zone close to the nozzle followed by a red-orange crown at the end of the flame, figure 4.5. Likely caused by the particular fluid conditions at these equivalence ratios which cooled down the flame to a point wherein some of the droplets were not completely consumed during the combustion process, thus reaching the end of the flame and making CO peaks.

Contrary to these cases, the biodiesel appears to be burning with low CO production under these conditions; it is believed that a process related to the saturated particles boost heat transfer at the bottom of the flame. It is known that these conditions will not be similar under higher pressures as the flame would retreat and faster reactions would take place at the bottom of the flame [18, 27].

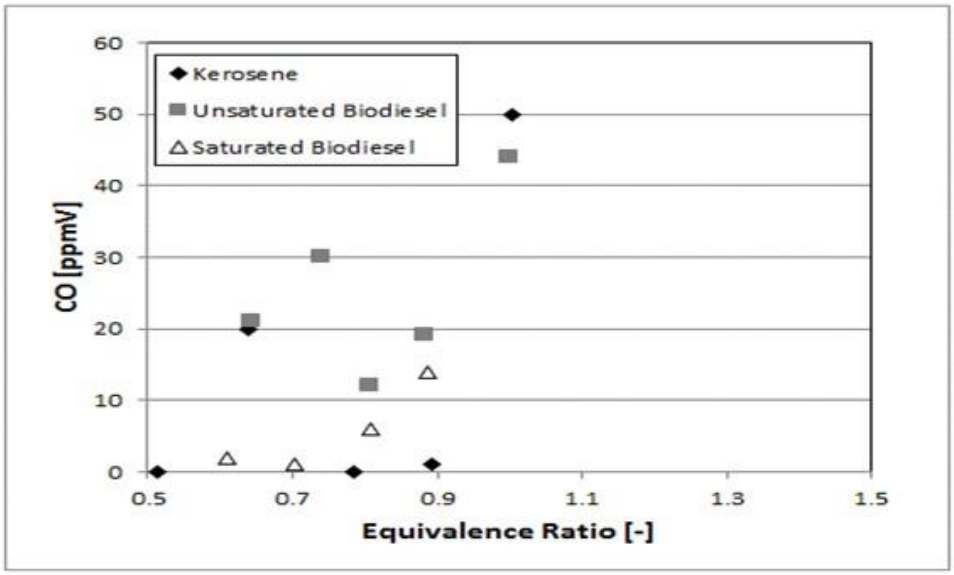

Figure 4-9 CO exhaust gas concentration (dry) as a function of equivalence ratio for kerosene and the two biofuels at atmospheric pressure.

4.3.3.5 NOx emissions

NOx emissions as a function of equivalence ratio for the kerosene and tested biofuels under atmospheric conditions are shown in figure 4.10.

NOx emissions boosted with increasing equivalence ratio towards stoichiometric conditions as the results indicate. Higher NOx emissions were produced by the saturated and unsaturated biodiesels than kerosene at all pressures [55].

Probably that higher NOx emissions from the biodiesels were correlated to a greater CH formation leading to induce NOx via CH+N→HCN reactions, as observed by others [141]. Furthermore, the greater temperature of reaction produced by the additional oxygen and enhanced combustion in the saturated biodiesel could also lead to higher Zeldovich emissions (thermal NOx).

Opposite to the experimental results, atomization performance was thought to be a parameter that would control the resultant NOx concentrations. For the bio-blends, as

reduced spray angle and bigger droplet size [57] would result in the fuel remaining unburned for longer periods of time and greater axial distances, decreasing NOx by a reduction in the combustion efficiency, burning more downstream to accomplish the reaction.

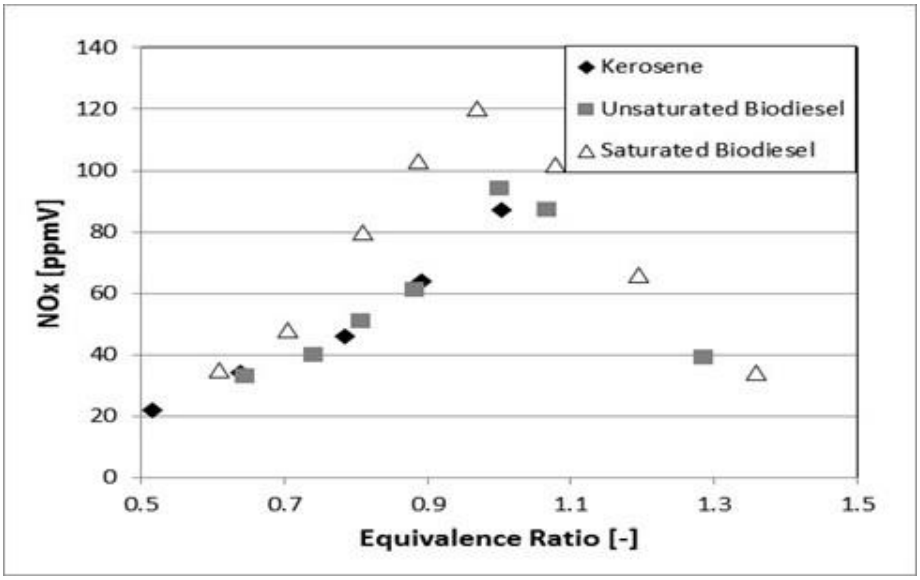

Figure 4-10 NOx exhaust gas concentration (dry) as a function of equivalence ratio for kerosene and the two biofuels at atmospheric pressure.

Both kerosene and the unsaturated biodiesel produce lower NOx emissions when compared with the saturated biodiesel, a phenomenon that could be associated with the content of nitrogen in the organic material carried by the saturated blend [54]. Moreover, solid particles showed traces of a more efficient combustion regime, i.e. lower CO and higher CO_2. Thus higher temperatures and augmented Zeldovich NOx.

It was also detected that NOx emissions are reduced significantly at higher pressures if the effect of pressure on NOx concentration is taken into consideration, with a peak of 120 ppm under atmospheric conditions decreasing to 25ppm at 2.9 bars for the saturated biofuel blend. Meanwhile, the power requirements for all cases are similar at 40 KW. It is believed that the high pressure forces the flame to retract towards the burner, compacting it and improving combustion and reactivity.

4.3.4 Chemical equilibrium calculations

By using GASEQ, the measured gas compositions were related to chemical equilibrium calculations as shown in table 4.3.

Pressures utilised for the analysis were 1, 10 and 100 bar with the purpose of clearly showing the progression of species with increasing pressure. Methyl-formate ($C_2H_4O_2$) was used as an alternative molecule linked to larger methyl esters [50, 52]. OH, radical has decreased at higher pressures as shown in the results.

The largest changes were detected in the evolution of hydrogen and oxygen towards the formation of complete combustion molecules, for instance, CO_2 and H_2O. Surprisingly, NO shows an acute decrease at higher pressures.

Although, temperatures are higher with the lack of oxygen in the blend that limits the production of NO. Furthermore, it is believed that OH radical formation is prevented by pressure, as discussed later.

Table 4-3 GASEQ equilibrium analyses. Molar fraction and adiabatic temperature of the flame.

Molecules	Pressure 1 bar	Pressure 10 bar	Pressure 100 bar
N_2	0.64381	0.64698	0.64927
H_2O	0.16593	0.16904	0.17109
CO_2	0.15452	0.16165	0.16674
CO	0.01704	0.01071	0.00617
O_2	0.00779	0.00456	0.00239
OH	0.00416	0.00256	0.00142
H	0.000481	0.000159	0.0000459
O	0.000372	0.000127	0.0000365
H_2	0.00332	0.00196	0.00109
NO	0.00258	0.00223	0.00176
Adiabatic Flame T	2272K	2331.6K	2372.4K

4.3.5 OH* Chemiluminescence analyses

Studies in OH* chemiluminescence were performed for all conditions. Comparisons between biofuels were carried out to detect the progression of OH* radicals at different pressures, as shown in figures 4.11 and 4.12. Abel inversion was applied to create intensity maps normalised by the greatest luminosity peak.

The highest pixel level for all the images shown here is used to set a nominal maximum luminosity, and all of the results are measured on this, which permits for a more accurate comparison of global intensity.

Apparently, results show a significant quantity of OH radicals at low pressure in the region where the swirling flame is placed. A significant difference between blends was observed at a high pressure, as shown in figures 4.11b and 4.12b. OH* production for

the unsaturated biodiesel has decreased, reducing the reaction zone length of this radical and thus chemiluminescence intensity, a phenomenon produced by the retraction of the flame and greater density as an outcome of increased downstream pressure.

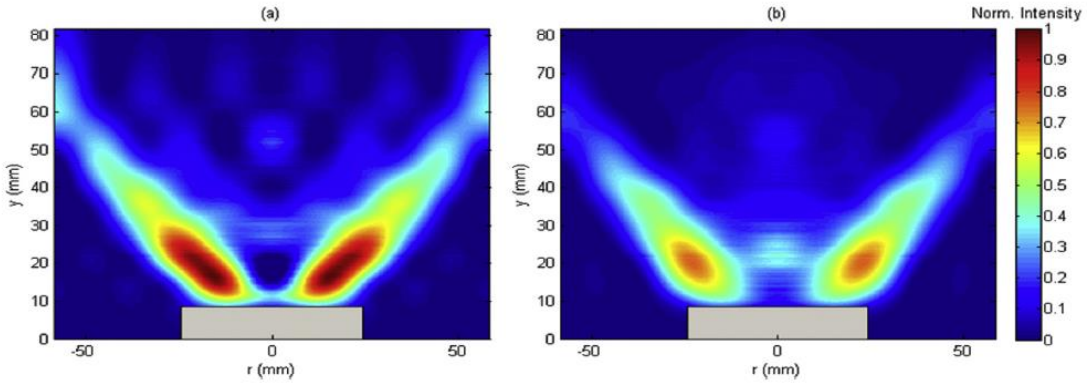

Figure 4-11 Abel inversion for OH* chemiluminescence for the Unsaturated biodiesel E.R. 0.550 at a) 1.9 bar, and b) 2.9 bar. The burner outlet is denoted as the grey rectangle at the bottom of the figure.

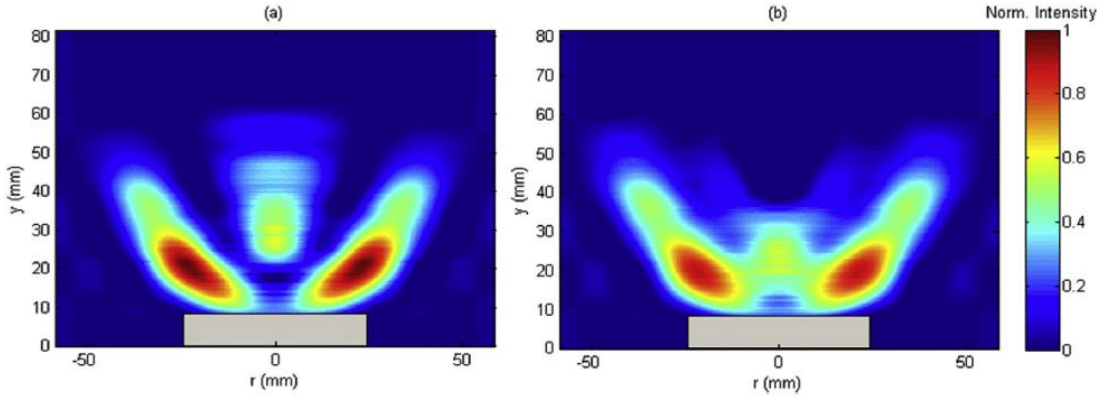

Figure 4-12 Abel inversion for OH* chemiluminescence Saturated blend E.R. 0.581 at a) 1.9 bar, and b) 2.9 bar.

However, the saturated mixture kept showing OH* intensity profiles similar to those observed at lower pressure, as shown in figure 4.12. From these results, some conclusions can be withdrawn; it looks as if oxygen from the biodiesel was reacting quicker than oxygen from the air when solid matter is existing in the fuel.

The changes in OH* intensity in the unsaturated biofuel at various pressures brought this assertion. Greater pressures mean higher densities, thus further air adjoining the flame leading to more OH* dilution, of a process driven by the surrounding atmosphere. However, since the OH* intensity in the saturated flame is similar at

various pressures, it is clear that the OH* production has been kept almost constant from a source independent of downstream conditions, i.e. pressure, with minor dilution effects at the OH* release location.

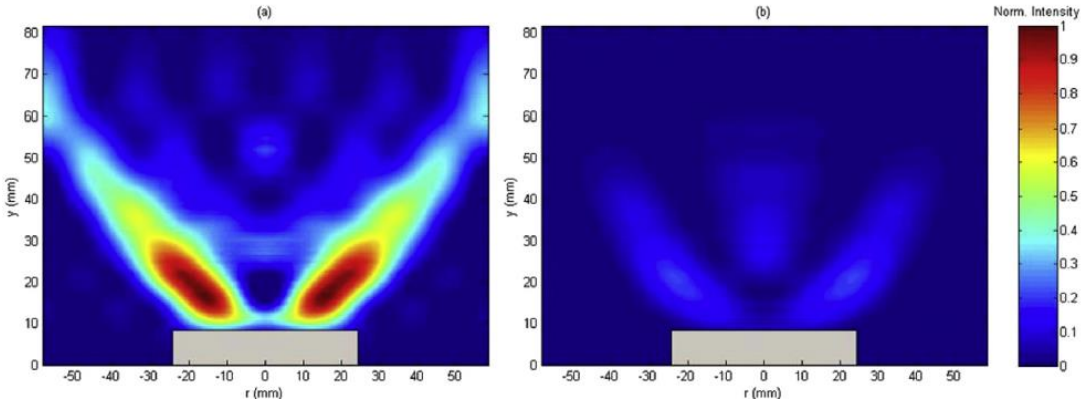

Figure 4-13 Abel inversion for OH* chemiluminescence at the same pressure (1.9 bars) and stoichiometry (~0.58). A) Unsaturated blend; B) Saturated blend.

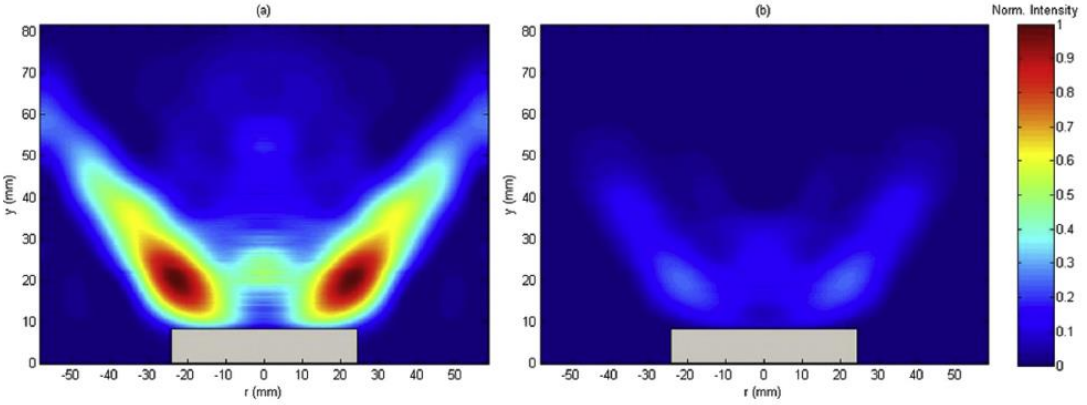

Figure 4-14 Abel inversion for OH* chemiluminescence at the same pressure (2.9 bars) and stoichiometry (~0.59). A) Unsaturated blend; B) Saturated blend.

An additional comparison was carried out between the different fuels at a similar pressure, figures 4.13 and 4.14. The unsaturated blend shows a significant increase in the OH* projections to those observed in the saturated biodiesel.

These changes emphasise the development of other species overtaking OH* production in the saturated blend more downstream of the burner nozzle. It can be concluded from other works [141] that CH production has been promoted for the saturated mixture which shows the highest NOx formation.

So, it can be deduced that solid matter in the fuel also acts as a catalytic substance for the production of other radicals. Although the particles keep forming CH radicals

downstream of the flame zone that augment NOx formation, at low equivalence ratios the use of these catalytic particles also increases fuel-bound oxygen reactions that remain almost unaltered at higher pressure. These properties could contribute to the improvement of combustion, wherein lead to a good fuel candidate at lean conditions.

Unluckily, visual notes showed that saturates would produce higher soot emission at the present concentrations, reducing the applicability of this particular fuel for gas turbines. Nevertheless, if the proper amount of particles in the biofuel is accomplished to reduce effects on materials and components noticeably, these particles could be an effective mechanism to improve gas turbine combustion at low cost.

4.4 Summary

Different fuels, kerosene and a biofuel in saturated and unsaturated form, were experienced to link the relative performance of the saturated biodiesel for gas turbine applications. It was detected that injection patterns are less likely to deliver efficient droplet breakup and atomization due to higher viscosity and surface tension in the saturated biodiesel.

Results showed that use of the saturated blend would be a product in higher NOx concentrations in the exhaust with less oxygen and CO emissions. Furthermore, the saturated solid organic compounds seem to have a catalytic effect to increase radical production downstream of the flame zone, thus increasing quick NOx formation. These mixtures also appear to be enhancing the production of OH radicals through reactions with the oxygen embedded in the fuel, thus increasing temperature even further with a related production of nitrogen oxides.

It has been shown that the perfect operability region for the saturated biodiesel is at very lean conditions and that under these situations its measured exhaust gas concentrations are comparable with the unsaturated biodiesel fuel. However, visual observations presented that saturates at these concentrations will incline to produce higher soot emission, reducing the applicability of the fuel for gas turbines.

Moreover, this research needs of further research to show in the future to improve combustion so the present research could be extended by adding biofuel preheating to

provide lower viscosity and then enhance atomization, along with higher injection pressures to be used for spraying the saturated biodiesel.

One of the main contributions of this thesis is focusing on two-phase flows by studying liquids and gaseous combinations for different alternative fuels using a swirl burner. Next evaluating emissions, CH*, temperature profile and stability. In this chapter, a comparative study between kerosene, and biodiesel was performed to understand the conclusion of using liquids fuels in a gas turbine and in particular the behaviour of biodiesel. Also, examine the application of saturated biodiesels in gas turbines for power generation and check if this type of fuel is appropriate to operate in a gas turbine. So, in next chapter (chapter five), experimental studies of alternative gases fuels using a 20 kW swirl burner were achieved to understand the conclusion of using gases fuels in a gas turbine.

Chapter 5

Emissions reduction by using different blends and various conditions under premixed combustion

Any sufficiently advanced technology is indistinguishable from magic

Arthur C. Clarke

5.1 Introduction

Increasing concern in alternative fuels for gas turbines has motivated research in gaseous fuels further than natural gas. Methane-enriched with hydrogen or diluted with carbon dioxide are of considerable interest. The latter seems quite relevant for the development of technologies such as oxyfuel combustion with CO_2 recirculation for carbon capture and storage to control temperatures in the combustion chamber.

The primary goal of introducing CO_2 into the gas turbine combustors is the reduction in emissions such as NO_X. That is achieved by cooling the flame. Thus the Zeldovich mechanism can be reduced [40]. Moreover, the use of CO_2 from carbon capture and storage facilities could reduce costs also capture equipment further downstream the combustion zone [41].

Also, the CO_2 injected through the premixed blend will decrease the reaction rate, thus lessening the temperature. The great temperature of the CO_2 in the CRZ will ensure a fast chemical reaction of the diluted reactants, thus permitting a stable regime with low NO_X and CO.

Thus, this chapter showed a trial study on the combustion of methane-carbon dioxide blends at atmospheric conditions. Gas combinations have been examined by using different levels of premixing with various injection methods with and without central injection and with and without swirl.

Moreover, an experimental study on the combustion of methane and methane-carbon dioxide with different conditions was achieved for the same burner, where the holes around the burner were closed by a premium black fire cement material that is a

smooth paste which sets rock hard when exposed to the air. Fire cement has excellent adhesion to most metals.

A 20 kW burner has been used to examine the flame stability, and emissions show by using these mixtures to consider the effect of CO_2 addition. The burner configuration consisted of a central body with an annular, premixed gas/air jet introduced through five, 60° swirl vanes.

A TESTO 350XL gas analyser was utilised to acquire NO_X and CO emission and other emissions concentration trends to characterise all the injection regimes while using different fuel blends. CH chemiluminescence diagnostics was also used and correlated with the levels of emissions produced during the trials.

The temperature distribution was examined for different heights from the burner outlet for the effect of CO_2 addition, equivalence ratio and different injection regimes. The resulting images were analysed using Photron FASTCAM PFV ver 2.4.1.1 software and MATLAB R2015a.

5.2 Experimental setup

5.2.1 Swirl burner and flow delivery system

An axial swirling flame burner was utilised to establish continuous swirling flames. The schematic of the swirl burner and the flow delivery system is shown in figure 5.1, while the placement position of swirler at the burner outlet is provided in figure 5.2. The swirl burner was used, in this experiment, consists of an axial swirler and a circular stainless steel tube placed as illustrated in figure 5.1.

The swirler is positioned concentrically into with the inner tube of the burner. It involves of five straight swirl vanes with a thickness of 1.5 mm each (figure 5.3). The swirler vanes are manufactured to be at the angle of 60° from the axial centerline axis.

The outside diameter of the swirler is 50 mm, while the swirler hub diameter is 10 mm (table 5.1). The geometrical swirl number, S is established on the following equation [150]:

$$S_N = \frac{2}{3}\left[\frac{1-\left(\frac{D_h}{D_s}\right)^3}{1-\left(\frac{D_h}{D_s}\right)^2}\right]\tan\theta \qquad (5.1)$$

Where D_h and D_s represent the swirler hub diameter and the swirler diameter, respectively, and θ is the vane angle orientation from the centre line axis. The calculated swirl number for the present burner was 1.2. This strong swirl permits the formation of a recirculation zone that recirculates hot products and assists in flame stabilisation [151]. Two methods of injection were used, one through the centre via a central injector, and one through the outer, primary premixed zone, figure 5.2.

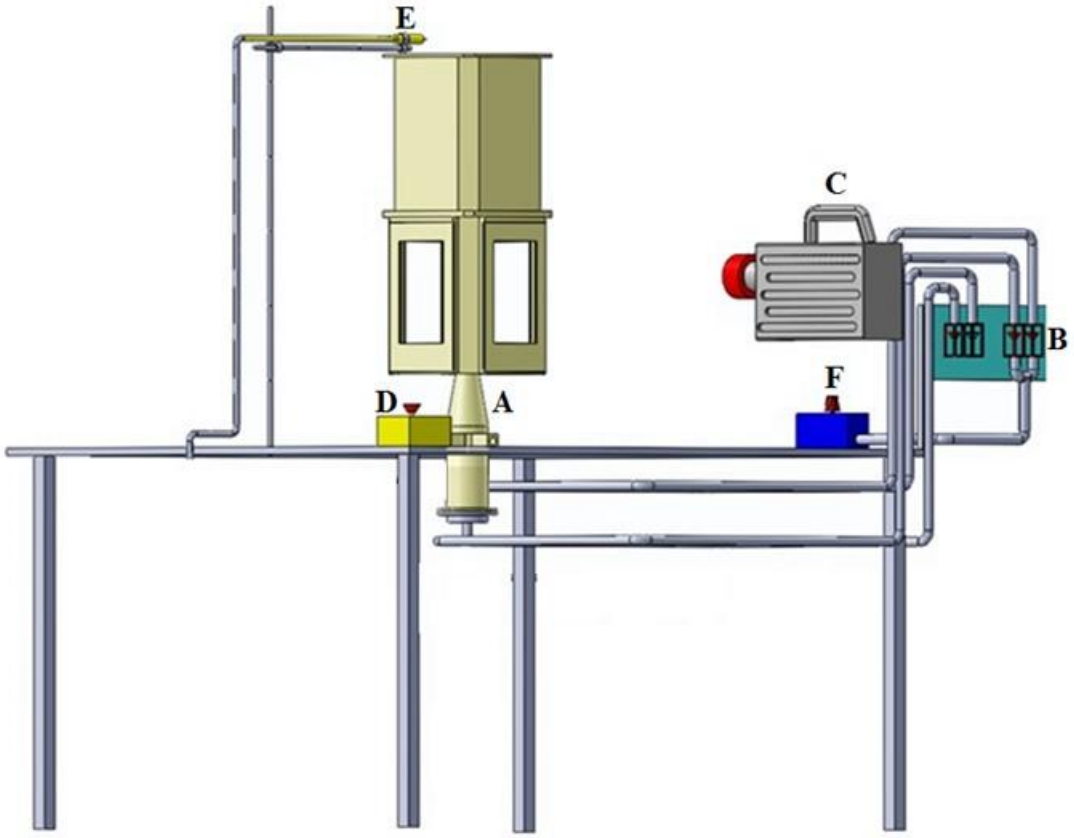

Figure 5-1 Generic swirl burner with Accessories. A - Swirl burner; B – Rotameters; C – High-speed camera; D – Emergency button; E – Pilot burners; F – Air regulator.

For flow delivery of methane and carbon dioxide, the gases were supplied and regulated via Platon glass Variable Area flowmeter and Platon NGX series glass. Variable Area with an accuracy of ± 1.25%, while air was supplied and controlled via

Platon glass, Variable Area flowmeter and Platon NGX series glass Variable Area with an accuracy of ±5% and ±1.25%, respectively.

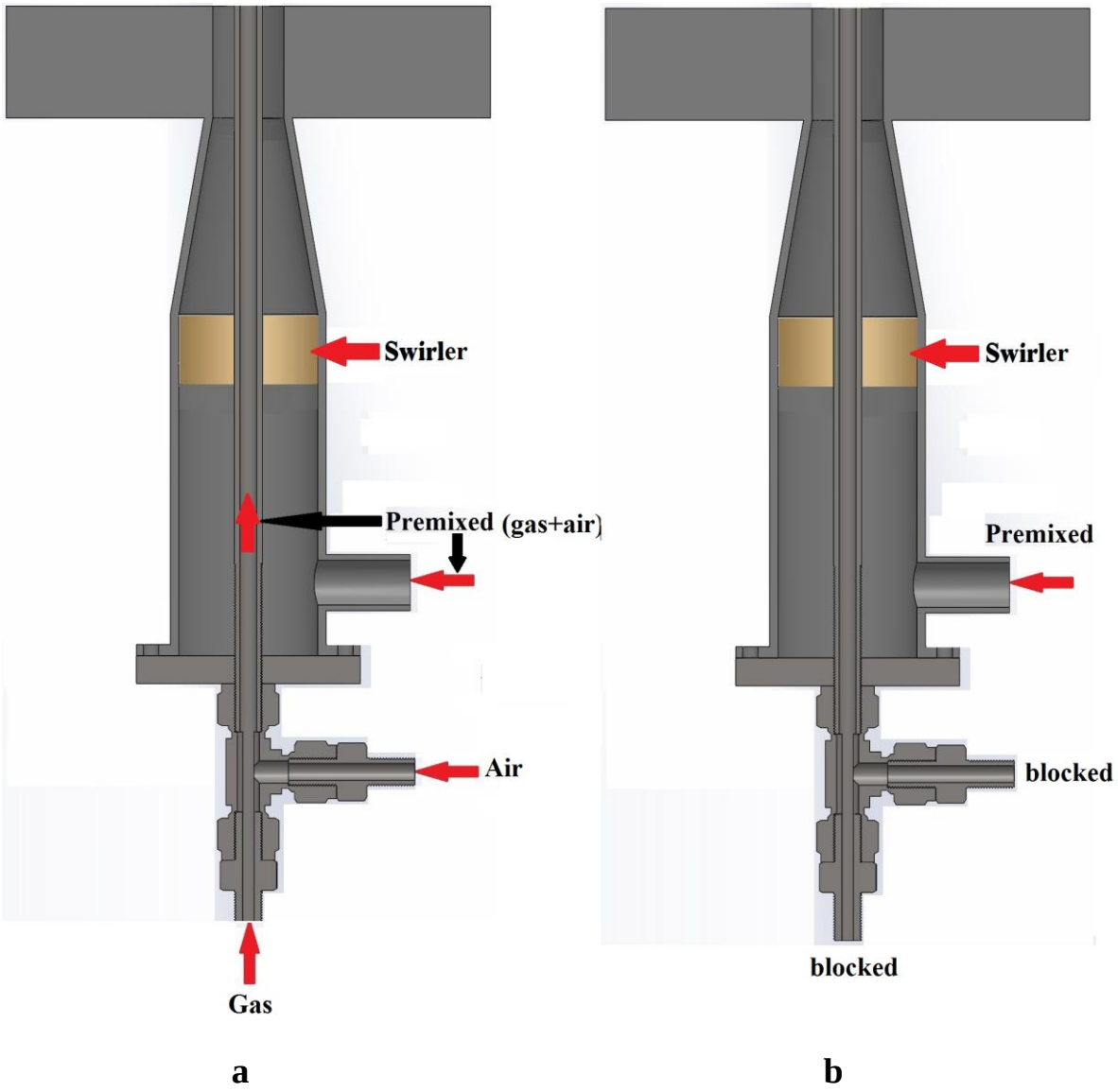

Figure 5-2 An example of a schematic burner and swirler a-open holes, b-closed holes

Gases and air for central and outer parts were premixed together in separate tubes to certify sufficient mixing before inflowing the burner. A pilot ignitor was used to burn the flame as shown in figure 5.1.

The rectangular combustion chamber has four quartz windows, providing full visual access to the combustion zone. The combustion chamber width and height are 118 mm and 410 mm, respectively. Details of the burner geometry are shown in table 5.1.

Moreover, the same burner was used without using the central injection and the flow delivery system is shown in figure 5.2b. The burner was operated with different power, compared with the first trials because all holes around the burner had closed by cement material.

Figure 5-3 Axial swirler.

Table 5-1 The geometry of axial swirl flame burner and relevant burner dimensions [mm].

Air swirler	
Material	Stainless steel
Type	Axial, straight vane
Swirl number, SN	1.2
Swirl angle, θ (°)	60
Number of blades	5
Blade thickness, *t* (mm)	1.5
Burner wall	
Material	Stainless steel
Width (mm)	118
Height (mm)	410
Burner geometry	
Burner outer diameter, Ds (mm)	50
Burner central diameter, Dh (mm)	10
Burner inner central diameter, d (mm)	6

5.2.2 Operating conditions

The rig was set up with two inputs of premixed air and gas for different blends as shown in figure 5.4. The central supply allowed a central diffusion flame to first ignite and stabilise combustion with the ability to provide larger amounts of methane and air to create a premixed flame and to compare different injection strategies by changing the central supply as shown in table 5.3. A larger external premixed supply was then used to demonstrate turbulent, fully premixed flames.

Rotameters controlled both the air and blends so their respective quantities could be monitored and altered. The system incorporates three solenoids that only allow combinations to pass once the system is stabilised.

CH_4 was blended with CO_2 as diluents impacts were investigated. Table 5.2 displays all tested mixtures. The influence of CO_2 as diluent on the emissions has been studied by incrementally addition CO_2 from 0% to 15% and 30%.

The combinations for all cases were supplied by cylinders that contained CO_2 already mixed with CH_4 at the required percentages. Several injection strategies were tracked to notice in what way the increase of central and outer injection affected the flame and decrease/increase NOx and CO emissions.

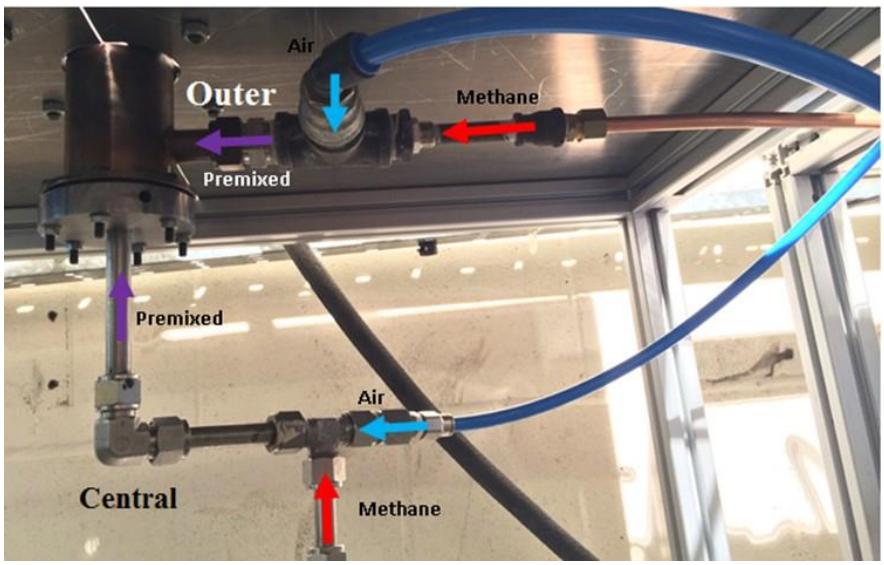

Figure 5-4 Premixed inputs of blends and air utilising the venturi effect to allow initial testing with gaseous fuel.

A TESTO 350XL gas analyser was used to measure NOx and CO and other emissions to characterise all the injection systems while using changed fuel mixtures. CH chemiluminescence diagnostics was studied and connected to the stability of each case. It was not likely to work under lean conditions using B2 and B3, table 5.2, as blowoff would happen. Thus, rich conditions were imposed for these combinations.

Table 5-2 Blend mixtures composition (vol. %)

Mixture	CH_4	CO_2
B1	100	0
B2	85	15
B3	70	30

Table 5-3 Injection strategies

strategies	Outer injection	Central injection
S1	Yes premixed	Yes premixed
S2	Yes premixed	NO
S3	Yes premixed	Yes diffusion

For the case of only the outer injection was used, where the central injection was not used as shown in figure 5.6 and it would be work, with different power compare with the first case, because all holes around the burner had closed by cement material to avoid a liquid leak. As a part of the preparation for the burner to work with various liquids and gases blends as a next step (chapter 6).

The rig was set up with two inputs of premixed air and gas for different combinations as can be realised in figure 5.5. The central supply was blocked to use it with liquid later by putting the Delevan nozzle at the end of the central pipe.

An external premixed supply was used to demonstrate turbulent, fully premixed flames, ignite and stabilise combustion with the ability to provide larger amounts of methane or blends and air to create a premixed flame and to compare different condition. Table 5.4 shows all experienced combinations. The effect of CO_2 as diluent on the emissions has been studied by incrementally adding CO_2 from 0%, 5%, 10% and 15%.

It was not possible to work with higher than 15% percent with new conditions of CO_2 as blowoff would occur and ignition was hard to achieve.

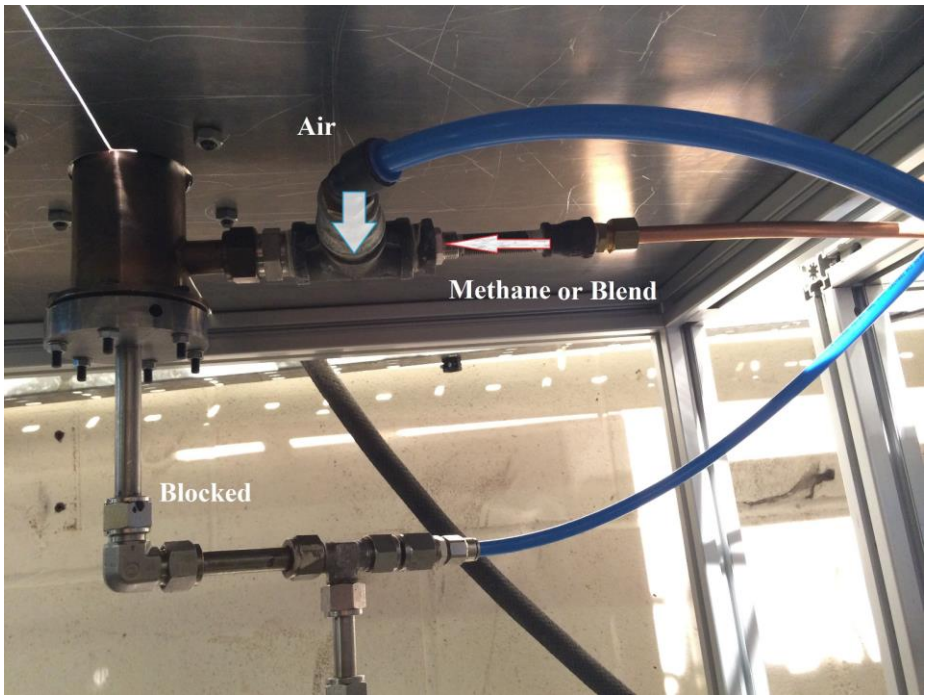

Figure 5-5 Premixed inputs of combinations and air utilising the venturi effect to allow initial testing with gaseous fuel.

Table 5-4 Blend mixtures composition (vol. %)

Mixture	CH_4	CO_2
D1	100	0
D2	95	5
D3	90	10
D3	85	15

5.2.3 Blowout limits

The injection of CO_2 seems to have a significant influence on the blowout limit. The increase in carbon dioxide displays the movement and progression of the boundaries of this instability, dropping the resistance of the flame as the diluent is augmented.

The higher the CO_2 flow rate, the higher the equivalence ratio at which blowout occurs. By gradually increasing the air flow rate of an established flame until the flame blows out. Comparison of the blowout limit of methane against the blends was performed.

The blowout phenomena, often regarded as the upper stability limit of combustors, occurs when the flame detaches from its location and physically blows off [152].

5.2.4 Equivalence ratio calculation method

Stoichiometric combustion reactions for methane, methane - carbon dioxide and gas mixtures, based on methane gas, can be written as follows:

$$CH4+2\cdot(O2+3.76\cdot N2)=CO2+2\cdot H2O+2\cdot 3.76N2 \quad (5.2)$$

$$CH4+k\cdot CO2+2\cdot(O2+3.76\cdot N2)=(k+1)\cdot CO2+2\cdot H2O+2\cdot 3.76\cdot N2 \quad (5.3)$$

Wherever k is the molar fraction ratios of additional gas in methane:

$K = XCO2/XCH4$

Stoichiometric air-fuel ratios (AFR) of methane, methane - carbon dioxide is calculated as,

$$AFR_{st}^{CH_4}=\frac{2\cdot(M_{O_2}+3.76\cdot M_{N_2})}{M_{CH_4}} \quad (5.4)$$

$$AFR_{st}^{CH_4\text{-}CO_2}=\frac{2\cdot(M_{O_2}+3.76\cdot M_{N_2})}{M_{CH_4}+k\cdot M_{CO_2}} \quad (5.5)$$

The mass flow rate of the gas blend and the air is measured, and the equivalence ratio is calculated from the formula:

$$ER=\frac{AFR_{st}}{\dot{m}_{air}/\dot{m}_{fuel}} \quad (5.6)$$

5.3 Results and discussion

5.3.1 Flame imaging

The gained flame images of CH* chemiluminescence were averaged and investigated via a Photron FASTCAM PFV Ver.3670 software and MATLAB R2015a, to acquire the planar flame structures and to study the flame appearance of methane and for the blends without and with swirl under various equivalence ratios for different injection regimes.

Figure 5.6 displays three sets of flame images with a swirl; each image represents average results out of 1000 images.

Imaging shows the radiation from the B2 flame is considerably different compared to methane and another blend. Methane flame demonstrates large CH* intensity peak at the axial profile.

The CH* concentration reduced at the further downstream axial location at equivalence ratio =1.6. A similar tendency was observed for 70%/30% Methane/CO_2 swirl flames respectively.

The high CH* intensity profiles for these blends is attributed to an inadequate mixing and lower OH* reactivity compared to combine B2, thus more production of soot and CO.

The figure shows that methane and B3 flame displays a relatively large area with high-intensity signals especially at equivalence ratio =1.9, B1-S3 and B3-S3 at the main post-reaction zone region.

B2-S2 represents the most stable flame; the post-reaction zone presented little luminosity at the downstream post-reaction zone of the flame, indicative of clean combustion with the low level of soot formation relatively.

The high CH of the post-reaction zone region for methane flame is reflected in the high-intensity count. However, the high luminosity of the post-reaction zone region for B3 blends is attributed to that small increase of CO_2 in the mixture seems to be acting as a supporter of better combustion, dropping the competition of reacting species for oxygen.

But, this phenomenon stops at higher CO_2 concentrations which cause combustion only at the tip of the burner and suffering from ignition will appear.

Increasing the equivalence ratio rises luminescing downstream of the initial reaction, as shown in figure 5.6 for S1 and S3, respectively.

The typical high-temperature environment under fuel-rich conditions increases the concentration formation of C/H radical, that would lead to the creation of acetylene and propargyl creation which are significant precursors for soot formation [135, 136].

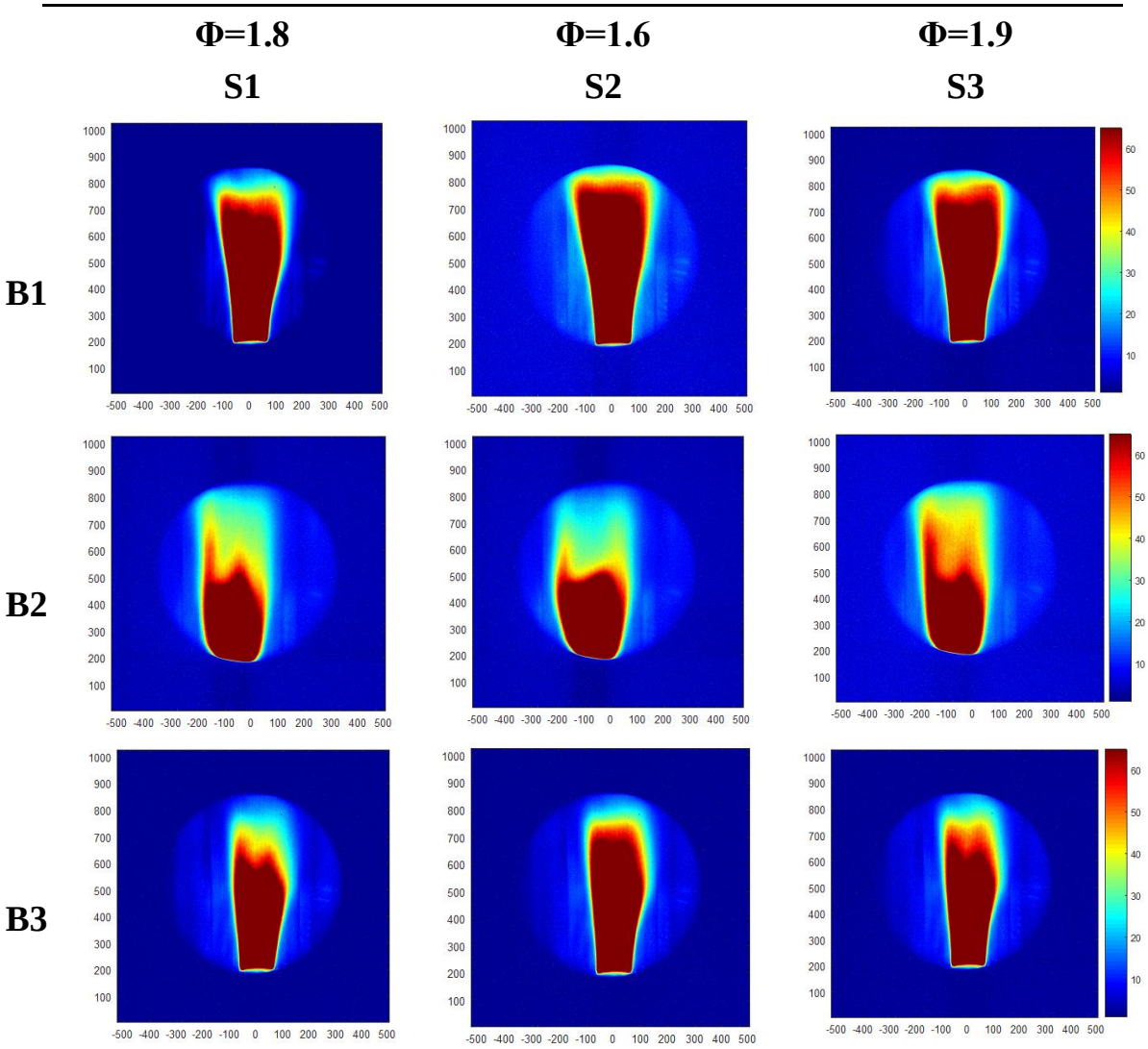

Figure 5-6 Abel inversion for CH* chemiluminescence of swirl gas mixtures at different equivalence ratios for various injection regimes.

Direct flame imaging was achieved to observe the flame appearance of methane and for the blends under various equivalence ratios for the case of closed holes. A digital camera (Nikon; Model D7200) was used to image the global flame appearance of blends swirl flame established at different equivalence ratios through the optically accessible quartz wall.

Figure 5.7 shows four sets of blends flame images, case D1, D2, D3 and D4 established at a constant composition of 0%,5%,10% and 15% CO_2 respectively. Bluish flames were observed because of the intense heat reaction zones. The fuels chemically react in this region under enough oxygen, leaving no unburned hydrocarbon for post-flame reaction or soot formation. Increasing the equivalence ratio to near stoichiometric

region results, in the luminous orange-yellow region downstream of the primary reaction zone. Visible orange-yellowish post flames are revealing of soot formation.

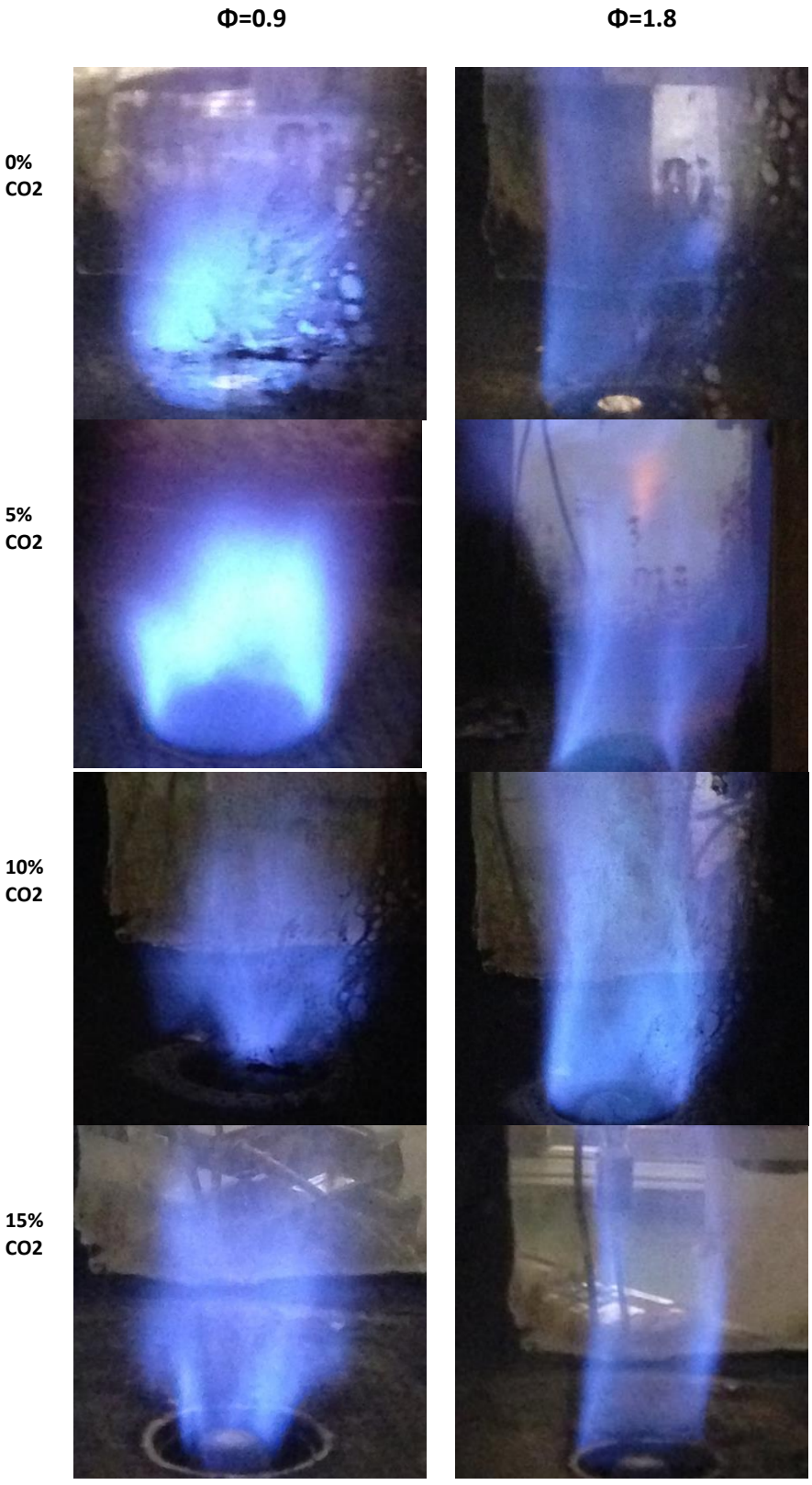

Figure 5-7 Global flame images of methane and different blends at various equivalence ratios.

The luminous post-flame region is evident for the fuel-rich mixture, as shown in figure 5.7 for baseline and different blends. The typical high-temperature environment under stoichiometric or fuel-rich conditions increases the concentration of vapour consisting of combustion product of H_2 component, e.g. H_2O, and formation of C/H radical play a significant role in the production of acetylene and propargyl formation which are essential precursors for soot formation [153, 154].

It is observed that 10% CO_2 blend (D3) shows less luminous post-flame region compared to other blends and methane under same equivalence ratio, which shows the lower trend for soot formation for the former as a result of reduced availability of C radicals. Moreover, the burning intensity is increased while the primary reaction zone length is decreased, as it is evident across the D3 flames.

5.3.2 Exhaust gas analysis

5.3.2.1 NOx emissions

Figure 5.8 shows the difference in the level of NOx emissions as a function of equivalence ratio with altered injection systems with and without swirl for all different blends.

The diluents of CO_2 for all the cases were supplied by cylinders that have CO_2 already mixed with CH_4 at different diluent ratios as shown in table 5.2.

Overall, all equivalence ratios tested presented a declining trend as the CO_2 diluent ratio rises from 0 to 30%. The lesser NOx can be attributed to the thermal effects of CO_2 dilution. The thermal effect decreases the flame temperature and thus the thermal NO [41].

CO_2 diluent lowers the adiabatic temperature due to its greater specific heat, which would result in a substantial reduction in overall burning rate via absorption of heat from the combustion process [155]. Dropping the flame temperature caused less NOx to be emitted, concurring with the thermal NOx formation mechanism [41].

The addition of diluent to the air stream too caused a matching decrease in oxygen mole fraction. So, the flame temperature and the mole fractions of H, O, and OH

radicals were reduced. For the chemical effect, the addition of diluents decreased N and HCN mole fractions and subsequently reduced the prompt NO [156].

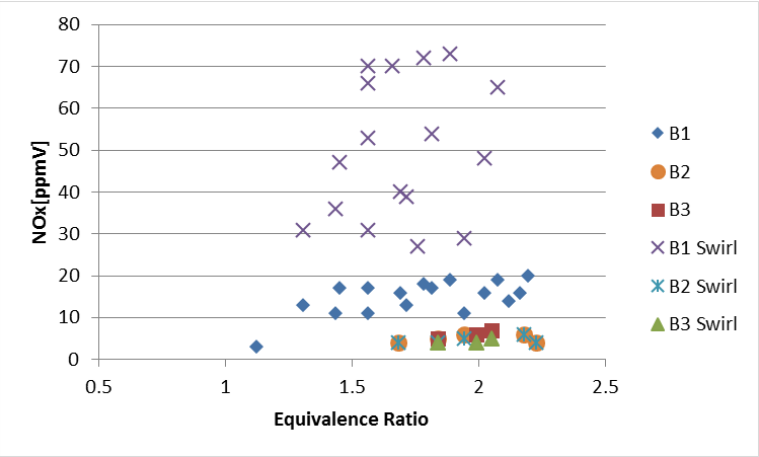

(S1)

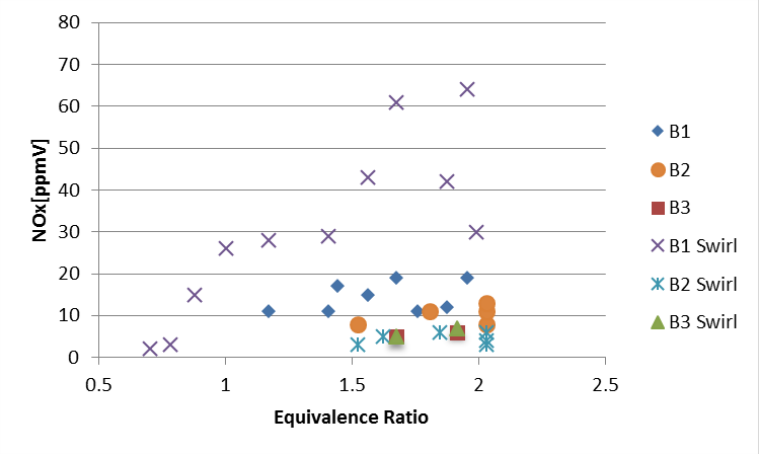

(S2)

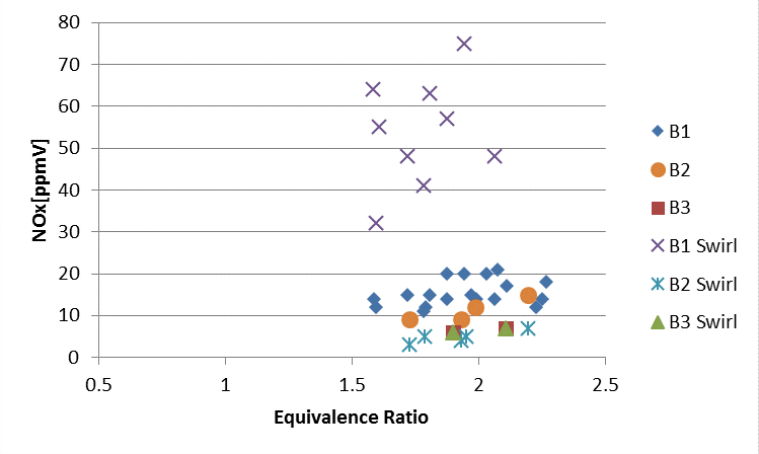

(S3)

Figure 5-8 NOx exhaust gas concentration (dry) as a function of equivalence ratio for B1, B2 and B3 for different injection regimes with swirl and without swirl.

Regarding injection approaches an external injection system using swirling vanes and no central injection (S2) has created the cleanest profiles, as predictable. About the other circumstances (S1, S3) the fuel is introduced out of the central injector; and as such it has single an axial velocity component that would cause a decrease in the swirl number.

For all blends, the trend is similar with low equivalence ratios showing the lowest NOx. Surprisingly, B3 with and without swirl produced the same NOx consequences. As before stated, this is an effect of the increase in a CO_2 diluent, thus decline of thermal NOx formation.

Further analyses will be achieved regarding CO for this blend. For pure methane, (B1), emissions are comparatively higher across all ranges of equivalence ratios, as expected [26].

Figure 5.9 gives the difference in the level of NOx emissions as a function of equivalence ratio for all different blends for the case of using only the outer injection with the holes around the burner were closed. The CO_2 dilution for all the cases was provided as shown in table 5.4.

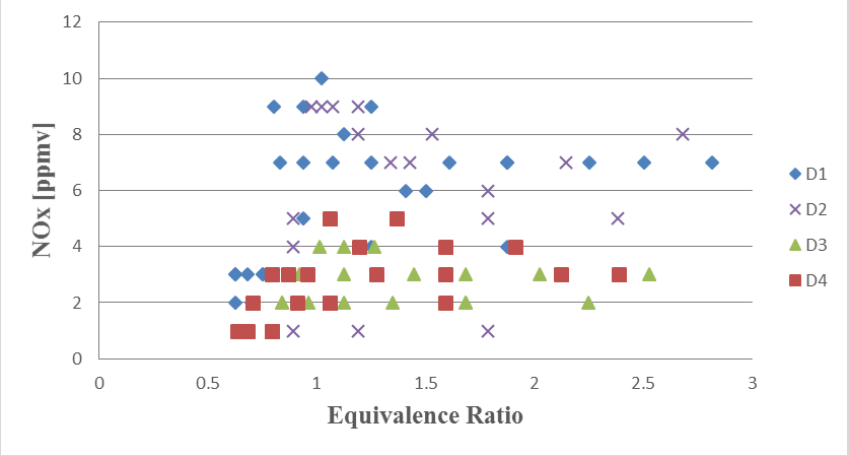

Figure 5-9 NOx exhaust gas concentration (dry) as a function of equivalence ratio for D1, D2, D3 and D4 blends.

Overall, all equivalence ratios experienced showed a decreasing trend as the CO_2 diluent ratio increases from 0 to 15%. The lesser NOx can be attributed to the thermal impacts of CO_2 dilution. The thermal effect decreases the flame temperature and thus the thermal NO [41].CO_2 diluent lowers the adiabatic temperature caused by its higher

specific heat, which would result in a major reduction in total burning rate via absorption of heat from the combustion process [155].

Lowering the flame temperature produced less NO_X to be produced, concurring with the thermal NOx formation mechanism [41]. For example, using 10%CO2/90% methane blends mixtures resulted in lower NOx production about 60% for the case of equivalence ratio=1, compared to methane.

Adding of diluent to the air stream likewise caused a corresponding decrease in oxygen mole fraction. Therefore, the flame temperature and the mole fractions of H, O, and OH radicals were reduced. For the chemical effect, the addition of diluents decreased N and HCN mole fractions and subsequently cut the prompt NO [156].

For all mixtures, the tendency is similar to low equivalence ratios viewing the lowest NOx. Relatively for pure methane, (D1), emissions are higher across all ranges of equivalence ratios, as expected [26].

5.3.2.2 CO emissions

Also, CO emissions are influenced by the injection mechanism, equivalence ratios and fuel blends at various operating conditions. Figure 5.10 shows the log form of CO emissions as a function of equivalence ratios for all combinations using different injection regimes and with two swirling cases. Overall, all tested equivalence ratios showed a decreasing trend as the CO_2 diluent ratio increases. However, the best trend was attained using B2 (85% CH_4-15 % CO_2) which created the lowest CO concentration.

The great creation of CO with B1 is due to the incomplete combustion of pockets of fuels. That could likewise be attributed to the short residence time when the system runs without swirl, so the CO formed in the combustion zone has less time to convert to CO_2 completely. Additionally, the low flame temperature under rich conditions prohibits the conversion of CO into stable species of CO_2 [157].

So, an increase in equivalence ratio resulted in a rise of CO formation by growing the amount of gas. Swirling flows through their coherent structures enhance proper mixing that results in the reduction of NOx and CO as shown in figures 5.8 and 5.10.

Interestingly, B2 with swirl presented the lowest CO profiles. Likewise, similar to NOx formation, B3 produces similar CO results with and without swirl.

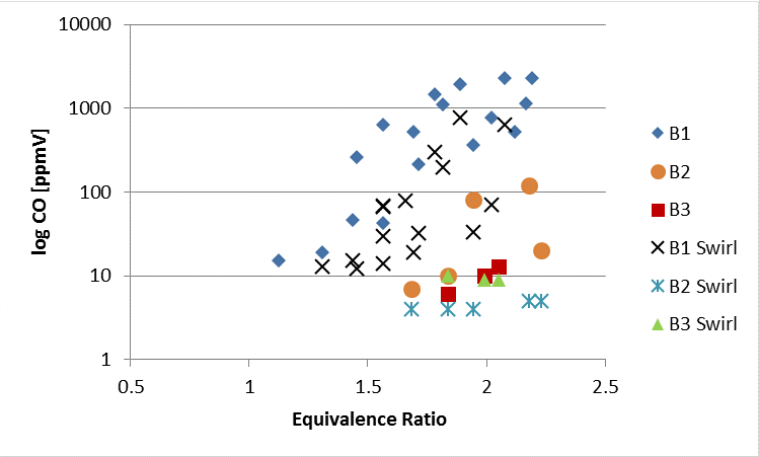

(S1)

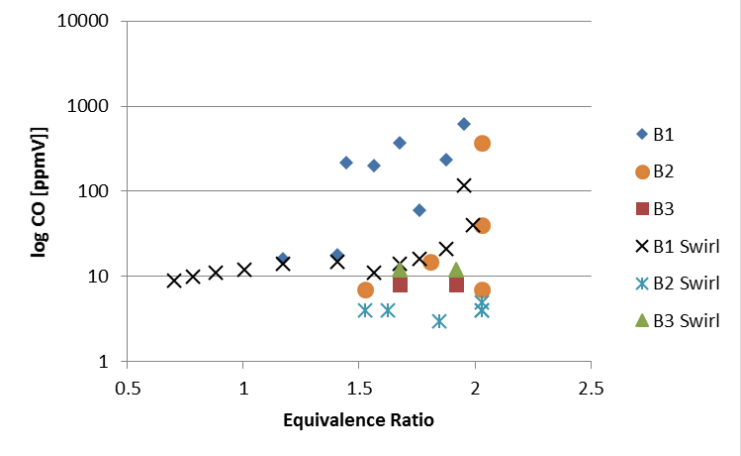

(S2)

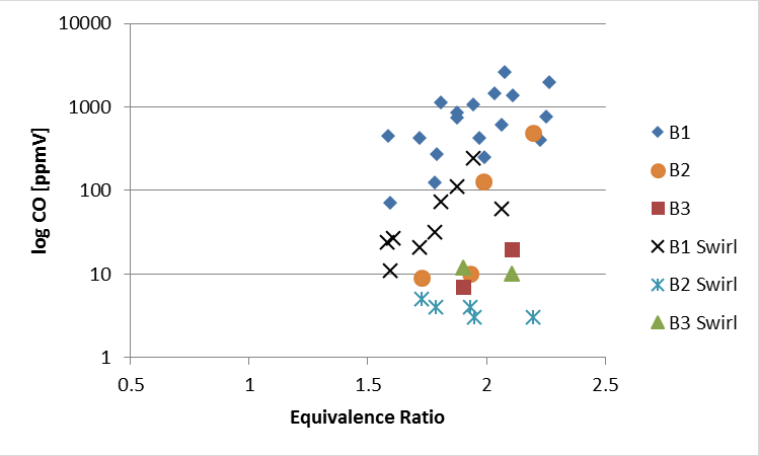

(S3)

Figure 5-10 CO exhaust gas concentration (dry) as a function of equivalence ratio for B1, B2 and B3 for different injection regimes with swirl and without swirl.

A slight increase in CO_2 in the mixture seems to be performing as a stimulus of better combustion, dropping the competition of reacting species for oxygen. However, this phenomenon stops at higher CO_2 concentrations which lead to combustion only at the tip of the burner.

The latter is established by the creation of the equal quantities of NOx (i.e. same temperature), low flame resistance (i.e. restricted equivalence ratios in the rich region), and equal CO emissions, (i.e. combustion only in a small section of the combustion zone).All proof that combustion occurs only at the tip of the burner outlet.

Figure 5.11 presents the log form of CO emissions as a function of equivalence ratios for all mixtures for the situation of the holes were closed, where CO emissions are influenced by the equivalence ratios and fuel blends at different operating conditions.

All tested equivalence ratios presented a decreasing trend as the CO_2 diluent ratio increases except for 15% CO_2 percent. Then, the best blend was found by using D3 (90% CH_4-10 % CO_2) with the new conditions which produced the lowest concentration of CO.

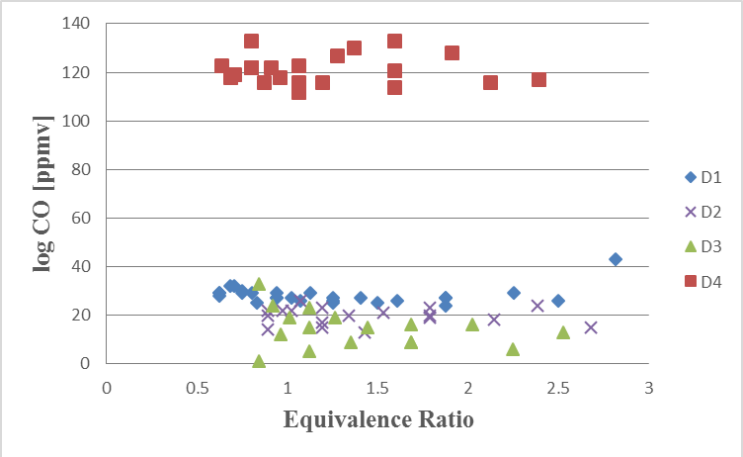

Figure 5-11 CO exhaust gas concentration (dry) as a function of equivalence ratio for D1, D2, D3 and D4 blends.

The high production of CO with D4 (85% CH_4-15 % CO_2) after closed the holes around the rig by using cement material is due to the incomplete combustion of pockets of fuels. The high percentage of CO_2 does not allow the gas to burn completely. That could also be attributed to the short residence time so the CO formed in the combustion zone has less time to convert to CO_2 completely.

Furthermore, the low flame temperature under rich conditions prohibits the conversion of CO into stable species of CO_2 [157].

Thus, a rise in equivalence ratio resulted in an augmentation of CO formation by increasing the quantity of gas. Remarkably, D3 showed the lowest CO profiles because of the reasonable amount of CO_2 in this case, indicating that the blend does not have any difficulties to burn.

As mentioned before, a slight increase in CO_2 in the mixture appears to act like an as an exciter of better combustion, reducing the competition of reacting species for oxygen. Nevertheless, this phenomenon stops at higher CO_2 concentrations which lead to combustion only at the tip of the burner.

5.3.2.3 CO_2 and O_2 emissions

The emissions index for CO_2 and O_2 for all mixtures are shown in figures.5.12 and figure 5.13 respectively. Both combinations showed higher CO_2 emissions compared to baseline B1.

The high carbon dioxide emissions for the mixtures was attributed to the presence of carbon monoxide in the fuels, with part of the CO produced was converted into CO_2 [158].

Regarding swirl, the emission increases when the swirl has been used for all blends, as the swirl makes the flame more efficient as a consequence of better mixing.

The O_2 emission profiles are shown in the figure 5.13, B2 produced the more efficient combustion. Therefore, B2 have lower O_2 emissions compared with B3. The highest O_2 emissions were measured mixture B1 and B3 without swirl that was evidence the combustion is not efficient enough.

For the case of round holes are closed, the emissions list for CO_2 and O_2 for all mixtures are shown in figure 5.14 and figure 5.15 respectively. D2 and D3 mixtures showed higher CO_2 emissions compared to baseline D1 and blended D4.

The high carbon dioxide emissions for the blends was attributed to the better reactivity combined with the already high carbon dioxide in the fuel, with part of the CO formed was converted into CO_2 [158], as previously stated.

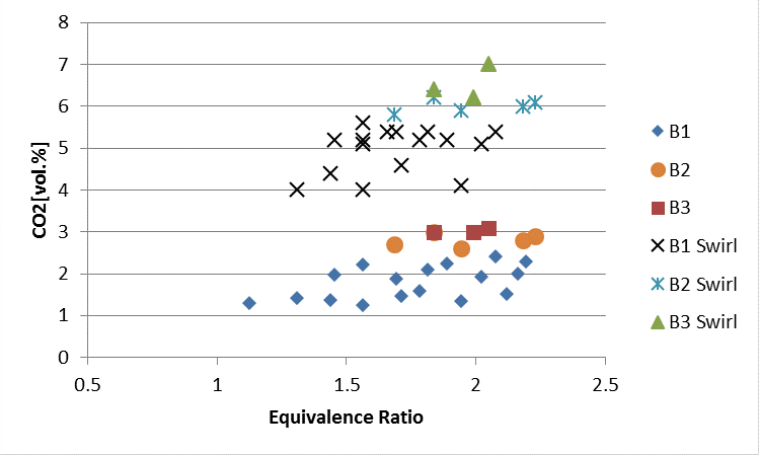

(S1)

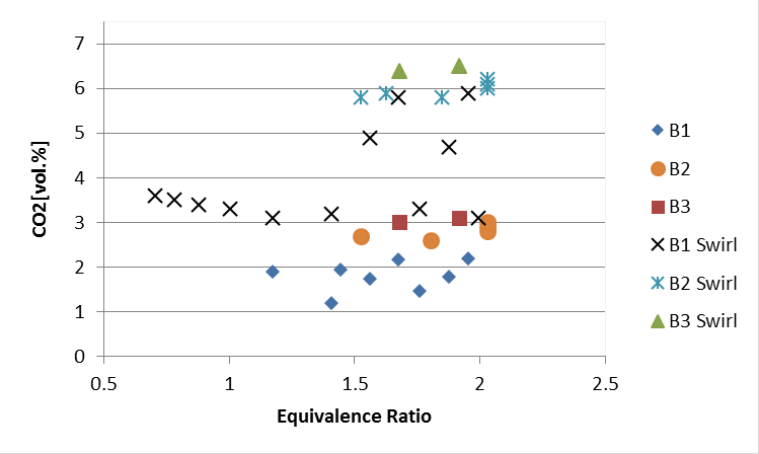

(S2)

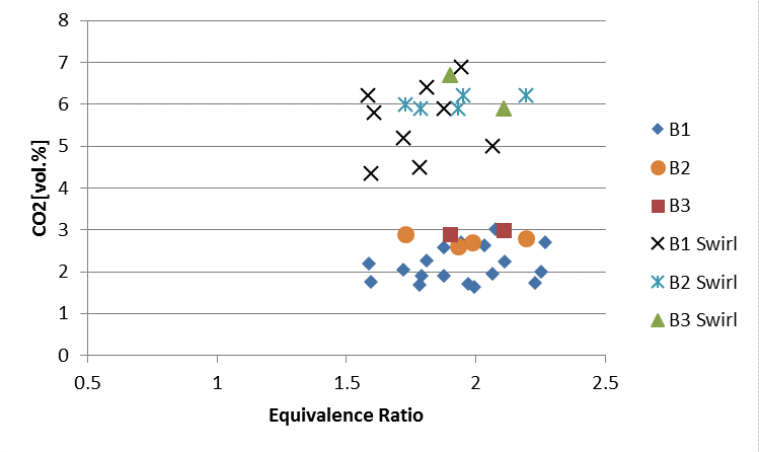

(S3)

Figure 5-12 CO_2 exhaust gas concentration (dry) as a function of equivalence ratio for B1, B2 and B3 for different injection regimes with swirl and without swirl.

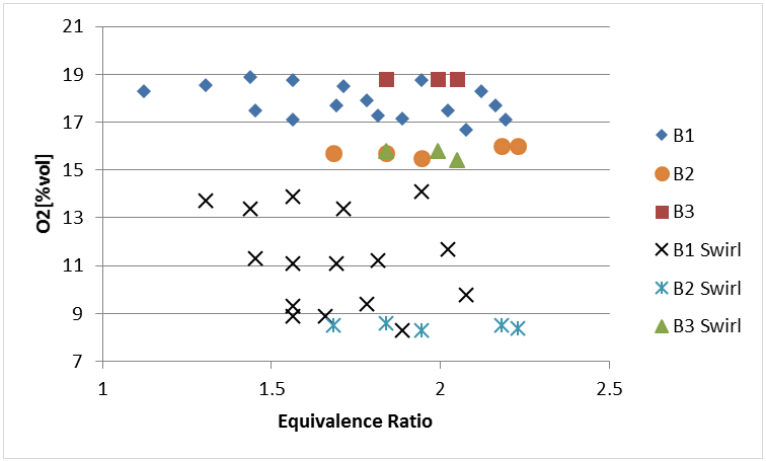

(S1)

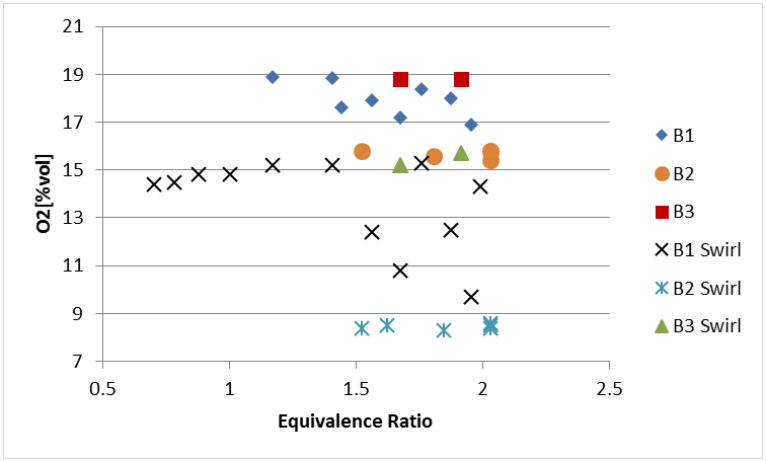

(S2)

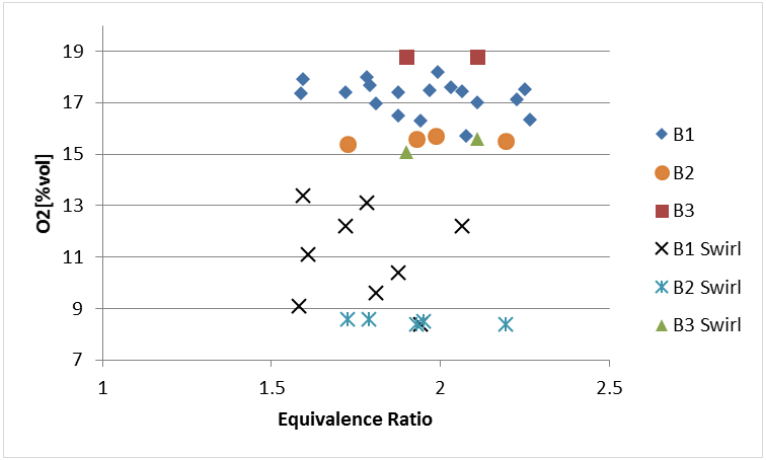

(S3)

Figure 5-13 O_2 exhaust gas concentration (dry) as a function of equivalence ratio for B1, B2 and B3 for different injection regimes with swirl and without swirl.

That is another evidence that the combustion for D4 combination was not good in addition to CO production for this blends that showed on earlier. That happened after closed the holes around the rig by using cement material and the reason for that is due to the incomplete combustion of pockets of fuels.

The high percentage of CO_2 relatively make the gas does not burn entirely. Moreover, that attributed to the short residence time, so the CO formed in the combustion zone has less time to convert to CO_2 [157] entirely.

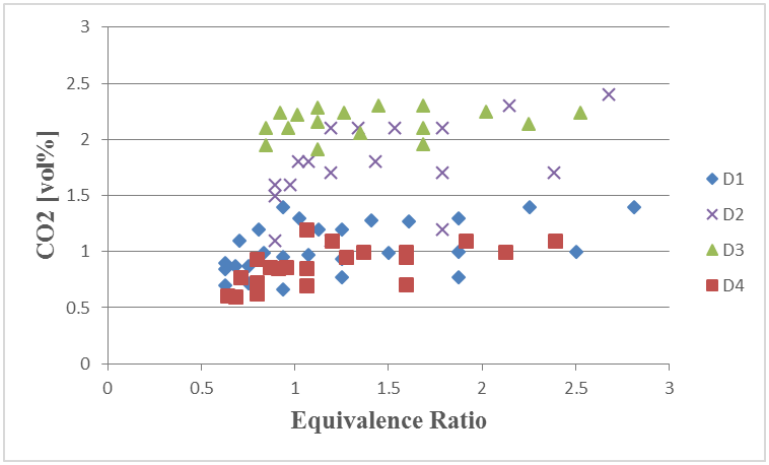

Figure 5-14 CO_2 exhaust gas concentration (dry) as a function of equivalence ratio for D1, D2, D3 and D4 blends.

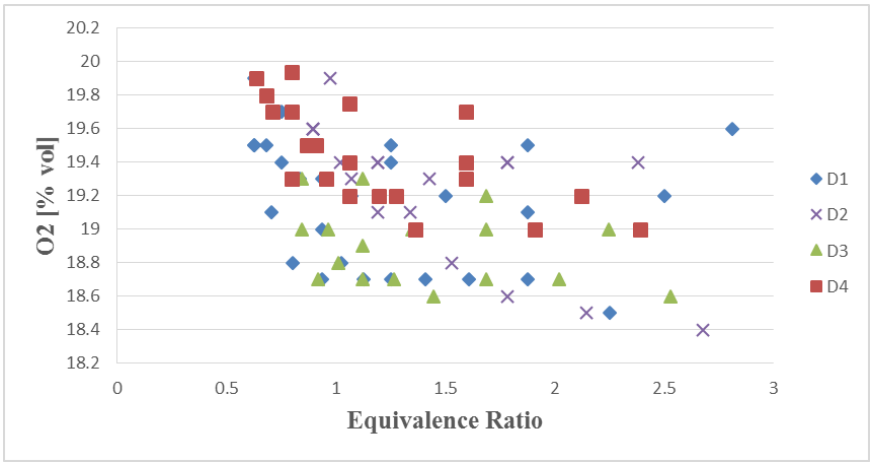

Figure 5-15 O_2 exhaust gas concentration (dry) as a function of equivalence ratio for D1, D2, D3 and D4 blends.

The O_2 emission profiles are shown in figure 5.15, demonstrating that D2 and D3 produced the more efficient combustion.

Therefore, D2 and D3 have lower O_2 emissions compared to D1 and D4. The peak O_2 emissions were measured using mixture D4; it is another indication that the combustion is not efficient enough.

5.3.3 Effect of CO_2 diluent addition on lean blow-off limits

Premixed combustion using pure methane and different blends was performed to determine the blow-off limits using open flame conditions.

Measurements were obtained for pure methane and then for various concentrations of CO_2 (table 5.2). Figure 5.16 shows the blow-off limit as a function of the mass flow rate at different CO_2 diluent rates.

CH_4 and gases blends flow rates were set to constant values, while the air was then gradually increased until blowoff was achieved.

The injection of CO_2 seemed to have a significant influence on the blowoff limit (figure 5.16). The increase in carbon dioxide from 0% to 15% and 30% apparently show the progression and movement of the boundaries of this instability, dropping the resistance of the flame as the diluent is augmented.

The higher the CO_2 flow rate, the higher the equivalence ratio at which blowoff occurs, for example, blowoff happened at equivalence ratio equal to 1.4 as shown in figure 5.16a for case B3.

The rise of carbon dioxide changes the limits of the instability, reducing the resistance of the flame. As the diluent is increased, the CO_2 could increase the strength of the central recirculation zone (CRZ) while keeping nearly the same equivalence ratio before blowoff.

That could improve the recirculation of other products in the field, augmenting their residence.

An increase in the flow rate of the blend will enhance the intensity of the shear layer, which will join into a new structure known as the High Momentum Flow Region (HMFR), which is highly correlated with the CRZ [44].

This fact indicates that operating in lean conditions may be impossible when CO_2 is added to the combustion mixture in an entirely premixed manner.

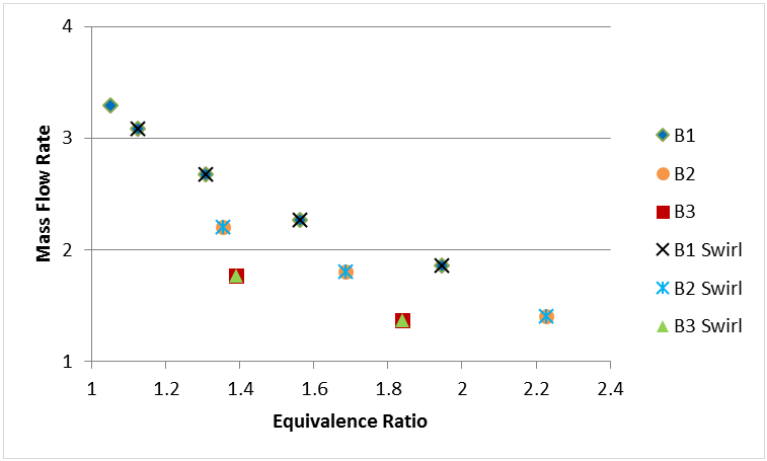

(S1)

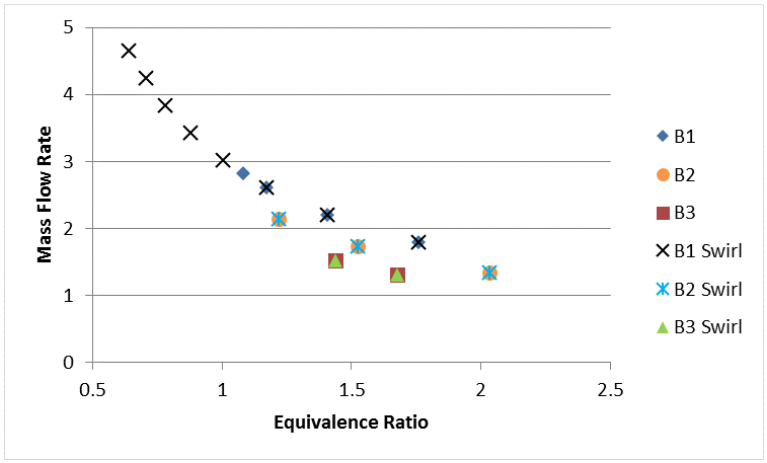

(S2)

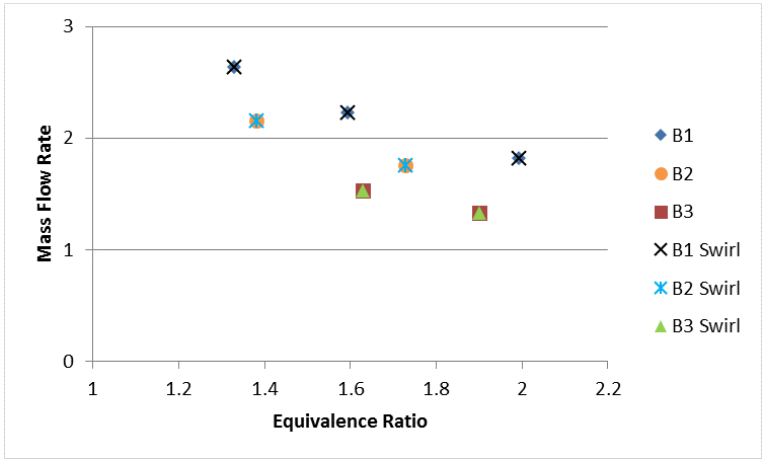

(S3)

Figure 5-16 Blowout limit as a function of mass flow rate for B1, B2 and B3 for different injection regimes with swirl and without swirl.

That could improve the recirculation of other products in the field, augmenting their residence. An increase in the flow rate of the blend will enhance the intensity of the shear layer, which will join into a new structure known as the High Momentum Flow Region (HMFR), which is highly correlated with the CRZ[44].

This fact indicates that operating in lean conditions may be impossible when CO_2 is added to the combustion mixture in an entirely premixed manner.

Regarding injection strategies, an external injection system with no central injection (S2) has produced the best stability profile, especially with swirling. For the other circumstances (S1, S3) the fuel is introduced out of the central injector; and as such it has just an axial velocity component which would cause a decrease in the swirl number.

Meanwhile, the central recirculation zone is a highly complex, chaotic recirculation region formed by the collision of vortices. Taking CH_4 as an example, it is obvious that the blow off occurred equivalence ratio equals 0.6. However, it happened at 1.05, 1.35 in the case of S1 and S3 respectively.

Methane and different combinations were performed to fix the blow-off limits using open flame conditions alongside premixed combustion. Measurements were attained for pure methane and then for various mixtures of CO_2 (table 5.4).

Figure 5.17 displays the blow-off limit as a function of the mass flow rate at different CO_2 diluent rates. CH_4 and gases mixtures flow rates were adjusted to constant values, whereas the air was then regularly increased until blowoff was accomplished.

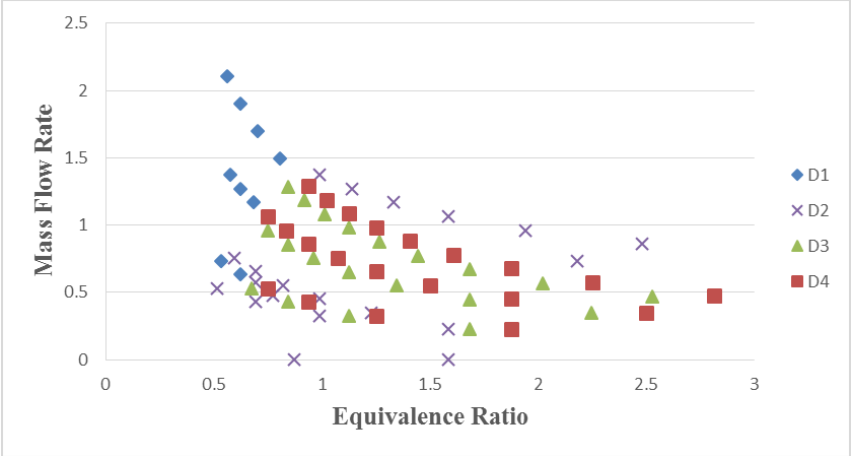

Figure 5-17 Blowout limit as a function of mass flow rate for D1, D2, D3 and D4 blends.

The injection of CO_2 appeared to have a major effect on the blowoff limit. The rise in carbon dioxide from 0% to 15% apparently shows the progress and movement of the

boundaries of this instability, dropping the resistance of the flame as the diluent is increased.

The higher the CO_2 flow rate, the higher the equivalence ratio at which blowoff arises, for instance, blowoff occurred at equivalence ratio equal to 0.9 as shown in figure 5.17, for case D4.

The increase of carbon dioxide varies the limits of the instability, dropping the resistance of the flame. As the diluent is increased, the CO_2 could raise the strength of the central recirculation zone (CRZ) while keeping nearly the same equivalence ratio before blowoff. That could expand the recirculation of other products in the field, extend their residence.

The strength of the shear layer will increase alongside the growth in the flow rate of the blend, which will join into a new structure known as the High Momentum Flow Region (HMFR), which is highly connected with the CRZ [44].

5.3.4 Temperature measurement

Measurement of temperatures on the burner wall is presented in figure 5.18 for different amounts of carbon dioxide addition to methane as well as several swirl conditions. From the temperature profiles for various injection systems shown in figure 5.18, it can be noted that the temperature decreases with carbon dioxide addition.

For example, with 15% and 30% carbon dioxide addition the temperature is lowered to 70 °C and 180 °C at the exit burner in the injection regime case S1, when compared to the real methane case. The difference in temperature for B1 to B2 is 12% however for B1to B3 is 31% as shown in figure 5.18 S1.

That is attributed to the CO_2 diluent that reduces the adiabatic temperature due to greater specific heat, which would result in a substantial decrease in overall burning rate because of the reduction flame speed [155].

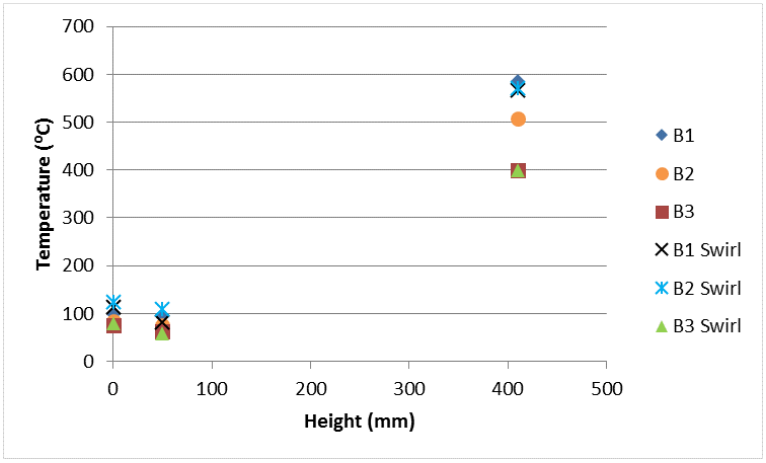

(S1)

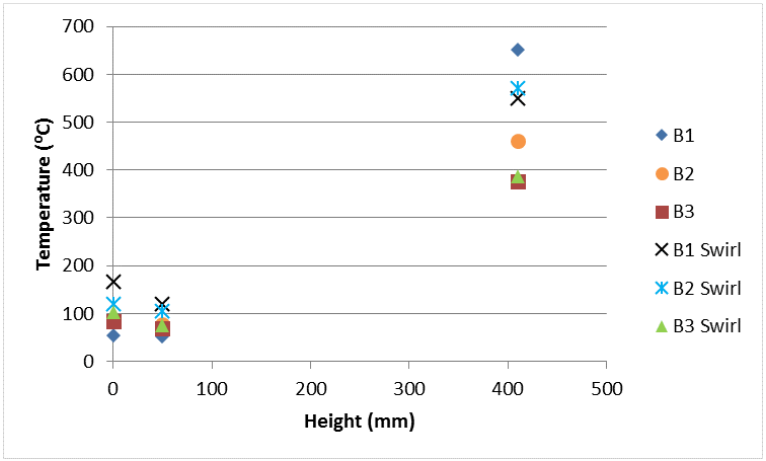

(S2)

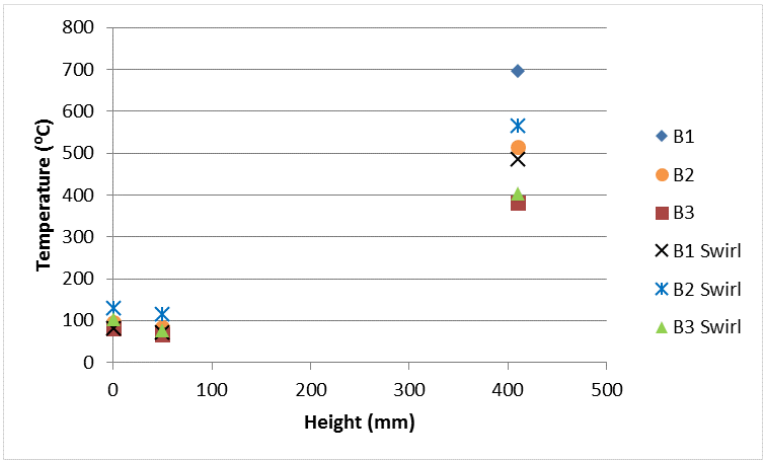

(S3)

Figure 5-18 Temperature profiles at a different height for B1, B2 and B3 for various injection regimes with swirl and without swirl (S1- Φ=1.8, S2- Φ=1.6, S3- Φ=1.9).

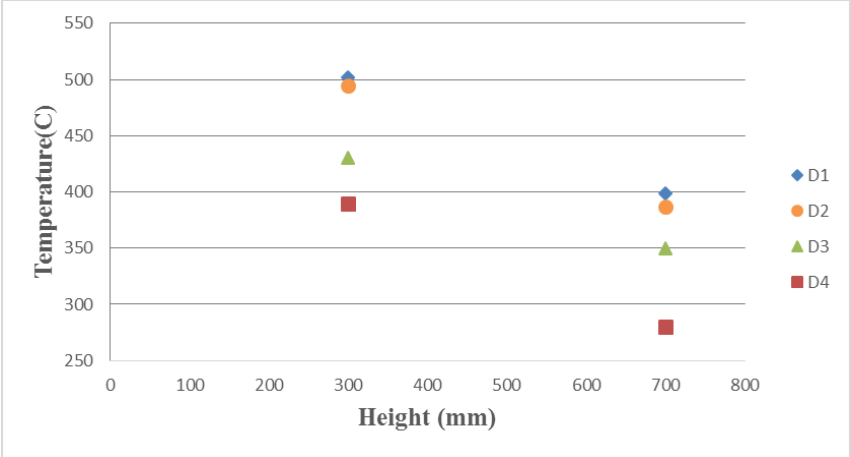

(a)

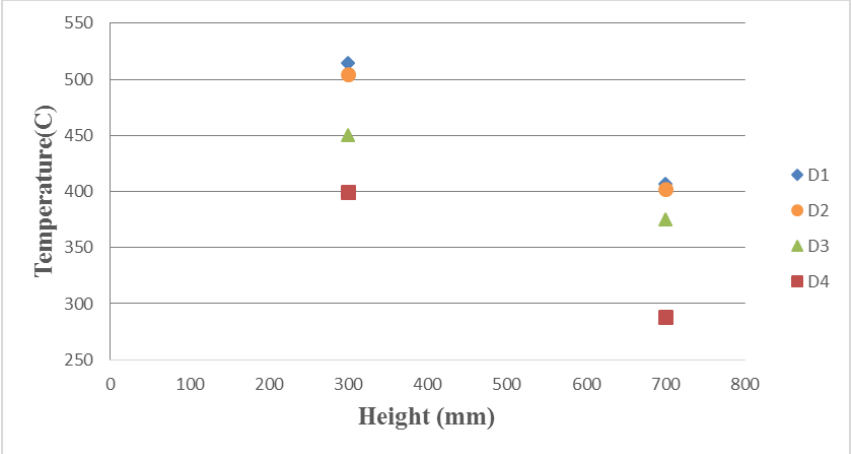

(b)

Figure 5-19 Temperature profiles at the different height for D1, D2, D3 and D4 for different equivalence ratio (a- Φ=1, b- Φ=1.5).

Regarding injection systems, there are no significant differences in temperatures for all cases. These differences are related to the variable equivalence ratio where the temperature increases with equivalence ratio, as noticed with the higher temperatures obtained at equivalence ratio 1.9 shown in figure 5.18 S1. Furthermore, S2 to S1 for methane is 10.1%. However, S3 to S1 temperature for the same blend is 17% as illustrated in figure 5.18.

Measurement of temperature profiles in the reaction zone is presented in figure 5.19 for different amounts of carbon dioxide addition to methane and various equivalence ratios for the rig after the round holes were closed. From the temperature profiles for various blends shown in figure 5.19, it can be noted that the temperature of the reaction zone decreases with carbon dioxide addition.

For example, with 10% carbon dioxide addition the temperature is lowered to 50 °C at the exit of the burner and 30 °C, at equivalence ratio =1,1.5 respectively, when compared to the clear methane case.

However, the difference in temperature between D1 to D4 is 22% as shown in figure 5.19a and figure 5.19b. That is attributed to the CO2 diluent that reduces the adiabatic temperature due to higher specific heat, which would produce in a significant decrease in overall burning rate due to the reduction flame speed [155].

Regarding equivalence ratio, it is apparent from both figures that the temperature increased with the rise in equivalence ratio from 1to 1.5.

5.3.5 Heat release

Heat release fluctuations were examined using the gain $(\overline{CH})/(CH)$ as a function of time for B1, B2 and B3 for all changed injection systems with and without swirl as shown in figure 5.20. Various equivalence ratios were used.

The contrast between blends was performed to observe the progression of CH radicals at different conditions. Results apparently showed a significant gain for B1-S1 and B1-S3, likely a consequence of reduced mixing compared to the blends.

S2 illustrations the most stable conditions, as predictable. Though, an unexpected result is the greater stability of the diffusive central injection compared to the premixed primary injection. The resulting images were analysed using a Photron FASTCAM PFV ver 2.4.1.1 software and MATLAB R2015a.

The augmented reaction of radicals produced by more oxygen in the central recirculation zone wherever the primary premixed injection is discharging its premixed mixture.

The central recirculation zone is a highly complex due to a quasi-chaotic recirculation region shaped by the impact of vortices of all sizes, the injection into the last will produce significant fluctuations of radicals, as observed.

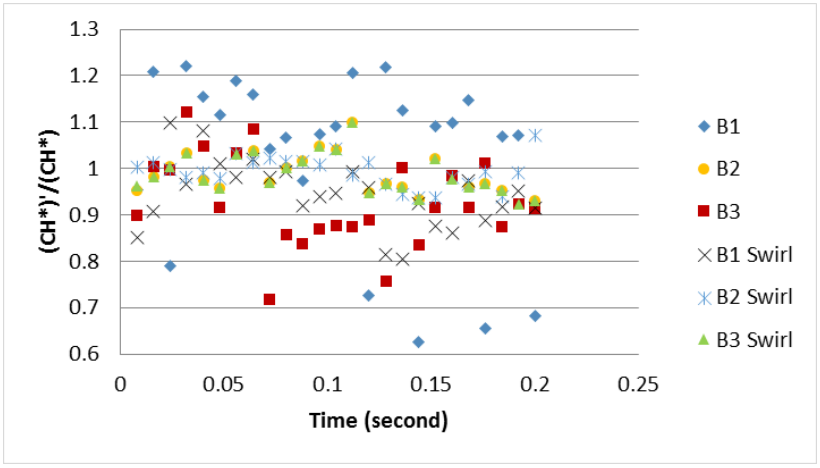

(S1)

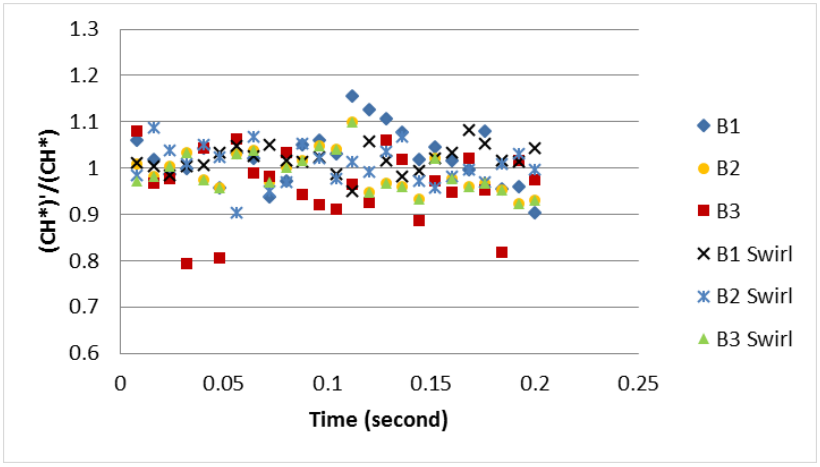

(S2)

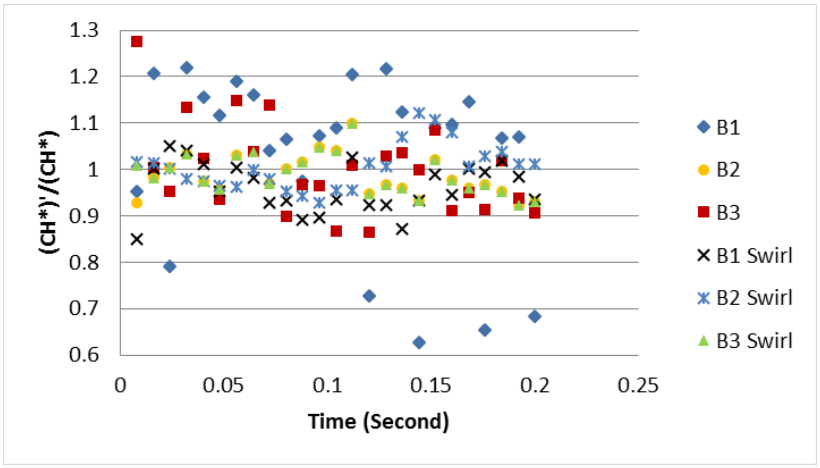

(S3)

Figure 5-20 Gain as a function of time for B1, B2 and B3 for different injection regimes with swirl and without swirl (S1- Φ=1.8, S2- Φ=1.6, S3- Φ=1.9).

However, this does not improve emissions reduction and barely augments flame stability, as demonstrated in the previously stated results.

5.3.6 CH* chemiluminescence analyses

The obtained flame images of CH* chemiluminescence were averaged (1000 images) and analysed via a Photron FASTCAM PFV Ver.3670 software and MATLAB R2016a, to get the planar flame structures for the situation of rig holes are closed. Figure 5.21 shows the planar flame structures of all the blends.

Imaging illustrates the radiation from the D3 flame is significantly different compared to methane and other blends.

Regarding CH*intensity, the CH* concentration located downstream in the axial location at equivalence ratios=0.9, which a high-intensity peak for methane, D1. A similar trend was observed for D2 and D4. The high CH* intensity profiles for these blends is attributed to an inadequate mixing and lower OH reactivity compared to combine D3, thus more production of soot and CO, as previously observed.

It seems that D3 has produced a flame with low CH* formation, high CO_2 production, low CO and NOx, and stable flame patterns. The figure shows that methane and D4 flame exhibits a relatively large area with high-intensity signals especially at equivalence ratios =1.8 at the post-reaction zone region.

This irregular post flame structure corresponds to the observed yellowish flame brush downstream the combustion zone, which indicates high soot tendency. For D2 and D3, the post-reaction zone showed little luminosity at the downstream post-reaction zone of the flame, indicative of clean combustion with the low level of soot formation.

The high luminosity of the post-reaction zone region for the methane flame is reflected in the high-intensity count as a result of soot radiation. However, the lower luminosity of the post-reaction zone region for D3 blends is attributed to that small increase of CO_2 that seems to be acting as a supporter of a better combustion, dropping the competition of reacting species for oxygen.

But, this phenomenon stops at higher CO_2 concentrations which lead to combustion only at the tip of the burner and trouble with the ignition. This idea is confirmed by the production of higher CO emissions as shown earlier.

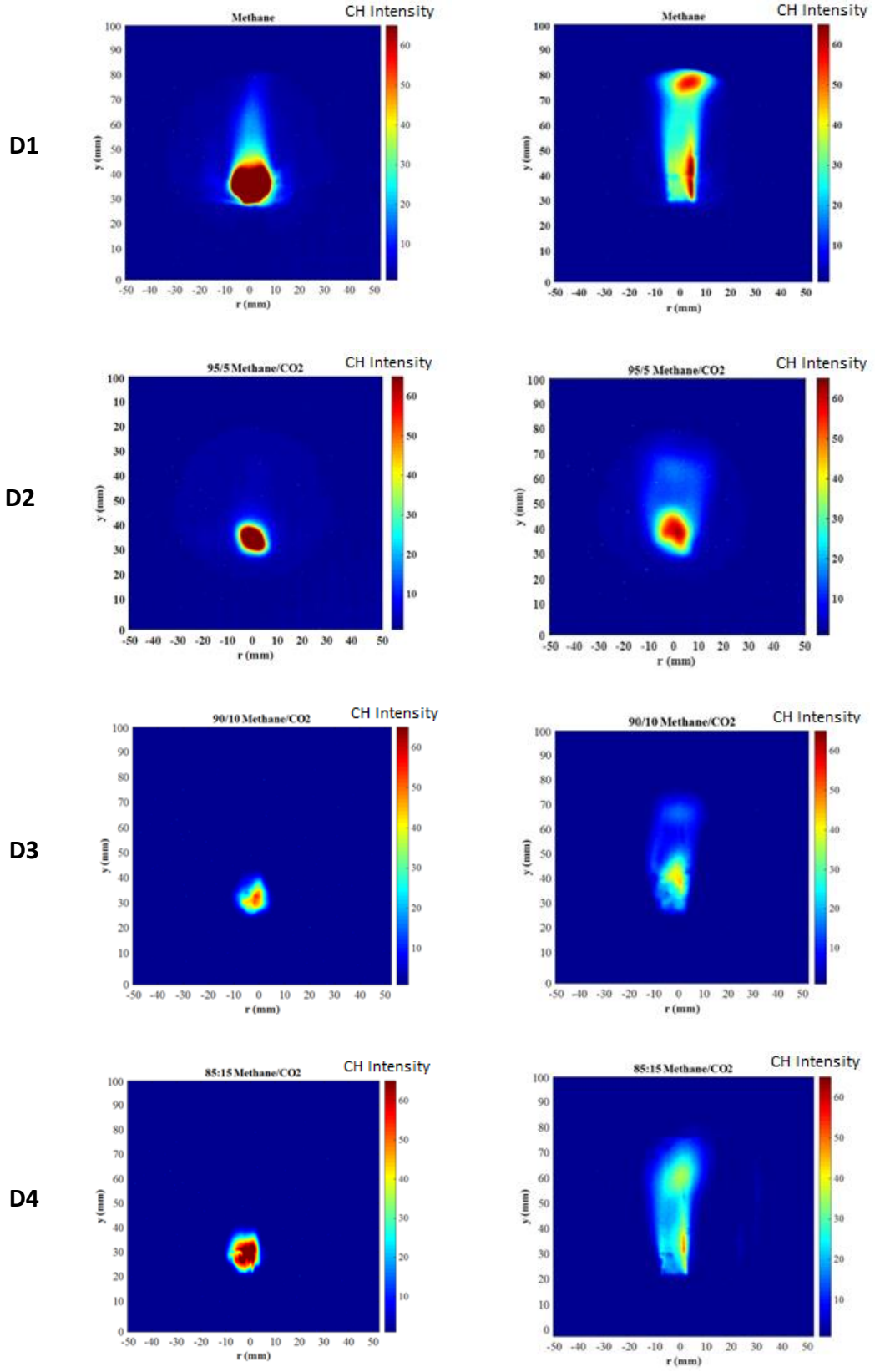

Figure 5-21 Abel inversion for CH* chemiluminescence for different blends and different equivalence ratios.

Figure 5-22 Leaking problem in the generic swirl burner

Regarding liquid fuel, it was tried to work with this type of fuels (diesel and biodiesel), in this chapter for the same burner then work with the combination (liquid and gas as shown in chapter six). However some problems had appeared, firstly because for the design of the burner, it leaked when placed on vertical position so many drops would be collected as shown in figure 5.22. Secondly, it was not possible to ignite the liquid alone, and it needed gas to help to ignite that cause the liquid to collect and had a leak.

5.4 Summary

A trial study on the combustion of methane-carbon dioxide mixtures at atmospheric conditions was carried out where gas mixtures have been examined by using different levels of premixing. Gas mixtures have been investigated by using changed levels of premixing with changed injection strategies with and without swirl and with and without central injection.

Outcomes showed that the introduction of limited amounts of CO_2 (15%) had controlled reaction rates and temperatures in the combustion zone, thus producing a decrease in emissions with a reduction in flame stability at low equivalence ratios. More dilution leads to even poorer combustion and flame extinction only above the burner tip. CH chemiluminescence distribution showed that B1-S1 and B1-S3 have

higher CH radical variations, as the creation of CH is greater but less controlled when compared to B1-S2.

The use of central premixed injection produces the most chaotic CH production case, possibly because of the production of radicals in a highly chaotic region such as the central recirculation zone.

Moreover, an experimental study on the combustion of methane and methane-carbon dioxide mixtures would present for the same burner, with different conditions where a premium black fire was used to close the holes around the burner, gas mixtures have been examined by using different levels of premixing without using central injection.

Results showed that the introduction of limited amounts of CO_2 (10%) had controlled reaction rates and temperatures in the combustion zone, thus producing a reduction in emissions with a decrease in flame stability at low equivalence ratios.

The results showed that a notable reduction in NOx was observed at all conditions for the CO_2/Methane blends in about 60% for 10% CO_2 addition. However, carbon monoxide emissions also decreased when using 5-10% CO_2 addition.

The use of CO_2/Methane blends mixtures led to lower CO production about 83% for the case of 10% CO_2. CH chemiluminescence analyses indicated that pure methane produced high heat fluctuation, with CO_2 at 5-10% showing the most stable CH profiles.

CH chemiluminescence distribution indicated that D1 and D4 have higher CH radical fluctuations, as the construction of CH is greater when compared to D2 and D3, with the latter showing good CO_2 production, low CO and NOx, with relatively high flame stability.

This chapter has been finished with one of the contributions of this thesis, by studying on the combustion of methane and methane-carbon dioxide mixtures at atmospheric conditions by using different levels of premixing for various conditions.

In addition to the work has done with chapter four with different types of liquids it is the time to start working with next chapter on two-phase flows. Studying liquids and

gaseous combinations of the various alternative fuels using a swirl burner, evaluating emissions, CH*, temperature profile and stability, and in this chapter the comparative study of methane and methane-carbon dioxide mixtures was performed to understand the conclusion of using these blends in a gas turbine. So, in next section, experimental studies of alternative gases and liquids in a two-phase system using a 20 kW swirl burner were achieved.

Chapter 6

Comparison performance of CO_2/CH_4/biodiesel and CO_2/ CH_4/diesel in a swirl burner generator

An experiment is a question which science poses to Nature, and a Measurement is the recording of Nature's answer

Max Planck

6.1 Introduction

There is an ever-increasing need to understand multiphase combustion because of their extensive application in energy, transportation, environment, propulsion, industrial safety, and nanotechnology.

More scientists and engineers with skills in these areas are required to solve many multifaceted problems. Multiphase reacting flows have been main research issues for many decades, and studies in these regions are expected to continue at an even greater speed.

Therefore, this chapter has been focused on that multi-phase studies by using a swirl burner. An experimental study on the combustion of CO_2/CH_4/diesel vs. CO_2/CH_4/ biodiesel mixtures at atmospheric conditions where the biodiesel derived from cooking oil.

The 20 kW swirl burner was employed to analyse gas turbine combustion features under atmospheric conditions to quantify flame stability and emissions by using these fuels. The burner configuration consisted of a centre body with an annular, premixed gas/air jet introduced through five, 60° swirl vanes.

A TESTO 350XL gas analyser was used to determine NOx and CO emission, and other types of emissions trends. Comparison between the blends was carried out at different equivalence ratios. CH* chemiluminescence diagnostics was likewise used and correlated with the levels of emissions produced during the trials at various flow rates. The resulting images were analysed using MATLAB R2016a and Photron FASTCAM PFV Ver.3670 software and to determine instability patterns that were correlated to fuel blend.

6.2 Experimental setup

6.2.1 Swirl burner and flow delivery system

An axial swirling flame burner was utilised to establish continuous premixed swirling flames at atmospheric conditions. This swirl injector consists of a liquid inlet, gas inlet, aeration tube, mixing chamber, swirl-generating vanes, swirl chamber, and the discharge orifice. The schematic of the swirl burner and the placement position of swirler are shown in figures 5.3 and 6.1.

The liquid flows were supplied independently to the atomiser through the centre via a central injector, whereas premixed gas was supplied through the outer, the gas is introduced into outer injector with a low velocity to get proper mixing with the liquid stream on the mouth burner.

The air-gas mixture passes through swirl-generating vanes which create swirling effects on the combination before exiting the injector through the discharge orifice figure 6.1.

Low liquid flow-rate was intended in this study to simulate low fuel consumption and to get better atomization compatible with the velocity of the premixed gas. One of trouble it had been faced that when the nozzle was close the mouth of the burner as shown in the figure 6.1b, it was impossible to attain stable flame because the high flow rate for the liquid compares with a gas push the premixed flow rate and no flame had happened.

So, the kind of nozzle was used, it was replaced by Delavan 0.75 x 60 WDB nozzle to Delavan 0.4 x 60 A, the first one had been used in Kurji's work, [70]. To get the less possible flow rate, even with that trouble had decreased but it had still existed, then the nozzle position had been moved to 50mm below the mouth to get a stable flame at some points.

There are several other parameters to take into consideration such as; the diameter of the chamber, the diameter of the exit orifice and air injection hole size, quantity and location [20, 160].

Literature has shown, depending on the parameters chosen for the design, the air to liquid ratio (ALR) and the pressures at which the fluids are supplied. The ALR appears to have a particularly significant effect on the mean droplet size; higher ALR tends to result in smaller mean droplet sizes. The schematic of the swirl flame burner and the flow delivery system is shown in figures 6.1 and 6.2.

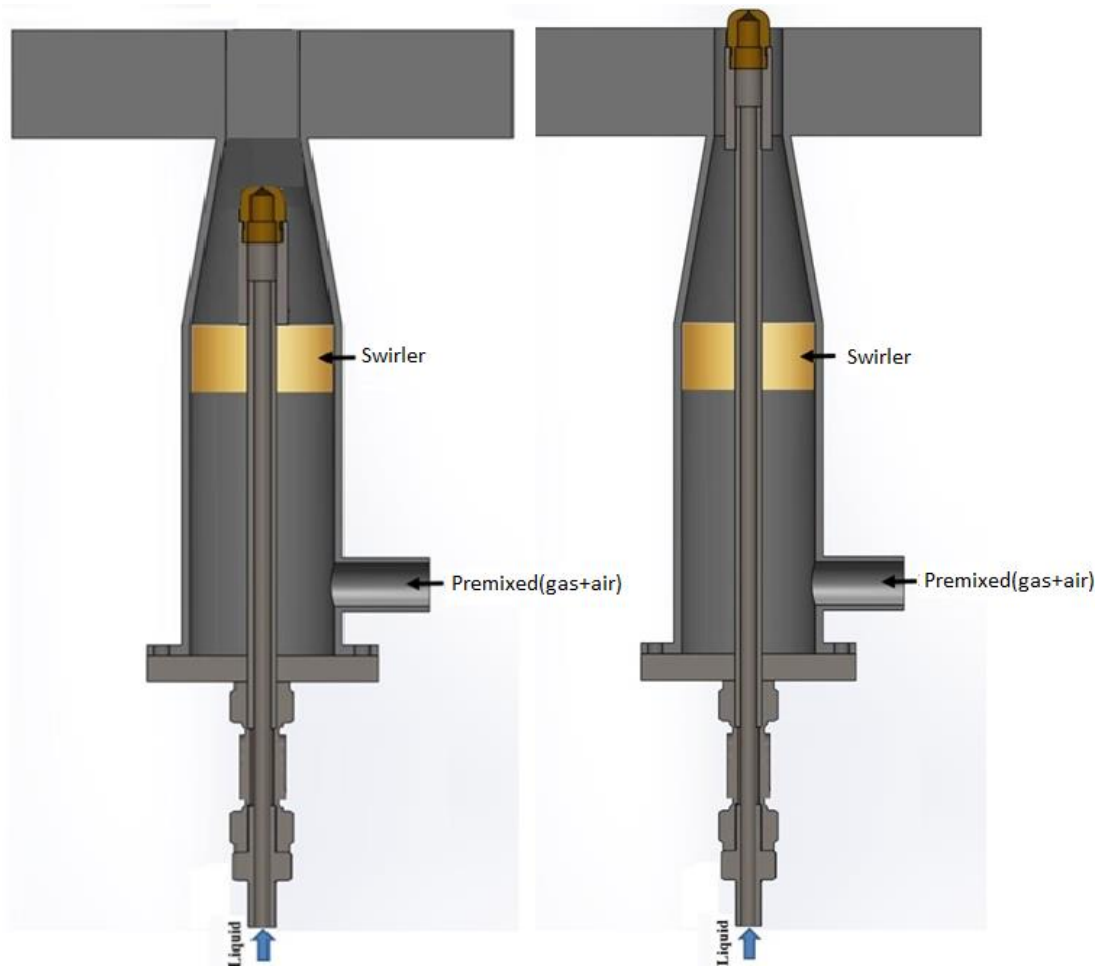

A B

Figure 6-1 A-Schematic burner with different swirler position B-Schematic burner and swirler.

A Delavan 0.4 x 60 A, nozzle atomiser was used as the fuel injector to atomise liquid fuel before mixing with swirling premixed. The atomiser nozzle was used operating pressures of 5 bar absolutes and with 0.54 litre/hour constant flow rate for the liquid fuel, using compressed nitrogen, passing into a liquid accumulator as shown in figure 6.2.

The swirl burner employed in this trial consists of an axial swirler and a circular stainless steel tube placed as illustrated in figure 6.1.

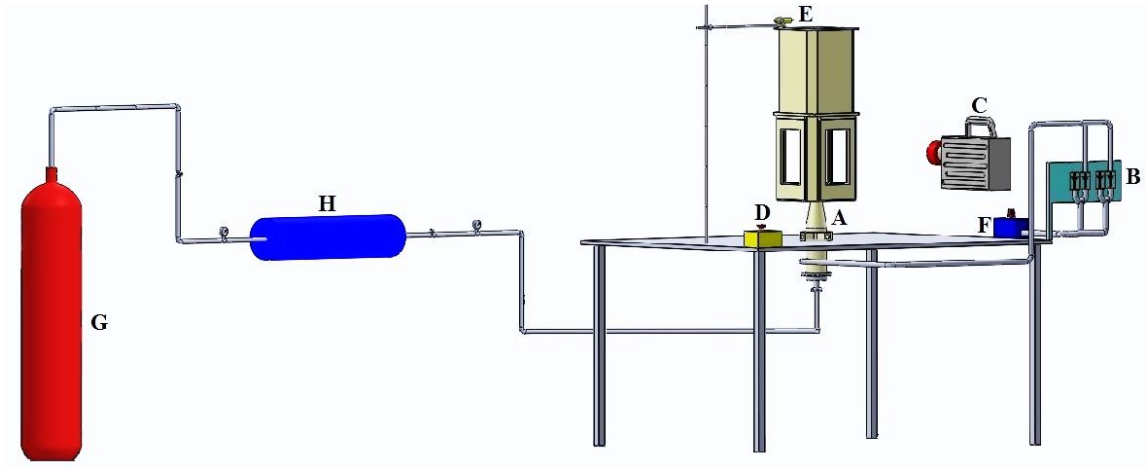

Figure 6-2 Generic swirl burner with accessories. A - Swirl burner; B – Rotameters; C – High-speed camera; D – Emergency button; E – Pilot burner; F – Air regulator; G- Nitrogen cylinder; H- Accumulator.

A pilot ignitor was used to ignite the flame as shown in figure 6.2, the combustion chamber is rectangular and has four internal quartz windows, giving full optical access to the combustion chamber. The width and the height of the combustion chamber are 118 mm, 410 mm, respectively, was used to form a combustor wall at the burner outlet, while one end of the tube was exposed to open atmospheric condition. More details of the burner geometry [43].

The swirler is placed in concentric with the atomiser at the burner outlet (100mm down the burner mouth). A circular quartz tube with a diameter of 100 mm and 180 mm in length was used to form a combustor wall at the burner outlet, while one end of the tube was exposed to open atmospheric condition. Details of the burner geometry are shown at [43].

A 1.5 mm thermocouple was positioned at various heights from the burner exit (300, and 700mm).The last point represents the exit point for the burner.

A Photron Fastcam APX-RS high-speed camera operating at 300 frames/s was also used with a 105 mm, 1:2.8 Nikon lens. The resultant images were analysed using Photron FASTCAM PFV ver 2.4.1.1 software and MATLAB R2016a.

6.2.2 Operating conditions

The swirling premixed was mixed before introduction into the burner where gas and air for the outer part was premixed in separate tubes to ensure adequate mixing before entering the burner then mixing with the liquid fuel spray. The atomising liquid fuel and swirling premixed were delivered independently at room temperature to the burner outlet at a different atomising air-to-fuel mass ratio (ALR), at which excellent atomization can be achieved at atmospheric condition. The operating conditions for the liquid fuels tested are shown in table 6.1.

However, table 6.2 shows all tested blends. The effect of two-phase flow on the emissions was investigated by using TESTO 350XL gas analyser to acquire NOx, CO and other emissions to characterise all two-phase flow conditions. CH chemiluminescence diagnostics was examined and correlated to the stability of each case.

Table 6.1 Fuel properties obtained

Property	Diesel [160]	Unsaturated Biodiesel[70]
Viscosity [m^2/s] 20°C	3×10^{-6}	7.40×10^{-6}
Viscosity [m^2/s] 40°C	2.00×10^{-6}	4.49×10^{-6}
Density [kg/m^3]	820	859
Surface Tension [mN/m]	28	29.1
HHV [MJ/kg]	46	38.9
Water content [wt%]	2.6	0.7

Both the air and blends were controlled by rotameters so their respective quantities could be monitored and altered. The system incorporates three solenoids that only allow combinations to pass once the system is stabilised CH_4 was blended with CO_2 as diluents then mixed with liquid depending on the combination and condition. The effect of CO_2 as diluent on the emissions has been studied by incrementally adding CO_2 from 0%, 5% and 10%. The blends for all cases were supplied by cylinders that contained CO_2 already mixed with CH_4 at the required percentages. Various combinations were followed to observe how the increment of CO_2 in the blends affected the flame and reduced/increased emissions. The TESTO 350XL gas analyser was used to measure NOx, CO and other emissions to characterise different

equivalence ratios while using different fuel mixtures. CH chemiluminescence diagnostics was examined and correlated to the stability of each case.

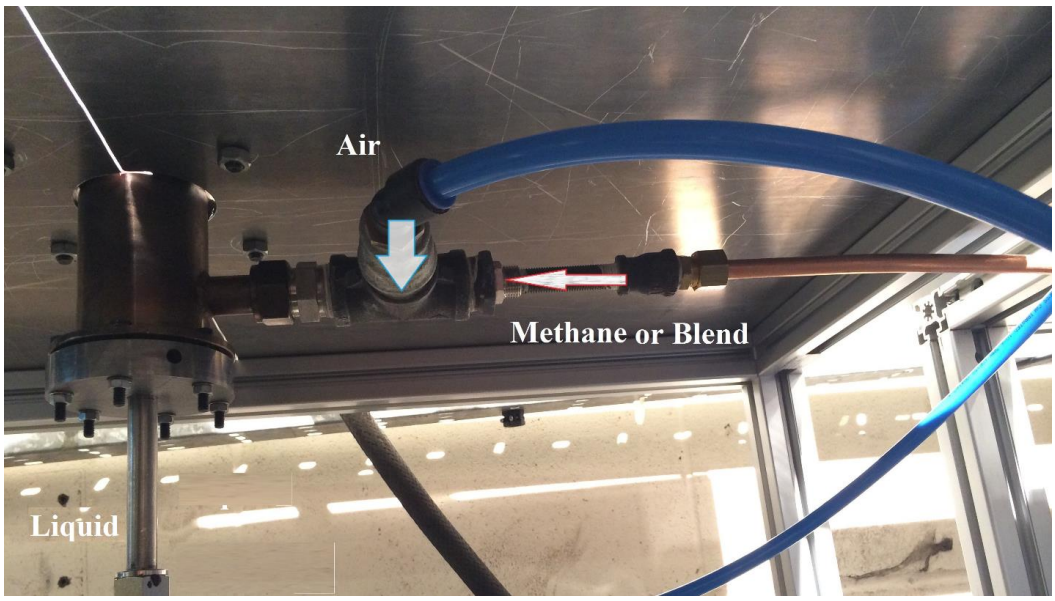

Figure 6-3 Premixed inputs of blends and air utilising the venturi effect to allow initial testing with gaseous fuel.

Table 6.2 Blend mixtures composition (vol. %)

Mixture	CH_4	CO_2	Liquid Fuel		Mixture	CH_4	CO_2	Liquid Fuel
B1	100	0	Diesel		B4	100	0	Biodiesel
B2	95	5	Diesel		B5	95	5	Biodiesel
B3	90	10	Diesel		B6	90	10	Biodiesel

6.2.3 Emissions measurements

Measurements of post-combustion emissions were performed using a gas analyser test 350-XL at approximately 300 mm downstream of the burner outlet. The sampling probe was placed 10 mm inside from the exit plane. The emissions measured include NOx, CO, O_2 and CO_2, with the measurement range of 0-1000 ppm, 0-10,000 ppm, 0-25% and 0-99.9% respectively. The emission readings from the gas analyser are reported in dry basis with the uncertainty of ± 5% ppm for NO, ± 5% ppm for CO, ± 0.8% for O_2 and ± 0.3% for CO_2. Measurements were taken 1 minute after the readings have become stabilised.

6.3 Results and discussion

6.3.1 Flame imaging

Direct flame imaging was performed to examine the flame appearance of CO_2/Methane blends, diesel or biodiesel derived from cooking oil. A digital camera (Nikon; Model D7200) was used to image the global flame appearance of blends swirl flame established through the optically accessible quartz wall.

Figure 6.4 shows six sets of blends flame images, cases B1, B2, B3, B4, B5 and B6 established at a constant composition of 0%, 5%, and 10% with diesel for a one time and with biodiesel for another respectively, as shown in table 6.2.

Blue flames were observed as a result of the intense heat reaction zones. The fuels chemically react in this region under sufficient oxygen, leaving no unburned hydrocarbon for post-flame reaction or soot formation. Visible orange-yellowish post flames are indicative of soot formation. The luminous post-flame region is evident for the fuel-rich mixture, as shown in figure 6.4 for B1, B2 and B3 respectively where it is obvious with these blends that the emissions increase.

The blueness of flame was due to lower carbon content in the fuel for the blends of biodiesel but yellowness for the blends of diesel due to higher carbon content. In other words, the blue coloured flame was due to the increase in the air-fuel ratio. The luminous bright yellow flame zone was due to the decrease in air-fuel ratio.

The luminosity of the flame was reduced in the case of biodiesel, and larger bluish zones are visible in flames. The length of the blue region observed in the near-burner area of the flame was increased in the case of biodiesel. The blue region is associated with the homogeneous gas phase reactions. The increase in the blueness was attributed to the increase in oxygen content of the fuel. The luminosity of flame was due to carbon content[161]. Biodiesel oil flames tended to have a smaller width and longer penetration, while diesel fuel flames have a wider and more even structure.

This difference was due to their relative densities and viscosities rather than their spray size. Since biodiesel cooking oil has higher density and viscosity values compared to

diesel oil, the momentum and shear resistance of waste cooking oil droplets made them less sensitive to swirling, and thus had longer penetration.

Comparison of the two fuels, diesel oil, tended to produce more sooty flames, where the quartz confinement tube was stained with black soot residue after only a few seconds of operation due to soot formation. The show time for every image in the figure was 5 seconds by taking the average. Every experiment was repeated five times to be sure from the result and take the average of them for each point in the results and the time was between one experiment and another one was one hour to cool the burner and get accurate results.

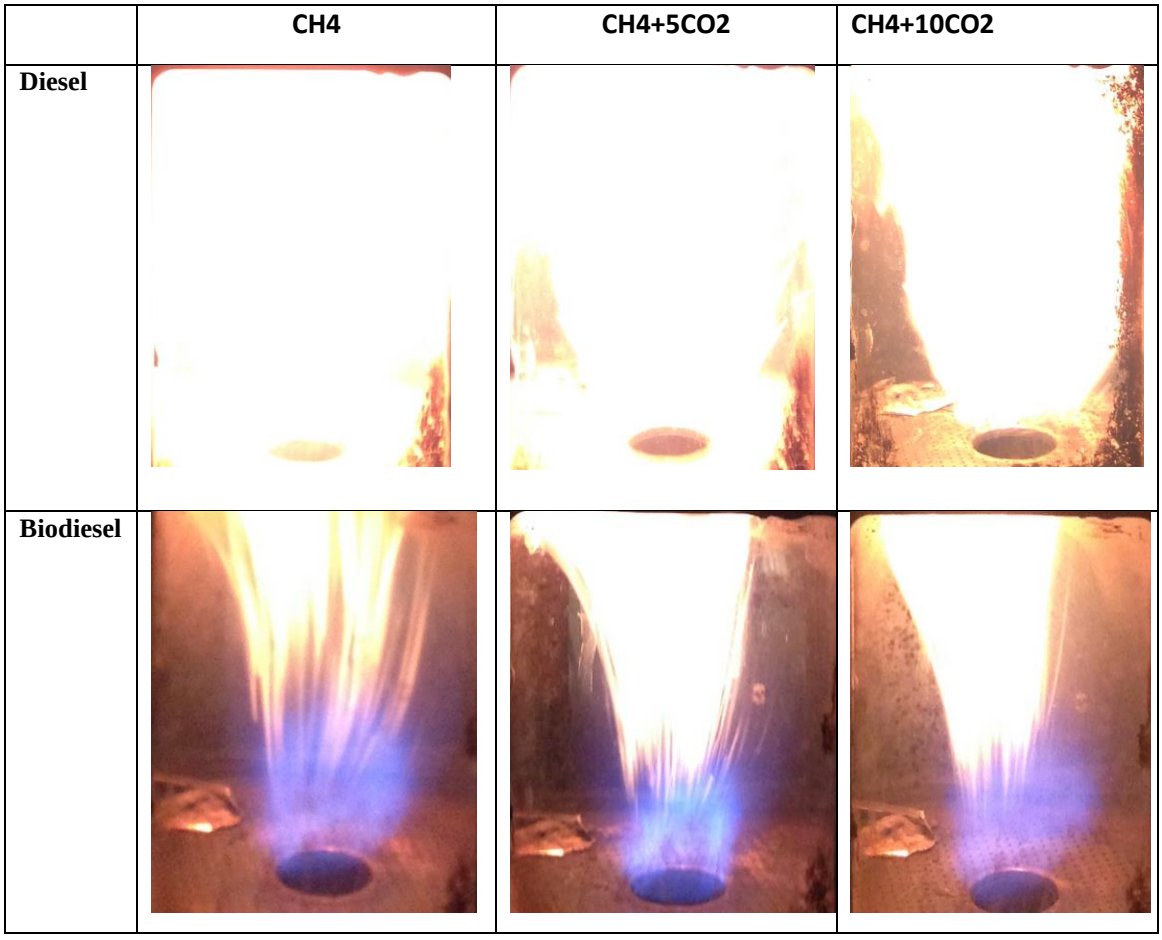

Figure 6-4 Global flame images of swirl gas mixtures at different equivalence ratio=1.7 for all different blends

Biodiesel cooking oil was considered as an oxygenated fuel which produced less soot due to the existence of oxygen molecules. Where formation of C/H radical play a significant role in the production of acetylene and propargyl formation which are

essential precursors for soot formation [153, 154]. The oxygen content in waste cooking oil improved the combustion efficiency compared to the case of diesel oil [161].

Furthermore, it is observed that 10% CO_2 with the blend (B3 and B6) shows less luminous post-flame region compared to other blends under same equivalence ratio, that indicating the lower tendency for soot formation for the former due to reduced availability of C radicals, where the bright flame decreased with increasing CO_2 percentage.

6.3.2 Exhaust gas analysis

6.3.2.1 NOx emissions

Comparison of the NOx emissions CO_2/CH_4/biodiesel and CO_2/CH_4 /diesel under various equivalence ratios are shown in figure 6.5. The diluents of CO_2 for all the cases were supplied by cylinders that have CO_2 already mixing with CH_4 at different diluent ratios as shown in table 6.2. Overall, emissions of NOx from all fuels decreases almost linearly with the increase of excess air ratio.

Lower NOx is produced at extreme high excess air ratios due to the lower flame temperature that suppresses the formation of thermal NOx [157, 163].

Biodiesel blends show lower NOx emissions compared to diesel blends for all the cases and different equivalence ratios. The trend of lower NOx emissions for biodiesel could be due to the role of oxygen in the molecule that suppresses CH production, thus reducing prompt NOx formation [67, 164].

Moreover, the lower NOx values must be attributed in part to the higher heat of vaporisation of the biodiesel spray. Regarding CO_2 dilution, overall, all tested equivalence ratio tested showed a decreasing trend as the CO_2 diluent ratio increases for both types of liquids.

The lower NOx can be attributed to the thermal effects of CO_2 diluents. The thermal effect decreases the flame temperature and thus the thermal NOx [41]. CO_2 diluent

reduces the adiabatic temperature due to higher specific heat, which would result in a significant decrease in overall burning rate [155].

That is a consequence of the cooling of the flame by absorbing heat from the combustion process, due to its high specific heat of the molecule.

Lowering the flame temperature caused less NOx to be emitted, concurring with the thermal NOx formation mechanism [41]. The addition of diluent to the air stream also causes a corresponding decrease in oxygen mole fraction.

Consequently, the flame temperature and the mole fractions of H, O, and OH radicals reduce. For the chemical effect, the addition of diluents may decrease the N and HCN mole fractions and subsequently reduces prompt NO [156].

According to the extended Zeldovich mechanism [40], as flame temperatures increase so do emissions of nitrous oxides, with reaction rates determined experimentally with reasonable accuracy [164].

Case B5 and B6 show significant lower NOx emissions. Results demonstrate the effect of biodiesel and CO_2 dilution on the NOx emissions, with a considerable impact. Using biodiesel and 10% CO_2 led to the average decrease of NOx by ~50% compared with B1 for equivalence ratios =1.6, as shown in figure 6.5.

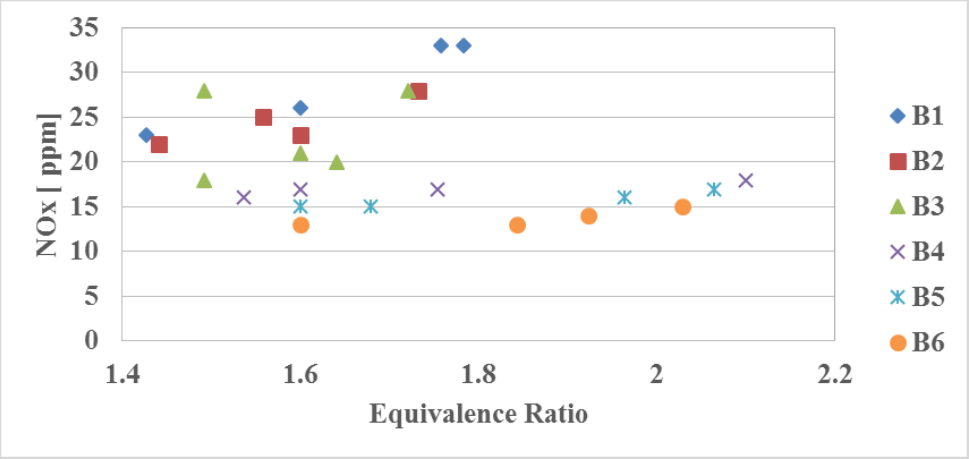

Figure 6-5 NOx exhaust gas concentration (dry) as a function of equivalence ratio for all different blends.

6.3.2.2 CO emissions

The emission index presented for CO as a function of equivalence ratios is shown in figure 6.6, for all mixtures, CO emissions are influenced by the equivalence ratio and fuel blend at different operating conditions. Overall, emissions of CO for all fuels decreases with the increase of excess air ratio. CO emissions are higher for low excess air ratios as too many rich pockets survive. For high excess rates, the temperatures are very low, and any CO formed in rich spray pockets are quenched by the low-temperature mixture, preventing re-burning. Also, shorter reaction times are expected at the higher mass flow rates. Biodiesel blends show lower CO emissions compared to diesel blends for all the cases and different equivalence ratios. The trend of lower CO emissions for biodiesel could be due to the oxygen content in biodiesel cooking oil resulted in a complete combustion than diesel oil [166, 167].

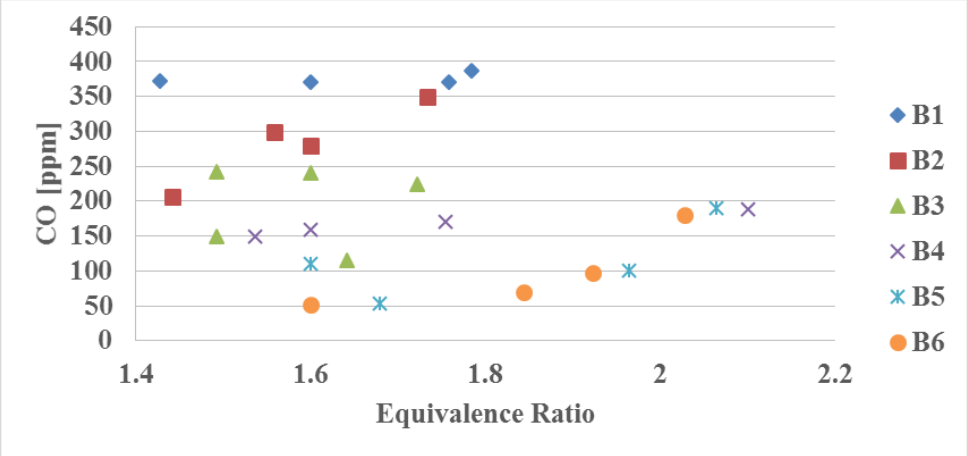

Figure 6-6 CO exhaust gas concentration (dry) as a function of equivalence ratio for all different combinations.

The variation in CO emission level according to different CO_2 dilution rates is also shown in figure 6.6. For example, the reduction between B2 and B3 is ~36% for the equivalence ratio =1.7. The reason for this behaviour is due to the incomplete combustion of pockets of fuel combined with the short residence time so the CO formed in the combustion zone has less time to convert into CO_2 completely [157]. Thus, the high production of CO at B1, B2 and B3 is due to the incomplete combustion of pockets of fuels and further aggravated by the presence of CO in the fuels. Moreover, incomplete combustion is a factor that caused unburned hydrocarbons to have short residence time to react to form CO [157].

6.3.2.3 CO_2 and O_2 emissions

Figure 6.7 displayed the variation of CO_2 formation as a function of equivalence for all blends. Carbon dioxide emissions values for biodiesel blends increased above that of diesel blends and increased CO_2 dilution mixtures showed higher carbon dioxide emissions compared to another blend. The high carbon dioxide emissions were attributed to the existence of carbon monoxide in the fuels, with part of the CO formed was converted into CO_2 [158]. And this is due to more efficient combustion [168, 169].

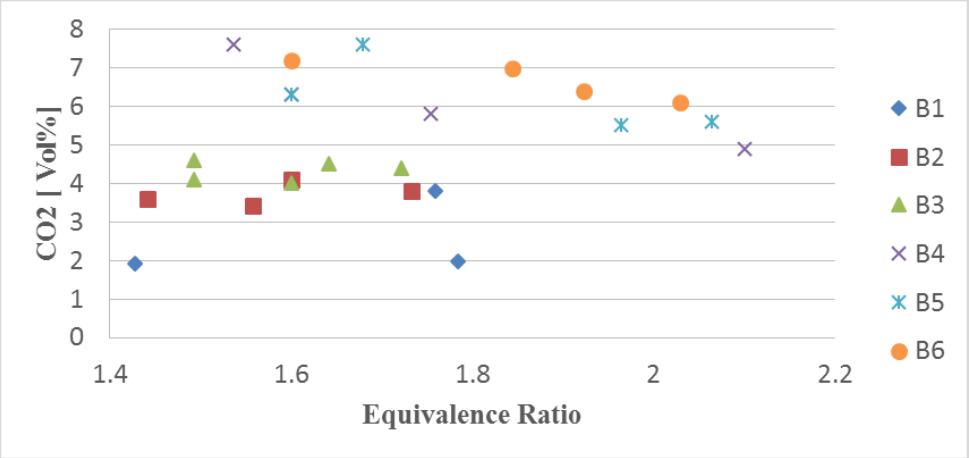

Figure 6-7 CO_2 exhaust gas concentration (dry) as a function of equivalence ratio for all different blends.

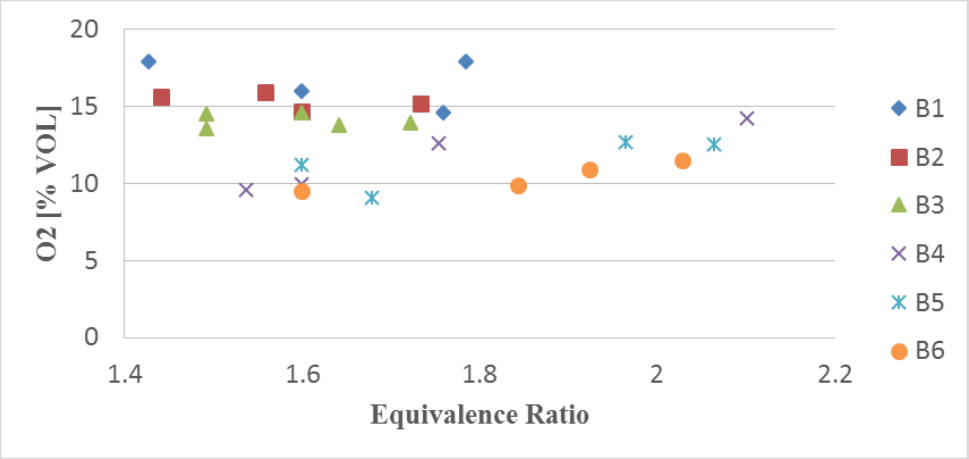

Figure 6-8 O_2 exhaust gas concentration (dry) as a function of equivalence ratio for all different blends.

That is another evidence that the combustion for diesel blends was not good in addition to CO production for this blends that showed. The O_2 emissions profiles were shown

in figure 6.8. Where the more efficient combustion was for B4, B5 and B6, therefore, the lowest O_2 emissions were for them. However, the lowest combustion and the peak O_2 emissions were measured for the mixture (B1) that another evidence that the combustion is not efficient enough.

6.3.3 Temperatures measurement

Measurements of temperature profiles on the burner wall are presented in figure 6.9 for a different amount of carbon dioxide addition to methane, and different liquid blends at various heights from the burner exit (300 and 700mm).The last position represents the exit point for the burner chimney. From the temperature profiles at Φ=1.7, it can be noted that the temperature decreases with carbon dioxide addition and increase with biodiesel blends.

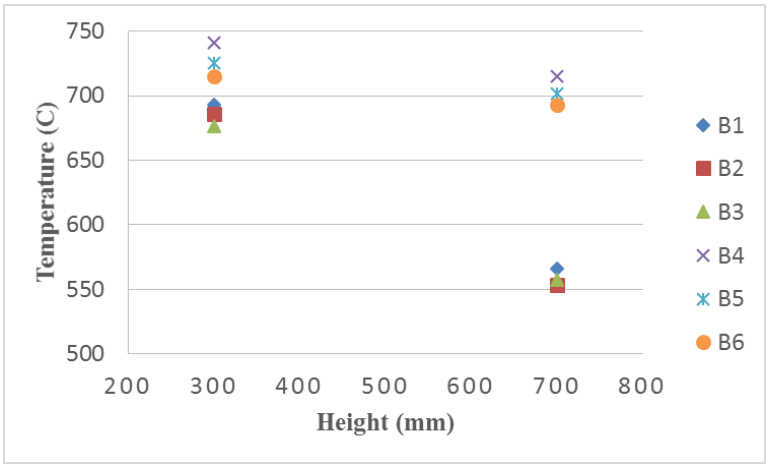

Figure 6-9 Temperature profiles at a different height for all different blends (Φ=1.7).

The reduction in temperature for CO_2 dilution can be attributed to that CO_2 diluent reduces the adiabatic temperature due to higher specific heat, which would result in a significant decrease in overall burning rate due to the reduction flame speed [155].

For example, with 0% and 10% carbon dioxide addition the temperature is lowered to 30 °C at the 700mm from the burner mouth. On the other hand, the increase in temperature biodiesel blends, it is attributed to that the higher oxygen content in biodiesel led to higher flame temperature. It may also belong due to the increase in fuel consumption. For instance, with the B1 blend and B4, the temperature is increased by 50 °C at the 300mm from the burner mouth.

6.3.4 CH* chemiluminescence analyses

CH* chemiluminescence images were averaged (300 images) and analysed to get the planar flame structures. Figure 6.10 shows the planar flame structures of different swirling flames using diesel and biodiesel at Φ=1.6.

CH* chemiluminescence excited from the flames can be utilised as a signal of heat release rate [169]. A Photron High-Speed Camera with a broadband long pass filter is used to reconstruct the region where soot is present.

The band-pass filter for the CH* radicals is centred at 430 nm ±15 nm. Results show that luminescence from biodiesel blends flame is significantly different to diesel. Diesel flame show high CH* intensity peaks compared to the biodiesel flames especially for B1 due to its high sooting tendency. The high luminosity of the post-reaction zone region for B1, B2 and B3 flame is reflected in the high-intensity count as a result of soot radiation

The powerful luminosity is attributed to CH* production as a consequence of the high content of aromatic rings in diesel. In contrast, biodiesel flames exhibit less CH* chemiluminescence intensity within the combustor indicative of cleaner combustion with a low level of soot formation.

The presence of oxygen in the biodiesel augments the local combustion of hydrocarbons, whereas the lack of aromatic rings reduces the formation of soot and the sooty yellowish flame brush downstream. Likewise, it has been reported that the soot generated from biodiesel is rapidly oxidised because of the initial combination of oxygen groups in the molecule [170].

On the other hand, results show greater CH* gain and soot for blends that did not contain CO_2 (B1, B4), likely a consequence of reduced mixing and high reactivity compared to other blends. Moreover, the high temperature of the CO_2 in the CRZ will ensure a fast chemical reaction of the diluted reactants, thus allowing low emissions and lower temperatures. The low relative CH* luminosity of the post-reaction zone region for blends with high CO_2 concentration shows an enhanced, cleaner combustion. However, this phenomenon stops at higher CO_2 levels, i.e. 20% when

tested, which led to combustion only at the tip of the burner and troubles during ignition. The high luminosity of the post-reaction zone region for B1, B2 and B3 flame is reflected in the high-intensity count as a result of soot radiation, and it produced a saturation CH* luminosity as shown in figure 6.10.

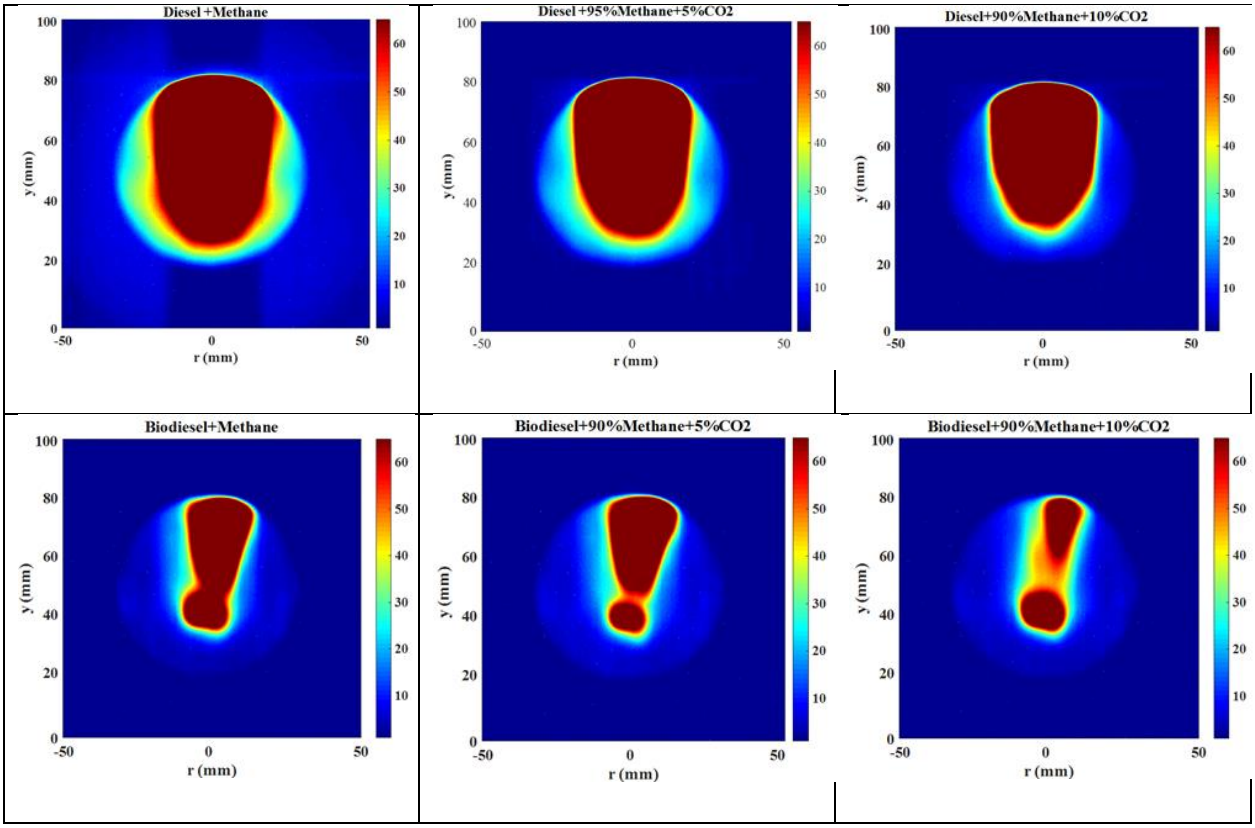

Figure 6-10 Abel inversion for CH* chemiluminescence for different blends at equivalence ratio = 1.6.

6.4 Summary

An experimental study on the combustion CO_2/CH_4/biodiesel and CO_2/CH_4/diesel mixtures at atmospheric conditions were carried. The combinations have been examined by using varying levels of premixing with various equivalences ratio. Results showed that biodiesel group blends reduced CO production at all tested conditions. Moreover, these combinations caused a reduction in emissions of nitrous oxides across all measurements.

The trend of lower CO emissions for biodiesel could be due to the oxygen content in biodiesel cooking oil resulted in a complete combustion than diesel oil. However, the lower NOx emissions compared to diesel blends for biodiesel blends for all the cases

and different equivalence ratios could be due to the role of oxygen in the molecule that suppresses CH* production, thus reducing prompt NOx formation and must be attributed in part to the higher heat of vaporisation of the biodiesel spray.

The introduction of CO_2 reduced the reaction rate and temperatures in the combustion zone, thus leading to a reduction in emissions of nitrous oxides as a consequence of decreases in flame temperature. CO_2 diluent decreased CO production at all tested conditions that belong to the incomplete combustion of pockets of fuels for blends without CO_2 and could also be attributed to the short residence time, so the CO formed in the combustion zone has less time to convert to CO_2 completely.

CH* intensity profiles downstream the burner outlet for diesel blends and biodiesel blends were carried as well. Diesel flames showed high CH intensity in the axial profile compared to biodiesel due to the high sooting tendency of the former. On the other hand, results showed greater CH* gain and soot for blends that did not contain CO_2. In general CO_2/CH_4/biodiesel mixtures have produced the cleanest profiles with the best flame stability.

Chapter 7

Conclusions and future work

For every fact, there is an infinity of hypotheses

Robert Maynard Pirsig

7.1 Conclusions

The condition to meet stringent environmental legislation and global depletion of fossil fuels have prompted continuous development for clean, sustainable alternative fuel and low-emissions combustion technology. In the field of the gas turbine, fuel flexibility is a required feature from the perspective of meeting emissions objective and reducing operating cost.

Even more, fuel flexibility is a required feature to meet all the above characteristics while minimising operating cost in gas turbines. Thus, some alternative fuels such as syngas or biodiesel can be used for gas turbines as these can comply with these requirements while being obtained from various processes, making them potential candidates for sustainable power generation. On the other hand in many combustion applications, the fuel is initially present as either liquid or solid. Most of the existing approaches dealing with combustion flows are limited to single-phase injection. To eliminate this limit, a new model for multiphase combustion has been developed.

Consequently, this work examined the performance of swirl burners using different injection strategies for various substitute fuels. The research procedure involved various stages;

- An assessment study between two liquid fuels, a pure biodiesel and saturated biodiesel, compared to kerosene. Atomization forms were obtained, and a combustion test campaign was initiated using a generic swirl burner.
- A trial study on the combustion of methane-carbon dioxide mixtures was achieved. Gas mixtures were examined by using different injection strategies with and without swirl and with and without central injection.

- The last burner was finally employed to carry out trials using multi-phase injection, where, experimental work investigated the performance of a swirl burner using various mixtures of CO_2/CH_4 blends with either diesel or biodiesel derived from cooking oil.

The most significant findings and conclusions of this study are listed below.

7.1.1 High-pressure optical chamber

- It was noticed in the saturated biodiesel that injection patterns are less to provide efficient droplet breakup and atomization caused by higher viscosity and surface tension.
- At atmospheric and elevated pressure, outcomes revealed that CO emissions are reduced with the biodiesels, perhaps as a result of the fuel-bound oxygen in the molecule which starts reacting further downstream than the oxygen contained in the air flow [50].
- Relatively, the saturated biodiesel also presented lower CO concentrations, in some points even lesser than the unsaturated biodiesel [48, 49]. The saturated biodiesel seems to be burning with low CO production; it is believed that a process related to the saturated particles boost heat transfer at the bottom of the flame.
- Higher NO_X concentrations in the exhaust were produced by using the saturated blend. The higher NO_X emissions from the biodiesels were connected to a greater CH* creation leading to induce NO_X via CH+N→HCN reactions, as observed by others [141].

  Additionally, the largest temperature of reaction produced by the additional oxygen and enhanced combustion in the saturated biodiesel could also cause higher Zeldovich emissions (thermal NO_X). Contrary to the experimental results, atomization performance was thought to be a parameter that would control the resultant NO_X concentrations. For the bio-blends, as reduced spray angle and bigger droplet size [57] would result in the fuel remaining unburned for longer periods of time and greater axial distances, reducing NO_X by a reduction in the combustion efficiency, burning more downstream to achieve the reaction.

- The saturated solid organic compounds appear to have a catalytic influence to increase radical production downstream of the flame zone, thus growing quick NO_X formation.

- The saturated solid organic seem to be improving the production of OH radicals through reactions with the oxygen embedded in the fuel, thus increasing temperature even further with an associated production of nitrogen oxides.

- The increase of operating pressure had the consequence of increasing combustion efficiency.
- It has been revealed that the perfect operability region for the saturated biodiesel is at very lean conditions.
- Both kerosene and the unsaturated biodiesel produce lower NOx emissions when related with the saturated biodiesel, a phenomenon that could be linked to the content of nitrogen in the organic material carried by the saturated blend[54].

  Furthermore, solid particles presented traces of a more efficient combustion regime, i.e. lower CO and higher CO_2. Thus higher temperatures and increased Zeldovich NOx.
- It was also noticed that NOx emissions are reduced considerably at higher pressures if the influence of pressure on NOx concentration is taken into consideration, with a peak of 120 ppm under atmospheric conditions decreasing to 25ppm at 2.9 bars for the saturated biofuel blend. Meanwhile, the power requirements for all cases are similar at 40 KW.

  It is believed that the high pressure forces the flame to withdraw towards the burner, compacting it and improving combustion and reactivity.

- Visual observations presented that saturated biodiesel will incline to produce higher soot emission, reducing the applicability of the fuel for gas turbines.

7.1.2 20 KW generic swirl burner with gases blends

- Results displayed that the introduction of limited amounts of CO_2 (15%) had controlled reaction rates and temperatures in the combustion zone, thus creating a decrease in emissions.
- All equivalence ratios tested presented a declining trend in the level of NOx emissions as the CO_2 diluent ratio rises from 0 to 30%. The lesser NOx can be attributed to the thermal effects of CO_2 dilution.
- The best trends were attained using B2 (85% CH_4-15 % CO_2) which created the lowest CO concentration.
- The great formation of CO with B1 is due to the incomplete combustion of pockets of fuels. That could be attributed to the short residence time when the system runs without swirl, so the CO formed in the combustion zone has less time to convert to CO_2 completely. Additionally, the low flame temperature under rich conditions prohibits the conversion of CO into stable species of CO_2.
- B2-S2 represents the most stable flame; the post-reaction zone showed little luminosity at the downstream post-reaction zone of the flame, indicative of clean combustion with the low level of soot formation relatively.
- CH chemiluminescence distribution presented that B1-S1 and B1-S3 have higher CH* radical variations, as the formation of CH* is greater but less controlled when compared to B1-S2.
- The use of central premixed injection produces the most chaotic CH* production case, perhaps because of the production of radicals in a highly chaotic region such as the central recirculation zone.
- Results for the case of closed holes revealed that the introduction of limited amounts of CO_2 (10%) had controlled reaction rates and temperatures in the combustion zone, thus reducing emissions.
- CH* chemiluminescence distribution showed that D1 and D4 have higher CH* radical fluctuations, as the construction of CH* is larger when compared to D2 and D3, and the latter showed a good CO_2 production, low CO and NOx, with relatively high flame stability.

- The high CH* production for D4 blends is attributed to that small increase of CO_2 in the mixture appears to be performing as a promoter of better combustion, reducing the competition of reacting species for oxygen.
- The results showed that a notable reduction in NOx was observed at all conditions for the CO_2/methane blends in about 60% for 10% CO_2 addition. However, carbon monoxide emissions also decreased when using 5-10% CO_2 addition.
- The use of CO_2/methane blends mixtures led to lower CO production about 83% for the case of 10% CO_2.
- CH* chemiluminescence analyses indicated that pure methane produced high heat fluctuation, with CO_2 at 5-10% showing the most stable CH* profiles.
- In general, more dilution of CO_2 leads to even poorer combustion and flame extinction only above the burner tip. This phenomenon ends at higher CO_2 concentrations which cause combustion only at the tip of the burner and trouble with ignition will appear.

7.1.3 20 KW generic swirl burner with multiphase

- Results showed that biodiesel group blends reduced CO production at all tested conditions that could be caused by the oxygen content in biodiesel cooking oil resulted in a complete combustion than diesel oil.
- The biodiesel combinations produced a reduction in emissions of nitrous oxides across all measurements.

  The lower NOx emissions compared to diesel blends for biodiesel blends for all the cases and different equivalence ratios could be due to the role of oxygen in the molecule that suppresses CH* production, thus reducing prompt NOx formation and must be attributed in part to the higher heat of vaporisation of the biodiesel spray.

- The introduction of CO_2 reduced the reaction rate and temperatures in the combustion zone, thus leading to a reduction in emissions of nitrous oxides as a result of decreases in flame temperature.

- CO_2 diluent decreased CO production at all tested conditions that belong to the incomplete combustion of pockets of fuels for blends without CO_2 and could also be attributed to the short residence time, so the CO formed in the combustion zone has less time to convert to CO_2 completely.
- Diesel flames showed high CH* intensity compared to biodiesel due to the high sooting trend of the first.

- Results showed greater CH* gain and soot for blends that did not contain CO_2 as a mixture.
- In general CO_2/CH_4/biodiesel mixtures have produced the cleanest profiles with the best flame stability.

7.2 Future work

The work of this research has been achieved at Cardiff university with 20 kW swirl burner while with HPOC were accomplished at the gas turbine research centre in Port Talbot. Many suggestions and ideas could be made for future studies, and can be summarised as follows:

- This research could be extended by adding biofuel preheating to provide lower viscosity. Then enhance atomization, along with higher injection pressures to be used for spraying the saturated biodiesel, that will improve combustion. Proposed solutions to this problem include biofuel preheating to deliver lower viscosity and hence improve atomization, besides higher injection pressures to be used for scattering the saturated biodiesel.
- A significant issue to be considered is the use of other methods of visualisation, such as Planar Laser Induced Fluorescence (PLIF).

  It has been used successfully in the analysis of swirling flames and the propagation of CH* and OH* radicals, which according to the theory are related to the burning region and temperature intensity.
- Moreover, the system needs to be run with a greater variety of fuels such as those with more hydrogen content, to see the effect of these fuels upon the emissions and stability limits.

- Computational fluid dynamics (CFD) is considered one of the branches of fluid mechanics, which uses numerical techniques and algorithms to resolve and analyse problems that include fluid flows.

  In the future, it is worth to use saturated biodiesel and compared to kerosene fuel using CFD. Moreover, using CFD with the two-phase flow with biodiesel, diesel and other blends.

- Incomplete gas-liquid mixing can have a significant impact on emissions. Premixed mixing for two phases is more susceptible to combustion instabilities.

  In the future, it is worth to investigate using effervescent atomization for better.

- One of the proposals of this project is to continue with the investigations on swirling flows with other fuels included methanol used to reduce NOx and carbon dioxide emissions, and a range other liquid biofuels.

- Study of the fuel droplet characteristics with biodiesels can be performed using a pressure swirl atomizer and compared to the present plain-jet air blast type atomizer.

- The methodology employed in this dissertation can be extended to other alternative fuels such as bioethanol, Fisher-Tropsch fuel or bio-oil.

- The instabilities affecting the two-phase exhaust jet are extraordinarily complex, and much more work needs to be done to understand the nature of the events at the phase interface.

  New diagnostic techniques are necessary here, as well. Small probes, inserted into the two-phase flow, might provide useful information about the frequency and scale of the instabilities.

References:

[1] R. K. Bhargava, L. Branchini, F. Melino, and A. Peretto, "Available and Future Gas Turbine Power Augmentation Technologies: Techno-Economic Analysis in Selected Climatic Conditions," *J. Eng. Gas Turbines Power*, vol. 134, no. 10, p. 102001, 2012.

[2] The carbon Brief, "Seven essential graphs from the IEA's World Energy Outlook," 2012. [Online]. Available: http://www.carbonbrief.org/blog/2012/11/favourite-graphs-from-iea.

[3] D. Eckardt, and P. Rufli, "Advanced gas turbine technology: ABB/BCC historical firsts," in *Journal of Engineering for Gas Turbines and Power*, vol. 124, no. 3, p. 542,2002.

[4] Frank J. Bartos, "High -Efficiency gas turbines add new flexibility," *Control Eng.*, 2011.

[5] Department of Energy and Climate Change, "Gas Generation Strategy," no. December, by the Stationery Office Limited, UK, pp. 1–68, 2012.

[6] Ashgriz N, *Handbook of Atomization and Sprays*. Springer Science & Business Media, 2011.

[7] S. H. I. . Cohen H., Rogers GFC., *Gas turbine theory*. Pearson Education, 1996.

[8] N. Hashimoto, Y. Ozawa, N. Mori, I. Yuri, and T. Hisamatsu, "Fundamental combustion characteristics of palm methyl ester (PME) as alternative fuel for gas turbines," *Fuel*, vol. 87, no. 15–16, pp. 3373–3378, 2008.

[9] S. Blakey, L. Rye, and C. W. Wilson, "Aviation gas turbine alternative fuels: A review," *Proc. Combust. Inst.*, vol. 33, no. 2, pp. 2863–2885, 2011.

[10] A. H. Lefebvre, *Gas Turbine Combustion*. 1999.

[11] T. Mosbach, G. C. Gebel, P. Le Clercq, R. Sadr, K. Kannaiyan, and A. Al-Sharshani, "Investigation of GTL-Like Jet Fuel Composition on GT Engine Altitude Ignition and Combustion Performance: Part II—Detailed Diagnostics," in *Volume 2: Combustion, Fuels and Emissions, Parts A and B*, p. 507–517,2011.

[12] D. Bulzan, B. Anderson, C. Wey, R. Howard, E. Winstead, A. Beyersdorf, E. Corporan, M. J. DeWitt, C. Klingshirn, S. Herndon, R. Miake-Lye, M. Timko, E. Wood, K. M. Tacina, D. Liscinsky, D. Hagen, P. Lobo, and P. Whitefield, "Gaseous and Particulate Emissions Results of the NASA Alternative Aviation Fuel Experiment (AAFEX)," in *Volume 2: Combustion, Fuels and Emissions, Parts A and B*, p. 1195–1207,2010.

[13] NASA and B. Bruce, "An Overview of the Aviation Fuel Experiment (AAFEX)," *Internaional Conf. Transp. Atmos. Clim.*, no. 10, p. 21–25,2009, 2009.

[14] A. N. Phan, and T. M. Phan, "Biodiesel production from waste cooking oils," *Fuel*, vol. 87, no. 17–18, pp. 3490–3496, 2008.

[15] A. Arrowsmith, "Atomization and Sprays.," *Chem. Eng. Sci.*, vol. 45, no. 5, p. 1435, 1990.

[16] F. Barreras, A. Lozano, J. Barroso, and E. Lincheta, "Experimental Characterization of Industrial Twin-Fluid Atomizers," *At. Sprays*, vol. 16, no. 2, pp. 127–146, 2006.

[17] B. S. Park, H. Y. Kim, Y. Kim, and J. T. Chung, "An experimental study on the spray characteristics of a dual-orifice type swirl injector at low fuel temperatures," *KSME Int. J.*, vol. 18, no. 7, pp. 1187–1195, 2004.

[18] N. Stuurman, and R. D. Vale, *Impact of new camera technologies on discoveries in cell biology*, vol. 231, no. 1. 2016.

[19] Y. Huang, and V. Yang, "Dynamics and stability of lean-premixed swirl-stabilized combustion," *Prog. Energy Combust. Sci.*, vol. 35, no. 4, pp. 293–364, 2009.

[20] A. H. Lefebvre, *Gas Turbine Combustion.second edition*. United states of America : Edwards brothers, 1998.

[21] J. S. Kurniawan, and S. Khardi, "Comparison of methodologies estimating emissions of aircraft pollutants, environmental impact assessment around airports," *Environ. Impact Assess. Rev.*, vol. 31, no. 3, pp. 240–252, 2011.

[22] S. Sgouridis, P. A. Bonnefoy, and R. J. Hansman, "Air transportation in a carbon constrained world: Long-term dynamics of policies and strategies for

mitigating the carbon footprint of commercial aviation," *Transp. Res. Part A Policy Pract.*, vol. 45, no. 10, pp. 1077–1091, 2011.

[23] R. Pavri, and G. D. Moore, "Gas Turbine Emissions and Control," *GE Power system*, vol. 1, no. 3, GE Power Systems, Atlanta, GA, 2008.

[24] G. E. Andrews, L. Hu, and W. Stephen, "Particulate Mass Emissions From Aircraft: A First Order Approximation Method Based on Experience From Diesel Particulate Mass Emissions Measurement," *ASME Turbo Expo Power Land, Sea, Air*, vol. 2, no. Combustion, Fuels and Emissions, pp. 465–487, 2009.

[25] M. N. Kim, "Design of Low NOx gas turbine combustion chamber," *Dep. Fuel Energy LeedsLeeds Univ.*, p. 181, 1995.

[26] C. Soares, *Gas Turbines. [recurso electrónico] : A Handbook of Air, Land and Sea Applications.* Butterworth-Heinemann, 2015.

[27] A. H. Lefebvre, *Gas Turbine Combustion*. CRC press, 1999.

[28] M. A. R. do Nascimento, L. de Oliveira Rodrigues, E. C. dos Santos, E. E. B. Gomes, F. L. G. Dias, E. I. G. Velásques, and R. A. M. Carrillo, "Progress in Gas Turbine Performance," *Prog. Gas Turbine Perform.*, pp. 107–142, 2013.

[29] T. Ai, C. Koeneke, H. Arimura, and Y. Hyakutake, "Development of an Air Cooled G Class Gas Turbine (the M501gac)," 2009.

[30] I. Eisaku, O. lkuo, T. Kelm, M. Akimasa, and M. Junichiro, "Development of Key Technologies for the Next Generation Gas Turbine," *Proc. ASME Turbo Expo*, vol. 1, p. 847, 2010.

[31] G. E. Andrews, "Short course, ultra Low NOx gas turbine combustion ," *Leeds Energy Resour. Res. Institute, Leeds Univ.* , 2009.

[32] G. E. Andrews, N. T. Ahmed, Phylaktou, and P. King, "Weak extinction in low NOx gas turbine combustion," in *Proceedings of the ASME Turbo Expo*, vol. 2, p. 623–638,2009.

[33] M. Moliere, "Expanding fuel flexibility of gas turbines*," *Proc. Inst. Mech. Eng. Part A J. Power Energy*, vol. 219, no. 2, pp. 109–119, 2005.

[34] P. Popovic, G. Myers, J. Citeno, R. Symonds, and A. Campbell, "Fuel Flexibility with Low Emissions in Heavy Duty Industrial Gas Turbines," in

ASME Turbo Expo : Power for Land, Sea, and Air, p. 163–172,2010.

[35] R. Jones, J. Goldmeer, and B. Monetti, "Addressing gas turbine fuel flexibility," *GE Energy*, vol. GER-4601, pp. 1–20, 2011.

[36] I. G. Wright, and T. B. Gibbons, "Recent developments in gas turbine materials and technology and their implications for syngas firing," *Int. J. Hydrogen Energy*, vol. 32, no. 16, pp. 3610–3621, 2007.

[37] J. and B. A. Meher-Homji, C. Zachary, "Gas turbine fuel system design. Combustion and operability," in *Proceedings of the Thirty-Ninth Turbomachinery Symposium*, p. 4–7,2010.

[38] J. Lewis, A. Valera-medina, S. Morris, R. Marsh, and H. Baej, "The Use of CO2 to Improve Stability and Emissions of an IGCC Combustor," in *ASME Turbo Expo : Turbine Technical Conference and Exposition GT2014-25446*, p. 1–11,2014.

[39] H. Baej, A. Valera Medina, N. Syred, R. Marsh, and P. J. Bowen, "Blowoff propensity, CRZs and flow turbulent nature using various syngases for gas turbines," 2015.

[40] J. Warnatz, U. Maas, and R. W. Dibble, *Combustion*, vol. 26, no. 5. Springer, 1999.

[41] M. C. Lee, S. Bin Seo, J. Yoon, M. Kim, and Y. Yoon, "Experimental study on the effect of N2, CO2, and steam dilution on the combustion performance of H2 and CO synthetic gas in an industrial gas turbine," *Fuel*, vol. 102, pp. 431–438, 2012.

[42] J. Pareja, H. J. Burbano, A. Amell, and J. Carvajal, "Laminar burning velocities and flame stability analysis of hydrogen/air premixed flames at low pressure," *Int. J. Hydrogen Energy*, vol. 36, no. 10, pp. 6317–6324, 2011.

[43] H. Kurji, A. Okon, A. Valera-Medina, and C. Cheng-Tung, "Reduction of emissions by using various syngases with different injection strategies under premixed combustion mode," in *International Conference for Students on Applied Engineering, ICSAE*, p. 407–412,2017.

[44] M. O. Vigueras-Zuniga, A. Valera-Medina, N. Syred, and P. Bowen, "High Momentum Flow Region and Central Recirculation Zone Interaction in

Swirling Flows," *Ing. Mec. Technol. Y Desarro.*, vol. 4, no. 6, pp. 195–204, 2014.

[45] J. Fu, C. Tang, W. Jin, L. D. Thi, Z. Huang, and Y. Zhang, "Study on laminar flame speed and flame structure of syngas with varied compositions using OH-PLIF and spectrograph," *Int. J. Hydrogen Energy*, vol. 38, no. 3, pp. 1636–1643, 2013.

[46] F. He, Z. Li, P. Liu, L. Ma, and E. N. Pistikopoulos, "Operation window and part-load performance study of a syngas fired gas turbine," *Appl. Energy*, vol. 89, no. 1, pp. 133–141, 2012.

[47] H. Shih, and J. Hsu, "A Computational Study of Flammability Limits of Opposed-Jet Syngas Diffusion Flames," *Int. J. Hydrogen Energy*, vol. 36, no. November, pp. 15868–15879, 2012.

[48] C. P. Fenimore, "Studies of Fuel-Nitrogen Rich Flame Gases," in *Proceedings of the Combustion Institute*, vol. 17, no. 1, p. 661,1979.

[49] K. K. Gupta, A. Rehman, and R. M. Sarviya, "Bio-fuels for the gas turbine: A review," *Renew. Sustain. Energy Rev.*, vol. 14, no. 9, pp. 2946–2955, 2010.

[50] K. K. Gupta, a Rehman, and R. M. Sarviya, "Evaluation of Soya Bio-Diesel as a Gas Turbine Fuel," *Iran. J. Energy Environ.*, vol. 1, no. 3, pp. 205–210, 2010.

[51] B. Esteban, J. R. Riba, G. Baquero, A. Rius, and R. Puig, "Temperature dependence of density and viscosity of vegetable oils," *Biomass and Bioenergy*, vol. 42, pp. 164–171, 2012.

[52] A. Rehman, D. R. Phalke, and R. Pandey, "Alternative fuel for gas turbine: Esterified jatropha oil-diesel blend," *Renew. Energy*, vol. 36, no. 10, pp. 2635–2640, 2011.

[53] A. Demirbas, "Progress and recent trends in biofuels," *Prog. Energy Combust. Sci.*, vol. 33, no. 1, pp. 1–18, 2007.

[54] M. A. R. Nascimento, E. S. Lora, P. S. P. Corrêa, R. V. Andrade, M. A. Rendon, O. J. Venturini, and G. A. S. Ramirez, "Biodiesel fuel in diesel micro-turbine engines: Modelling and experimental evaluation," *Energy*, vol. 33, no. 2, pp. 233–240, 2008.

[55] Z. Habib, R. Parthasarathy, and S. Gollahalli, "Performance and emission

characteristics of biofuel in a small-scale gas turbine engine," *Appl. Energy*, vol. 87, no. 5, pp. 1701–1709, 2010.

[56] S. A. Basha, K. R. Gopal, and S. Jebaraj, "A review on biodiesel production, combustion, emissions and performance," *Renew. Sustain. Energy Rev.*, vol. 13, no. 6–7, pp. 1628–1634, 2009.

[57] H. V. Panchasara, B. M. Simmons, A. K. Agrawal, S. K. Spear, and D. T. Daly, "Combustion Performance of Biodiesel and Diesel-Vegetable Oil Blends in a Simulated Gas Turbine Burner," *J. Eng. Gas Turbines Power*, vol. 131, no. 3, p. 31503, 2009.

[58] A. Campbell, J. Goldmeer, T. Healy, R. Washam, M. Moliere, and J. Citeno, "Heavy Duty Gas Turbine Fuel Flexibility," *Proc. ASME Turbo Expo*, vol. GT2008-513, pp. 1077–1085, 2008.

[59] M. Canakci, "Combustion characteristics of a turbocharged DI compression ignition engine fueled with petroleum diesel fuels and biodiesel," *Bioresour. Technol.*, vol. 98, no. 6, pp. 1167–1175, 2007.

[60] A. Senatore, M. Cardone, L. Allocca, S. Vitolo, and V. Rocco, "Experimental Characterization of a Common Rail Engine Fuelled with Different Biodiesel," 2005.

[61] X. W. Zhao, X. K. Han, C. He, and J. W. Tan, "Experimental study on spray characteristics of biodiesel oil," *Chin Intern Combust Engine Eng*, vol. 1, pp. 16–19, 2008.

[62] C. S. Lee, S. W. Park, and S. Il Kwon, "An experimental study on the atomization and combustion characteristics of biodiesel-blended fuels," *Energy and Fuels*, vol. 19, no. 5, pp. 2201–2208, 2005.

[63] C. Grimaldi, and L. Postrioti, "Experimental Comparison Between Conventional and Bio-derived Fuels Sprays from a Common Rail Injection System," 2000.

[64] J. M. Desantes, R. Payri, F. J. Salvador, and V. Soare, "Study of the Influence of Geometrical and Injection Parameters on Diesel Sprays Characteristics in Isothermal Conditions," *SAE Pap. 2005-01-0913*, vol. 2005, no. 724, 2005.

[65] E. Bocci, A. Di Carlo, S. J. McPhail, K. Gallucci, P. U. Foscolo, M. Moneti, M.

Villarini, and M. Carlini, “Biomass to fuel cells state of the art: A review of the most innovative technology solutions,” *Int. J. Hydrogen Energy*, vol. 39, no. 36, pp. 21876–21895, 2014.

[66] R. Prakash, R. K. Singh, and S. Murugan, “Experimental investigation on a diesel engine fueled with bio-oil derived from waste wood-biodiesel emulsions,” *Energy*, vol. 55, pp. 610–618, 2013.

[67] J. A. Martin, and A. A. Boateng, “Combustion performance of pyrolysis oil/ethanol blends in a residential-scale oil-fired boiler,” *Fuel*, vol. 133, pp. 34–44, 2014.

[68] J. Lehto, A. Oasmaa, Y. Solantausta, M. Kytö, and D. Chiaramonti, “Review of fuel oil quality and combustion of fast pyrolysis bio-oils from lignocellulosic biomass,” *Appl. Energy*, vol. 116, pp. 178–190, 2014.

[69] A. Cappelletti, A. M. Rizzo, D. Chiaramonti, and F. Martelli, “CFD redesign of micro gas turbine combustor for bio-fuels fueling,” *XXI Int. Symp. Air Breath. Engines*, vol. 1506–1513., no. SEPTEMBER, pp. 1199–1206, 2013.

[70] H. Kurji, A. Valera-Medina, J. Runyon, A. Giles, D. Pugh, R. Marsh, N. Cerone, F. Zimbardi, and V. Valerio, “Combustion characteristics of biodiesel saturated with pyrolysis oil for power generation in gas turbines,” *Renew. Energy*, vol. 99, pp. 443–451, 2016.

[71] N. Hashimoto, H. Nishida, and Y. Ozawa, “Fundamental combustion characteristics of Jatropha oil as alternative fuel for gas turbines,” *Fuel*, vol. 126, pp. 194–201, 2014.

[72] C. T. Chong, and S. Hochgreb, “Spray Combustion Characteristics of Palm Biodiesel,” *Combust. Sci. Technol.*, vol. 184, no. 7–8, pp. 1093–1107, 2012.

[73] C. T. Chong, and S. Hochgreb, “Measurements of non-reacting and reacting flow fields of a liquid swirl flame burner,” *Chinese J. Mech. Eng.*, vol. 28, no. 2, pp. 394–401, 2015.

[74] D. Sequera, A. K. Agrawal, S. K. Spear, and D. T. Daly, “Combustion Performance of Liquid Biofuels in a Swirl-Stabilized Burner,” *J. Eng. Gas Turbines Power*, vol. 130, no. 3, p. 32810, 2008.

[75] C. D. Bolszo, and V. G. McDonell, “Emissions optimization of a biodiesel fired

gas turbine," *Proc. Combust. Inst.*, vol. 32 II, no. 2, pp. 2949–2956, 2009.

[76] C. D. Bolszo, and V. G. McDonell, "Evaluation of Plain-Jet Air Blast Atomization and Evaporation of Alternative Fuels in a Small Gas Turbine Engine Application," *At. Sprays*, vol. 19, no. 8, pp. 771–785, 2009.

[77] C. T. Chong, and S. Hochgreb, "Flame structure, spectroscopy and emissions quantification of rapeseed biodiesel under model gas turbine conditions," *Appl. Energy*, vol. 185, pp. 1383–1392, 2017.

[78] W. A. Sirignano, "Fluid Dynamics of Sprays— Freeman Scholar Lecture," *J. Fluids Eng.*, vol. 115, no. 3, pp. 345–378, 1993.

[79] H. H. Chiu, "Advanced and Challenges in Droplet and Spray Combustion," *Prog. Energy Combust. Sci.*, vol. 26, no. 4, pp. 381–416, 2000.

[80] C. T. Crowe, T. R. Troutt, and J. N. Chung, "Numerical Models for Two-Phase Turbulent Flows," *Annu. Rev. Fluid Mech.*, vol. 28, no. 1, pp. 11–43, 1996.

[81] V. S. Santoro, D. C. Kyritsis, and A. Gomez, "An experimental study of vortex-flame interaction in counterflow spray diffusion flames," *Proc. Combust. Inst.*, vol. 28, no. 1, pp. 1023–1030, 2000.

[82] A. Lemaire, T. R. Meyer, K. Zahringer, J. R. Gord, and J. C. Rolon, "PIV/PLIF Investigation of Two-Phase Vortex-Flame Interactions," in *the 11th International Symposium on Applications of Laser Techniques to Fluid Mechanics*, 2002.

[83] G. Gouesbet, and A. Berlemont, "Eulerian and Lagrangian approaches for predicting the behaviour of discrete particles in turbulent flows," *Prog. Energy Combust. Sci.*, vol. 25, no. 2, pp. 133–159, 1998.

[84] E. Loth, "Numerical approaches for motion of dispersed particles, droplets and bubbles," *Prog. Energy Combust. Sci.*, vol. 26, no. 3, pp. 161–223, 2000.

[85] V. IYER, and J. ABRAHAM, "Penetration and Dispersion of Transient Gas Jets and Sprays," *Combust. Sci. Technol.*, vol. 130, no. 1–6, pp. 315–334, 1997.

[86] F. H. Harlow, "Fluid dynamics in group T-3 Los Alamos national laboratory:(LA-UR-03-3852)," *J. Comput. Phys.*, vol. 195, no. 2, pp. 414–433, 2004.

[87] S. P. Lin, and R. D. Reitz, "Drop and Spray Formation From a Liquid Jet,"

Annu. Rev. Fluid Mech., vol. 30, no. 1, pp. 85–105, 1998.

[88] C. Baumgarten, "Mixture Formation in Internal Combustion Engines," *J. Chem. Inf. Model.*, pp. 1–312, 2013.

[89] A. W. Kerst, B. Judat, and E.-U. Schlünder, "Flow regimes of free jets and falling films at high ambient pressure," *Chem. Eng. Sci.*, vol. 55, no. 19, pp. 4189–4208, 2000.

[90] A. H. Lefebvre, "Fifty Years of Gas Turbine Fuel Injection," *At. Sprays*, vol. 10, no. 3–5, 2000.

[91] E. Goldstein, *the Theory and Practice of*, vol. 42, no. 3. CRC Press, 2015.

[92] C. Tricou, and K. Knasiak, "Development of a high transfer efficiency painting technology using effervescent atomization," *ILASS (Institute Liq. At.*, no. May, 2005.

[93] F. J. Petersen, O. Wørts, T. Schæfer, and P. E. Sojka, "Design and Atomization Properties for an Inside- Out Type Effervescent Atomizer," *Drug Dev. Ind. Pharm.*, vol. 30, no. 3, pp. 319–326, 2004.

[94] M. V. Panchagnula, and P. E. Sojka, "Spatial droplet velocity and size profiles in effervescent atomizer-produced sprays," *Fuel*, vol. 78, no. 6, pp. 729–741, 1999.

[95] C. A. W. Allen, and K. C. Watts, "Comparative analysis of the atomization characteristics of fifteen biodiesel fuel types," *Trans. ASAE*, vol. 43, no. 2, p. 207, 2000.

[96] A. S. V. and Sankar, "Swirl effervescent atomizer for spray combustion," in *Proceedings of the ASME Heat Transfer Division*, vol. 37, no. 2, p. 18–22,1995.

[97] M. E. C. Ferreira, J. J. G. Martins, and J. C. F. Teixeira, "Optimization of an Effervescent Atomizer to the Combustion of Residue Oils," in *ASME Summer Heat Transfer Conference collocated with the ASME Pacific Rim Technical Conference and Exhibition on Integration and Packaging of MEMS, NEMS, and Electronic Systems*, p. 751–757,2005.

[98] A. Mostafa and S. Khalil, "Measurements of Coal Water Slurry Sprays Produced by an Effervescent Atomizer," in *Compressed Air*, no. July, p. 1–7,2006.

[99] S. D. Sovani, J. D. Crofts, P. E. Sojka, J. P. Gore, and W. A. Eckerle, “Spray performance of a prototype effervescent diesel injector,” *ASME INTERN COMBUST ENGINE DIV PUBL ICE.*, vol. 32, pp. 81–88, 1999.

[100] R. R. Su TF, Chang CT, “Effects of injection pressure and nozzle geometry on spray SMD and D.I. emissions.,” 1995.

[101] T. R. Ohrn, D. W. Senser, and A. H. Lefebvre, “Geometrical Effects on Discharge Coefficients for Plain-Orifice Atomizers,” *At. Sprays*, vol. 1, no. 2, pp. 137–153, 1991.

[102] R. A. Coffee, *Electrostatic spraying of liquids and powders*, vol. 10, no. 10. Wiley New York etc, 1964.

[103] S. D. Sovani, P. E. Sojka, and A. H. Lefebvre, “Effervescent atomization,” *Prog. Energy Combust. Sci.*, vol. 27, no. 4, pp. 483–521, 2001.

[104] S. K. Chen, and A. H. Lefebvre, “Spray Cone Angles of Effervescent Atomizers,” *At. Sprays*, vol. 4, no. 3, pp. 291–301, 1994.

[105] J. D. Whitlow, A. H. Lefebvre, and R. J. Rollbuhler, “Experimental studies on effervescent atomizers with wide spray angles,” in *In AGARD, Fuels and Combustion Technology for Advanced Aircraft Engines 11 p (SEE N94-29246 08-25)*, 1993, vol. 1,1993.

[106] N. Carolina, “Numerical Simulation of Two-Phase Flow within an Aerated Liquid Injector,” in *48th AIAA Aerospace Sciences Meeting Including the New Horizons Forum and Aerospace Exposition*, no. January, p. 1–23,2010.

[107] R. Pavri, and G. D. Moore, “Gas Turbine Emissions and Control,” *GE Power Syst.*, vol. 1, no. 3, 2008.

[108] N. H. Escott, G. E. Andrews, H. S. Alkabie, Afa. AlShaikhly, and B. George, “Large airflow capacity radial swirlers for ultra low No sub (x) at high inlet temperatures.,” *Asme, New York, Ny(Usa).*, vol. 8, pp. 241–253, 1993.

[109] G. E. Andrews, I. D. Andrews, D. W. Dixon-Hardy, B. M. Gibbs, H. Li, and S. Wright, “Airport PM,” in *Volume 2: Combustion, Fuels and Emissions, Parts A and B*, p. 363–375,2010.

[110] R. M. Harrison, J. P. Shi, S. Xi, a. Khan, D. Mark, R. Kinnersley, and J. Yin, “Measurement of number, mass and size distribution of particles in the

atmosphere," *Philos. Trans. R. Soc. A Math. Phys. Eng. Sci.*, vol. 358, no. 1775, pp. 2567–2580, 2000.

[111] P. Schmittel, B. Günther, B. Lenze, W. Leuckel, and H. Bockhorn, "Turbulent swirling flames: Experimental investigation of the flow field and formation of nitrogen oxide," *Proc. Combust. Inst.*, vol. 28, no. 1, pp. 303–309, 2000.

[112] A. Ishak, M. Shaiful, M. Jaafar, and M. Nazri, "The effect of swirl number on discharge coefficient for various orifice sizes in a burner system," *J. Mek.*, no. 17, pp. 99–108, 2004.

[113] G. E. Andrews, N. Escott, and M. C. Mkpadi, "Radial Swirler Designs for Ultra-Low NOx Gas Turbine Combustors," in *ASME Turbo Expo : Power for Land, Sea, and Air*, 2008, no. 21, p. 277–289,2008.

[114] G. E. Andrews, M. N. Kim, M. C. Mkpadi, and S. a. Akande, "Liquid Fuelled Low NOx Radial Swirlers With Central Pilot Combustion," in *Volume 2: Turbo Expo 2007*, p. 311–321,2007.

[115] M. Barr, and F. A. Williams, "Comparison of combustion instabilities found in various types of combustion chambers," in *Symposium (International) on Combustion*, vol. 12, no. 1, p. 169–181,1969.

[116] T. Lieuwen, H. Torres, C. Johnson, and B. T. Zinn, "A Mechanism of Combustion Instability in Lean Premixed Gas Turbine Combustors," *J. Eng. Gas Turbines Power*, vol. 123, no. 1, p. 182, 2001.

[117] H. C. Mongia, T. J. Held, G. C. Hsiao, and R. P. Pandalai, "Incorporation Of Combustion Instability Issues Into Design Process: Ge Aeroderivative And Aero Engines Experience," *Combust. Instab. Gas Turbine Engines*, vol. 210, pp. 43–63, 2006.

[118] D. Sun, G. Lu, H. Zhou, Y. Yan, and S. Liu, "Quantitative assessment of flame stability through image processing and spectral analysis," *IEEE Trans. Instrum. Meas.*, vol. 64, no. 12, pp. 3323–3333, 2015.

[119] A. G. Gaydon, and H. G. Wolfhard, *Flames: Their structure, radiation and temperature*, vol. 24, no. 10. Halsted Press, 1971.

[120] G. J. Pendley, "High speed imaging technology: yesterday, today, and tomorrow," in *25th international Congress on High-Speed photography and*

Photonics, p. 110–113,2003.

[121] O. Chns, "w w w . p e r k i n e l m e r . c o m / i n s t r u m e n t s."

[122] D. Pavia, G. Lampman, and G. Kris, *Introduction To ORGANIC LABORATORY TECHNIQUES*. Cengage Learning, 2005.

[123] C. Harris, Daniel C. (Michelson Laboratory/China Lake, *Quantitative Chemical Analysis*, vol. 53, no. 9. Macmillan, 2010.

[124] N. Docquier, F. Lacas, and S. Candel, "Closed-loop equivalence ratio control of premixed combustors using spectrally resolved chemiluminescence measurements," *Proc. Combust. Inst.*, vol. 29, no. 1, pp. 139–145, 2002.

[125] E. Stresing, "High Speed Cameras." [Online]. Available: http://www.stresing.de/highspeed.html.

[126] L. Zimmer, S. Tachibana, T. Yamamoto, Y. Kurosawa, and K. Suzuki, "Evaluation of chemiluminescence as sensor for lean premixed combustion," *Continuum (N. Y).*, vol. 387, pp. 431–434, 2003.

[127] A. G. Gaydon, "Measurements of Effective Temperature and Studies with Special Sources," in *The Spectroscopy of Flames*, Springer, p. 182–220,1974.

[128] V. Nori, and J. Seitzman, "Chemiluminescence Measurements and Modeling in Syngas, Methane and Jet-A Fueled Combustors," in *45th AIAA Aerospace Sciences Meeting and Exhibit*, no. January, p. 1–14,2007.

[129] D. Sheet, "Agilent 6890N Network Gas Chromatograph."

[130] "High-Speed Photography," *Physics Today*, 1956. [Online]. Available: https://en.wikipedia.org/wiki/High-speed_photography.

[131] M. R. Morrell, J. M. Seitzman, M. Wilensky, E. Lubarsky, J. Lee, and B. Zinn, "INTERPRETATION OF OPTICAL EMISSIONS FOR SENSORS IN LIQUID FUELED COMBUSTORS Georgia Institute of Technology Atlanta , GA 39 th Aerospace Sciences Meeting & Exhibit," *39th Aerosp. Sci. Meet. Exhib.*, 2001.

[132] J. Kojima, Y. Ikeda, and T. Nakajima, "Basic aspects of OH (A), CH (A), and C 2 (d) chemiluminescence in the reaction zone of laminar methane--air premixed flames," *Combust. Flame*, vol. 140, no. 1, pp. 34–45, 2005.

[133] B. Higgins, M. Q. McQuay, F. Lacas, J. C. Rolon, N. Darabiha, and S. Candel, "Systematic measurements of OH chemiluminescence for fuel-lean, high-pressure, premixed, laminar flames," *Fuel*, vol. 80, no. 1, pp. 67–74, 2001.

[134] J. Kojima, Y. Ikeda, and T. Nakajima, "Multi-point time-series observation of optical emissions for flame-front motion analysis," *Meas. Sci. Technol.*, vol. 14, no. 9, pp. 1714–1724, 2003.

[135] K. Schreel, "Laser velocimetry techniques: LDV, PTV, PIV," 2005.

[136] F. Guethe, D. Guyot, G. Singla, N. Noiray, and B. Schuermans, "Chemiluminescence as diagnostic tool in the development of gas turbines," *Appl. Phys. B Lasers Opt.*, vol. 107, no. 3, pp. 619–636, 2012.

[137] C. O. Co, and N. O. No, "Portable Flue Gas Analyzer System testo 350 Measurements on stationary engines and burners , gas turbines and complex thermoprocesses," 2008.

[138] EPA, "Testo 350 Verification EPA."

[139] Testo, "Portable Emission Analysis." [Online]. Available: http://www.testo350.com/testo-350/350anadefsx/350faqs.html.

[140] C. Morley, "GASEQ; Chemical Equilibria in Perfect Gases ," *Gaseq*, 2005. [Online]. Available: www.gaseq.co.uk,.

[141] C. Pereira, G. Wang, and M. Costa, "Combustion of biodiesel in a large-scale laboratory furnace," *Energy*, vol. 74, no. C, pp. 950–955, 2014.

[142] "Tensiometer – For the measurement of surface and interfacial tension Precise measuring instruments for research and industry."

[143] "6100 Compensated Calorimeter 6100 Ordering Guide," p. 6120.

[144] I. C4000 and Calorimeter, "http://www.geminibv.nl/labware/ika-c4000-adiabatic-calorimeter." .

[145] Agilent Technologies, "Agilent 700 Series ICP Optical Emission Spectrometers User Guide," 2006.

[146] N. Cerone, F. Zimbardi, L. Contuzzi, E. Alvino, M. O. Carnevale, and V. Valerio, "Updraft gasification at pilot scale of hydrolytic lignin residue," *Energy and Fuels*, vol. 28, no. 6, pp. 3948–3956, 2014.

[147] S. H. Park, H. J. Kim, H. K. Suh, and C. S. Lee, “Atomization and spray characteristics of bioethanol and bioethanol blended gasoline fuel injected through a direct injection gasoline injector,” *Int. J. Heat Fluid Flow*, vol. 30, no. 6, pp. 1183–1192, 2009.

[148] S. M. Morris, P. J. Bowen, Y. Sevcenco, R. Marsh, and N. Syred, “Preliminary Results from a High Pressure Optical gas Turbine Combustor Model with 3D Viewing Capability,” *AIAA Int Meet. Orlando*, 2015.

[149] E. M. Fisher, W. J. Pitz, H. J. Curran, and C. K. Westbrook, “Detailed chemical kinetic mechanisms for combustion of oxygenated fuels,” *Proceedings of the Combustion Institute*, vol. 28, no. 2. on Combustion at the University of Edinburgh, Scotland, pp. 1579–1586, 2000.

[150] J. M. BEÉR, “Combustion Aerodynamics,” *Combust. Technol.*, vol. 3, pp. 61–89, 1974.

[151] V. TANGIRALA, R. H. CHEN, and J. F. DRISCOLL, “Effect of Heat Release and Swirl on the Recirculation within Swirl-Stabilized Flames,” *Combust. Sci. Technol.*, vol. 51, no. 1–3, pp. 75–95, 1987.

[152] T. Lieuwen, V. McDonell, D. Santavicca, and T. Sattelmayer, “9 Operability Associated with Issues Steady Flowing Combustors,” in *Synthesis Gas Combustion: Fundamentals and Applications*, CRC Press, p. 261,2009.

[153] S. S. Su, S. J. Hwang, and W. H. Lai, “On a porous medium combustor for hydrogen flame stabilization and operation,” *Int. J. Hydrogen Energy*, vol. 39, no. 36, pp. 21307–21316, 2014.

[154] L. Wu, N. Kobayashi, Z. Li, H. Huang, and J. Li, “Emission and heat transfer characteristics of methane-hydrogen hybrid fuel laminar diffusion flame,” *Int. J. Hydrogen Energy*, vol. 40, no. 30, pp. 9579–9589, 2015.

[155] Y. Zhang, W. Shen, H. Zhang, Y. Wu, and J. Lu, “Effects of inert dilution on the propagation and extinction of lean premixed syngas/air flames,” *Fuel*, vol. 157, pp. 115–121, 2015.

[156] D. E. Giles, S. Som, and S. K. Aggarwal, “NOx emission characteristics of counterflow syngas diffusion flames with airstream dilution,” *Fuel*, vol. 85, no. 12–13, pp. 1729–1742, 2006.

[157] T. García-Armingol, and J. Ballester, “Operational issues in premixed combustion of hydrogen-enriched and syngas fuels,” Int. J. Hydrogen Energy, vol. 40, no. 2, pp. 1229–1243, 2015.

[158] K. J. Whitty, H. R. Zhang, and E. G. Eddings, “Formation 6 Pollutant and Control,” *Group*, p. 169,2010, 2010.

[159] J. S. Chin, and a. H. Lefebvre, “A Design Procedure for Effervescent Atomizers,” *J. Eng. Gas Turbines Power*, vol. 117, no. 2, p. 266, 1995.

[160] U. E. L. Properties, “Fuel properties 1 FUEL PROPERTIES,” pp. 1–22.

[161] N. Khan, and V. Raghavan, “Structure and reaction zones of hydrogen e Carbon-monoxide laminar jet diffusion flames,” *Int. J. Hydrogen Energy*, vol. 39, no. 34, pp. 19832–19845, 2014.

[162] I. Glassman, and R. A. Yetter, *Glassman, Yetter Combustion*. 2008.

[163] İ. Çelikten, E. Mutlu, and H. Solmaz, “Variation of performance and emission characteristics of a diesel engine fueled with diesel, rapeseed oil and hazelnut oil methyl ester blends,” *Renew. Energy*, vol. 48, no. x, pp. 122–126, 2012.

[164] L. Spadaccini, “Pollutant formation and energy release in liquid-fuel turbulent diffusion flames,” in *Archive Set 140*, vol. 16, no. 1, p. 105–117,1963.

[165] G. V. Subbaiah, K. R. Gopal, and S. A. Hussain, “The effect of biodiesel and bioethanol blended diesel fuel on the performance and emission characteristics of a direct injection diesel engine,” *Iran. J. Energy Environ.*, vol. 1, no. 3, pp. 211–221, 2010.

[166] M. Gumus, and S. Kasifoglu, “Performance and emission evaluation of compression ignition engine using a biodiesel (aprocot seed kernel oil methyl ester) and its blends with diesel fuel,” *Biomass and Bioenergy*, vol. 34, no. 1, pp. 134–139, 2010.

[167] G. Labeckas, and S. Slavinskas, “The effect of rapeseed oil methyl ester on direct injection Diesel engine performance and exhaust emissions,” *Energy Convers. Manag.*, vol. 47, no. 13–14, pp. 1954–1967, 2006.

[168] S. Puhan, N. Vedaraman, G. Sankaranarayanan, and B. V. B. Ram, “Performance and emission study of Mahua oil (madhuca indica oil) ethyl ester in a 4-stroke natural aspirated direct injection diesel engine,” *Renew. Energy*,

vol. 30, no. 8, pp. 1269–1278, 2005.

[169] Y. Hardalupas, and M. Orain, “Local measurements of the time-dependent heat release rate and equivalence ratio using chemiluminescent emission from a flame,” *Combust. Flame*, vol. 139, no. 3, pp. 188–207, 2004.

[170] J. Song, M. Alam, A. L. Boehman, and U. Kim, “Examination of the oxidation behavior of biodiesel soot,” *Combust. Flame*, vol. 146, no. 4, pp. 589–604, 2006.